

CORRELATION AND OPTIMISATION OF THERMODYNAMIC MODEL  
PARAMETERS WITH EXPERIMENTAL DATA TO PREDICT EMISSIONS  
FROM A DIESEL ENGINE

by

Onur Barış

B.S., Mechanical Engineering, Middle East Technical University, 2008

Submitted to the Institute for Graduate Studies in  
Science and Engineering in partial fulfillment of  
the requirements for the degree of  
Master of Science

Graduate Program in Mechanical Engineering

Boğaziçi University

2012

CORRELATION AND OPTIMISATION OF THERMODYNAMIC MODEL  
PARAMETERS WITH EXPERIMENTAL DATA TO PREDICT EMISSIONS  
FROM A DIESEL ENGINE

APPROVED BY:

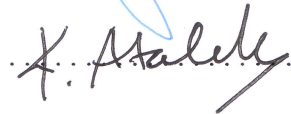
Assoc Prof. Hasan Bedir  
(Thesis Supervisor)



Prof. A. Erhan Aksoylu



Assoc. Prof. Kunt Atalık



DATE OF APPROVAL: 30.01.2012

*Dedicated to my family since nothing will be possible without them.*

## **ACKNOWLEDGEMENTS**

I want to thank my thesis supervisor Assoc. Prof. Hasan Bedir for his patience and guidance throughout the work. I want to also thank my supervisors Tolga Şenoğuz for helping to find a suitable thesis project and Kayhan Özdemir for his full support during my work whenever I needed help. I want to thank Dietmar Hermann, for the injection testing support, Robert Wang for his support on issues with GTpower software, Emre Korkmaz for his support on dynamometer test data supplement. I want to thank Ford Motor Company and Ford OTOSAN for allowing me to do this work. Lastly, I want to thank TUBITAK for the scholarship given to MSc. students.

## **ABSTRACT**

### **CORRELATION AND OPTIMISATION OF THERMODYNAMIC MODEL PARAMETERS WITH EXPERIMENTAL DATA TO PREDICT EMISSIONS FROM A DIESEL ENGINE**

The biggest challenge in engine development is emission regulation today, which gets more stringent with time. Computer aided engineering (CAE) has also increasing importance together with increasing potential of processors for easy and quick calculations and also it is less expensive compared to conducting tests. Therefore it is highly important and challenging to predict emissions by using computer models and simulations precisely. For diesel engines, NO<sub>x</sub> and particle (soot) emissions have the highest importance. 3D CFD of combustion systems and phenomenological combustion models can provide such information. Phenomenological combustion models have the advantage of much lower runtimes compared to 3D CFD and can be used for wide variety of engine operating points for prediction. Such a phenomenological diesel combustion model is used and correlated with limited amount of test data for the prediction of emissions and is compared to a larger set of emission test data to see its performance. Assessments are made how well the emissions can be predicted by using such a model. The sensitivity of the model against different start of injection and exhaust gas recirculation values is tested. NO<sub>x</sub> model show good accuracy whereas soot model needs some modification. Both emission models can provide some insight in terms of direction (increase-decrease).

## ÖZET

### **DİZEL MOTORLARDA EMİSYON ÖNGÖRMEK AMAÇLI TERMODİNAMİK MODEL PARAMETRELERİNİN OPTİMİZASYONU**

Günümüzde motor geliştirmenin önündeki en büyük kısıtlamalardan birisi giderek daralan emisyon sınırı standartlarıdır. Bilgisayar destekli mühendisliğin de önemi günümüzde gittikçe artmaktadır çünkü bilgisayarların artan kapasitesi hızlı ve detaylı analize olanak sağlamaktadır ve bilgisayar bazlı analiz yapmak teste oranla çok daha ucuz ve kolay olmaktadır. Bu sebeple bilgisayarda yapılan modelleri ve analizleri kullanarak emisyon öngörüsü yapmak oldukça kritik ve zorlayıcı bir prosedürdür. Dizel motorlarda özellikle azot oksit ( $\text{NO}_x$ ) ve partikül emisyonları büyük önem taşımaktadır. 3 boyutlu hesaplamalı akışkanlar dinamiği (HAD) veya öngörü yapabilen sıfır boyutlu yanma modelleri bu gibi emisyon öngörüsünü sağlamak için kullanılabilir. Sıfır boyutlu yanma modelleri 3 boyutlu HAD yöntemine göre çok daha az sürede sonuçları verebildiğinden birçok motor operasyonu noktasında öngörü yapabilmek için daha kullanışlıdır. Bu çalışmada bu tarz bir modelin sınırlı sayıda test ölçümü kullanarak korrelasyonu yapıldı ve emisyon sonuçlarının çok daha fazla noktada test ile nasıl uyduğu karşılaştırıldı. Böylece modelin performansı hakkında sonuçlar elde edildi. Ayrıca modelin farklı enjeksiyon zamanlaması ve farklı içeri giren egzoz gazı oranlarında ne kadar doğru öngörü yapabildiği test edildi. Azot oksit modelinin gerçeğe oldukça yakın sonuçlar verdiği fakat partikül modelinde bazı değişikliklere ihtiyaç olduğu tespit edildi. Her iki emisyon modeli de belli seviyede yönsel olarak bilgi almak açısından kullanılabilir.

## TABLE OF CONTENTS

ACKNOWLEDGEMENTS.....	iv
ABSTRACT.....	v
ÖZET.....	vi
LIST OF FIGURES.....	viii
LIST OF TABLES.....	xii
LIST OF SYMBOLS.....	xiii
LIST OF ACRONYMS/ABBREVIATIONS.....	xv
1. INTRODUCTION.....	1
2. LITERATURE SURVEY.....	2
2.1. Combustion Model.....	2
2.1.1. Model of Hiroyasu and GTpower modifications.....	3
2.2. Emission Model.....	2
3. MODEL CORRELATION AND OPTIMIZATION.....	20
3.1. Introduction.....	20
3.2. Test Data and Pre-processing.....	20
3.3. Combustion Correlation.....	26
3.4. Emission Correlation.....	33
3.5. Results.....	36
3.6. SOI and EGR Sensitivity.....	45
4. CONCLUSION.....	52
APPENDIX A: PHENOMENOLOGICAL COMBUSTION MODELS.....	54
APPENDIX B: SENSITIVITY STUDY.....	62
APPENDIX C: TEST SETUP.....	77
APPENDIX D: DESIGN OF EXPERIMENTS.....	80
REFERENCES.....	82

## LIST OF FIGURES

Figure 2.1.	Diesel fuel jet divided into small sub-region. ....	4
Figure 2.2.	Diagram showing the mixing and combustion step. ....	4
Figure 2.3.	Diagram of the mass system in the subzones during the process. ....	5
Figure 2.4.	Spray arrangement during impingement event. ....	8
Figure 2.5.	Spray arrangement for swirl event. ....	8
Figure 2.6.	Process chart for net production of particulates in diesel engines. ....	18
Figure 3.1.	Pressures during processing (a) pressure with and without smoothing and (b) the comparison of measured vs. recalculated from burn rate. ....	22
Figure 3.2.	Injection profiles at 1800 bar rail pressure at different quantities. ....	24
Figure 3.3.	RMS errors at each case with optimum correlation parameters. ....	28
Figure 3.4.	Cylinder pressure comparison for all cases (straight line – measured, dotted line – predicted). ....	29
Figure 3.5.	RMS errors by using a single optimized parameter set. ....	32
Figure 3.6.	NO <sub>x</sub> emission zero error curves for different cases. ....	34
Figure 3.7.	Soot emission zero error curves for different cases. ....	35



Figure 3.8.	NO <sub>x</sub> emission map for (a) test and (b) model. ....	37
Figure 3.9.	NO <sub>x</sub> error of the model compared to the test data. ....	38
Figure 3.10.	Soot emission map for (a) test, (b) single multiplier model, (c) four multipliers model and (d) interpolated multiplier model. ....	39
Figure 3.11.	Soot error map for (a) single multiplier model, (b) four multipliers model and (c) interpolated multiplier model. ....	41
Figure 3.12.	Soot emissions for (a) around 1500 rpm 41% load and (b) around 4000 rpm 83% load. ....	43
Figure 3.13.	RMS errors when SOI changes at 2000 rpm 50% load. ....	45
Figure 3.14.	Cylinder pressure comparison for different SOI values. ....	46
Figure 3.15.	NO <sub>x</sub> emissions for different SOI values (test vs. model). ....	47
Figure 3.16.	Soot emissions for different SOI values (test vs. model). ....	48
Figure 3.17.	Burn rate RMS errors for different EGR rates (in percentage). ....	49
Figure 3.18.	Cylinder pressures for different EGR rates (test vs. model). ....	50
Figure 3.19.	NO <sub>x</sub> emission for different EGR rates (test vs. model). ....	50
Figure 3.20.	Soot emission for different EGR rates (test vs. model). ....	51
Figure A.1.	Temporal sequence of the premixed combustion model. ....	55
Figure A.2.	Zone description. ....	58

Figure A.3.	Slice propagation through the combustion chamber. ....	60
Figure B.1.	Pressure vs crank angle plots for timestep sensitivity. ....	62
Figure B.2.	Temperature vs crank angle plots for timestep sensitivity. ....	63
Figure B.3.	NO <sub>x</sub> concentration vs CAD. ....	64
Figure B.4.	Soot concentration vs CAD. ....	64
Figure B.5.	Change of burn rate with CBAIR multiplier. ....	67
Figure B.6.	Change of burn rate with CAAIR multiplier. ....	68
Figure B.7.	Change of burn rate with CWALL multiplier. ....	69
Figure B.8.	Change of burn rate with CIGN1 multiplier. ....	70
Figure B.9.	Change of burn rate with CIGN8 multiplier (full load). ....	72
Figure B.10.	Change of burn rate with CIGN8 multiplier with 20% EGR. ....	72
Figure B.11.	Change of burn rate with TBMULT multiplier. ....	74
Figure B.12.	Change of burn rate with CRATE multiplier. ....	75
Figure C.1.	Diesel engine flow layout schematic. ....	78
Figure D.1.	Test matrix for full factorial (a) and latin hypercube (b) methods. ....	81

## LIST OF TABLES

Table 2.1.	Reaction rates and temperatures for Zeldovich mechanism reactions. ....	15
Table 3.1.	Engine properties. ....	20
Table 3.2.	Operating points chosen for correlation (Speed and Torque). ....	25
Table B.1.	Case setup for parameter sensitivity. ....	66
Table B.2.	Emissions and maximum temperature for CBAIR sensitivity. ....	67
Table B.3.	Emissions and maximum temperature for CAAIR sensitivity. ....	68
Table B.4.	Emissions and maximum temperature for CWALL sensitivity. ....	69
Table B.5.	Emissions and maximum temperature for CIGN1 sensitivity. ....	70
Table B.6.	Emissions and maximum temperature for CIGN8 sensitivity (full load). ....	73
Table B.7.	Emissions and maximum temperature for CIGN8 sensitivity (part load). ....	73
Table B.8.	Emissions and maximum temperature for TBMULT sensitivity. ....	74
Table B.9.	Emissions and maximum temperature for CRATE sensitivity. ....	75
Table C.1.	Smoke meter properties. ....	79
Table C.2.	HORIBA NO <sub>x</sub> Analyzer properties. ....	79

## LIST OF SYMBOLS

B	Quantity of fuel injected per stroke (mg/stroke)
$c_p$	Specific heat at constant pressure (J/kgK)
$C_n$	Nozzle discharge coefficient
D	Diameter of a droplet (m)
$D_{32}$	Sauter mean diameter (m)
$D_n$	Nozzle orifice diameter (m)
F	Wall area of a combustion cylinder ( $m^2$ )
$F_{st}$	Stoichiometric equivalence ratio
$H_u$	Calorific value of fuel, lower heating value (J/kg)
$h^*$	Heat transfer coefficient between burned gas and cylinder wall ( $W/m^2K$ )
$h_{fg}$	Heat of vaporization (J)
G	Mass flux from liquid to vapor (fuel)
I	Factor representing order of injection
J	Factor representing crank angle at ignition of packages
$k^*$	Mass transfer coefficient at high mass transfer
L	Factor representing the radial location of the package
$L_n$	Injector nozzle length (m)
m	Mass (kg)
$\Delta m_{fci}$	Mass of fuel burned at stoichiometric ratio (kg)
$\Delta m_{fg}$	Mass of vaporized fuel (kg)
$\Delta m_{fi}$	Mass of fuel burned (kg)
$\Delta m_{fui}$	Mass of fuel evaporated in the package (kg)
N	Number of droplets in the package
n	Engine speed (rpm)
P	Cylinder pressure (MPa)
$P_{O_2}$	Partial pressure of oxygen (MPa)
$\Delta P$	Difference between injection pressure and cylinder pressure (Pa)
Q	Net amount of heat release (J)
R	Gas constant (kJ/kmolK)

$r_s$	Swirl ratio
$S$	Spray tip penetration (m)
$T$	Temperature (K)
$t$	Time (s)
$V$	Cylinder volume ( $m^3$ )
$u$	Velocity of fuel jet (m/s)
$Y_{NO}$	NO concentration
$Y_A$	Mass fraction of vaporized fuel
$z$	Coordinate (m)
$\alpha$	Mass diffusivity
$\xi$	Flow rate ratio of air to fuel at droplet surface
$\theta$	Crank angle (degree)
$\lambda$	Heat of evaporation
$\kappa$	Specific heat ration ( $c_p/c_v$ )
$\rho_x$	Density of x ( $kg/m^3$ )
$\tau_i$	Ignition delay (ms)
$\tau$	Ignition delay of gaseous mixture at constant conditions (ms)
$\phi_g$	Equivalence ratio concerning the vaporized fuel
$\omega$	Angular velocity (rad/s)

**LIST OF ACRONYMS / ABBREVIATIONS**

Re	Reynolds number
We	Weber number
Nu	Nusselt number
Pr	Prandtl number
Sh	Sherwood number
Sc	Schmidt number
0	Surface or initial condition
2	Bulk condition
a	Air
f	Fuel
g	Gas
l	Liquid
b	Burned gas
k	Kinetics
n	Injector nozzle
s	Soot or swirl
v	Vapor
w	Wall
inj	Injection
ig or ign	Ignition
cyl	Cylinder
sf	Soot formation
sc or so	Soot consumption or Soot oxidation
CAD	Crank angle degree
SOI	Start of injection
EGR	Exhaust gas recirculation
NO <sub>x</sub>	Nitrogen oxides such as NO and NO <sub>2</sub>
FSN	Filter smoke number
DOE	Design of experiments

## 1. INTRODUCTION

Internal combustion engines are one of the most important power units used for transportation for the last 100 years. Many researches have been done on engines using different methods. Together with improved technology, importance of computer aided design (CAE) has become more and more important nowadays. It is simply cheaper and easier to model the phenomenon in a computer and process the results instead of testing it physically. Increasing performance of computers is also a big advantage. However it is important to model the physical phenomena correctly and to know what is included / excluded in the models. This is the case since it is very hard to exactly have the same physical phenomena inside a computer model.

Flow and combustion inside the engine is one of the key design issues for the engine. Computational fluid dynamics (CFD) is widely used to simulate the flows inside engine parts and systems. Commercial CFD codes are available to use for any geometry so that the designer does not need to develop his/her own code.

GTpower is one of the commercial codes available, which is a one dimensional fluid dynamics code. In the code, whole flow path of the engine is modeled 1-D; i.e. intake system, cylinders and exhaust system. Heat release profiles are used for modeling the combustion or available methods are used to create heat release profiles if it is not available. GTpower is a useful code for simulating the whole engine and to see its behavior at different operating conditions (at different loads and speeds).

It is also important to predict engine behavior from such a code. Nowadays; emission legislations are extremely important. Therefore it is important to predict emissions beforehand and take necessary steps in the design stage of the engine. Therefore a predictive simulation model is necessary and can be highly useful. Effect of many different design parameters on emissions can be seen using such a model.

## 2. LITERATURE SURVEY

### 2.1. Combustion Model

There are a number of different phenomenological combustion models available in the literature. Some are created by the authors themselves and some of them (most of them) are the modified versions of one of the available models or mix of different models. The purpose is to obtain data about heat release and emissions from a simple combustion model. This type of model requires less amount of time compared to 3D CFD in-cylinder combustion analysis. However empirical constants are needed to correlate the model since details such as 3D turbulent flow and exact 3D geometry is missing in such models. Different models will be explained here. Only modifications done to the first model will be explained, which is the model used in GTpower named as DIjet model and the equations will be given in detail.

First the combustion model details will be explained then the emission modeling details will be explained.

All models do certain main assumptions about which parameter depends on which event and which events have the most importance for combustion. All models have a certain number of correlation parameters, which are empirical coefficients in the equations. Since it is diesel combustion, most of the models divide the combustion into two main parts: pre-mixed and diffusion. All models have a certain ignition delay model and wall impingement (i.e. fuel spray wetting cylinder and piston walls) assumption. Another purpose of the models is to be able to account for several fuel injections per cycle (pre-, main and post-injection events which are used mostly in modern diesel engines. Also there can be more than one pre-, main and post injection).

Four models are listed here, first being model of Hiroyasu *et al.* [1,2] and the modification made in GTpower [3]. This model is explained in detail. Another model available in the literature is the model by Barba *et al.* [4], where some of the mathematical models are implemented from [5] and [6]. In this model fuel jet is not modeled in detail.



Another example is the work by Maiboom *et al.* [7], where fuel jet is modeled with less detail compared to [1] and injection models from other sources such as [8-10] are used. This model is the modified version of a previous work explained in [11]. Another and last example is the work by Rether *et al.* [12] where some of the modeling is referenced to [13]. These models will not be explained in much detail here, some explanations can be found in the appendix section.

In all the works listed above; the model is judged by the comparison of cylinder pressure or net heat release diagrams for test and the model mostly. There is no given numerical measure of the model for its exactness. Only plots of heat release, burn rate or cylinder pressure is given so that one can see have the experimental and model graphs fit with each other.

It can also be seen that all these models have certain number of empirical coefficients that should be calibrated. Most geometrically detailed model is the one from Hiroyasu *et al.* and GTpower DIjet model, which is build based on the fuel jet model by Hiroyasu *et al.*. There are also many additional modeling work conducted by many others but most recent and different models are investigated.

Since  $\text{NO}_x$  and soot particles are the most important and critical emissions for a diesel engine, the focus in this study is on  $\text{NO}_x$  and soot emission prediction.

### **2.1.1. Model of Hiroyasu and GTpower modifications**

Hiroyasu *et al.* has worked on such a model as explained in [1], in which he models the fuel jet injected to the cylinder. The fuel jet is divided into small elements in the axial and radial direction as shown in Figure 2.1 taken from [1].

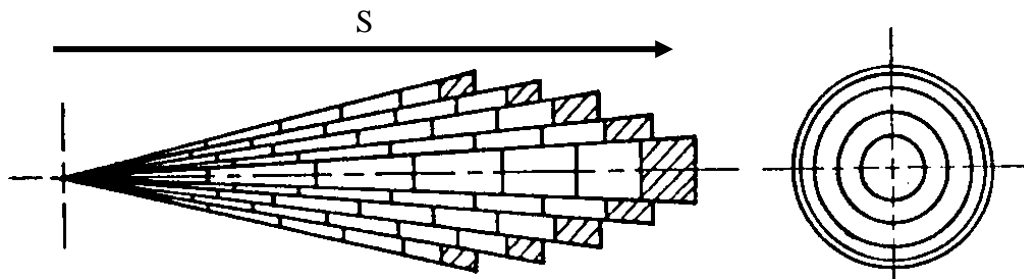


Figure 2.1. Diesel fuel jet divided into small sub-regions [1].

Air is entrained to these zones and it is mixed with fuel. Air entrainment is modeled using conservation of momentum, i.e. the speed of the subzones decrease as more air is entrained into it. Therefore the subzones in the edge of the spray which are in direct contact with air will be slower compared to the subzones in the centerline of the spray, which can be seen in Figure 2.1. All the calculations are done for these subzones (burn rate, emission etc.). Figure 2.2 from [1] shows the schematic diagram of mixing and combustion.

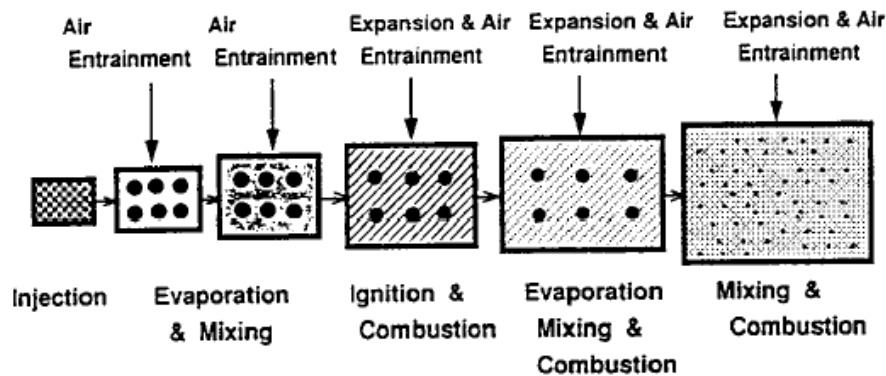


Figure 2.2. Diagram showing the mixing and combustion steps [1].

Figure 2.3 from [1] shows the change of mass fractions in each subzone during the injection and combustion processes. As can be seen, the combustion can be limited by entrained air or evaporation rate of the fuel at that subzone.

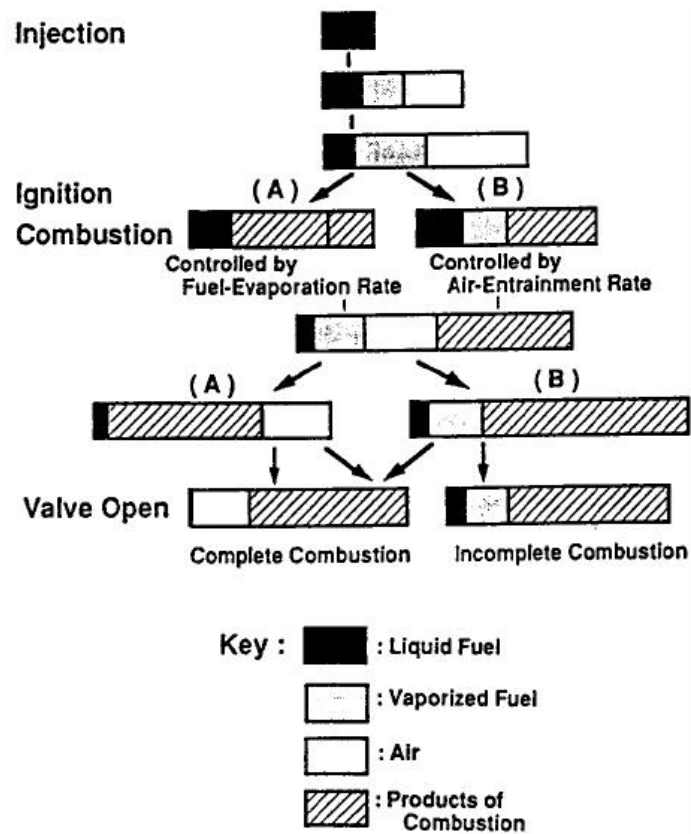


Figure 2.3. Diagram of the mass system in the subzones during the process [1].

Spray penetration (shown in Figure 2.1) and breakup are also modeled other than air entrainment. Penetration of the spray changes according to break-up time. Equation 2.1 and Equation 2.2 are used for the calculation of penetration distance and Equation 2.3 gives breakup time.

Since more air is entrained into the edges of the spray (due to the direct contact with surrounding air), edges will be slower than the centerline subzones. This modification for axially outer zones is done by using another equation.  $L$  denotes the radial distance from the center and  $L=1$  means the center axis. This effect is calculated by Equation 2.4, where the penetration distance is modified.

$$S = 0.39 \sqrt{\frac{2\Delta P}{\rho_l}}, \quad \text{for } 0 < t < t_b \quad (2.1)$$

$$S = 2.95 \left(\frac{\Delta P}{\rho_l}\right)^{0.25} \sqrt{\alpha_0 t}, \quad \text{for } t \geq t_b \quad (2.2)$$

$$t_b = 28.65 \frac{\rho_l D_n}{\sqrt{\rho_a \Delta P}} \quad (2.3)$$

$$S_L = S \cdot \exp(-8.577 \cdot 0.001(L - 1)^2) \quad (2.4)$$

To include the effect of the swirl within the chamber (which is effective in diesel engines), the following modification is made to the penetration distance.

$$S_S = C_S \cdot S \quad (2.5)$$

$$C_S = \left(1 + \frac{\pi r_s n S}{30 u_o}\right)^{-1} \quad (2.6)$$

As was mentioned earlier, conservation of momentum is used for air entrainment. This means that the momentum of the subzone at the exit of the injector nozzle is equal to the momentum of the subzone at any distance. This leads to Equation 2.7 and Equation 2.8.

$$m_f u_o = (m_f + m_a) u \quad (2.7)$$

$$m_a = m_f \left(u_o \cdot \frac{dt}{ds} - 1\right) \quad (2.8)$$

Air entrainment rate can be found by taking the time derivative of both sides in Equation 2.8.

As the spray ignites and its periphery covers with flame, the air entrainment rate decreases. Another event that changes the air entrainment rate is the impingement of the spray to piston bowl or cylinder wall. After this event, momentum of the spray decreases and air entrainment value is modified. Air entrainment rate after ignition and after wall impingement are given by Equation 2.9 and Equation 2.10, respectively (subscript f for firing and w for wall).

$$\frac{dm_{af}}{dt} = C_f \frac{dm_a}{dt} \quad (C_f = 0.7) \quad (2.9)$$

$$\frac{dm_{aw}}{dt} = C_w \frac{dm_a}{dt} \quad (C_w = 1.5) \quad (2.10)$$

In GTpower there are separate multipliers for this equation for before combustion (CBAIR), after combustion (CAAIR) and after wall impingement (CWALL) and the default values are different. Modifications made on this model in GTpower will be covered in detail in the following sections.

The deformation in the path of the injected fuel due to swirl is calculated by Equation 2.11.

$$r_{\text{def}} = S \cdot \frac{m_a}{m_a + m_f} \cdot \frac{\frac{n}{60} r_s 2\pi S}{\frac{u_0 + u}{2}} \quad (2.11)$$

For clarity, Figures 2.4 and 2.5 from [1] show the configuration of the spray during impingement and swirl of the air, respectively. Figure 2.4a shows the case without impingement. Fuel spray is assumed to move along the wall surface as constant thickness packages as shown in Figure 2.4b. When the fuel gets close to the neighbor spray injected from other injector nozzle, side swell is limited and thickness increases as shown in Figure 2.4c. Figure 2.5 shows that axial center of the spray is shifted when swirl is present and center of mass of the spray corresponds to the deformation calculated using Equation 2.11. Figure 2.5 shows arrangements for no swirl, weak and strong swirl cases.

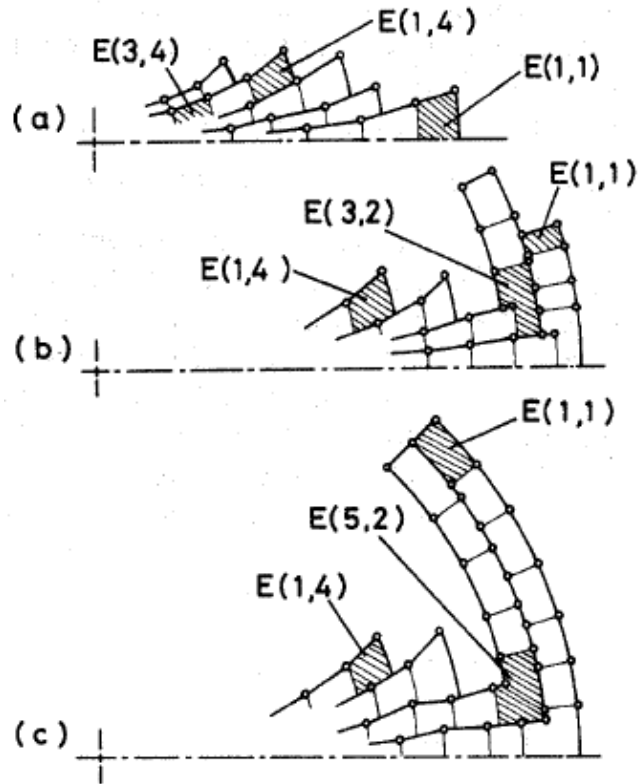


Figure 2.4. Spray arrangement during impingement event [1].

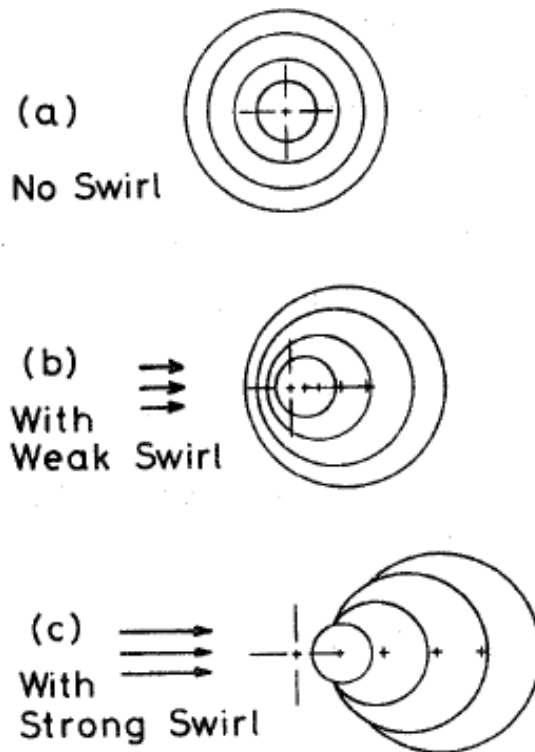


Figure 2.5. Spray arrangement for swirl event [1].

Spray evaporation is modeled by considering the liquid fuel as droplets after break-up and mean diameter of the droplets are calculated in each zone. This mean diameter is also called Sauter mean diameter (SMD). Sauter mean diameter, which is assumed to depend on pressure difference, density and fuel quantity, is calculated as shown in Equation 2.12. Equation 2.13 shows the temperature change of liquid fuel and change of the droplet diameter is given by Equation 2.14. Change of the liquid fuel mass is calculated by Equation 2.15. Evaporated fuel mass is calculated using Equation 2.16.

$$D_{32} = 23.9(\Delta P)^{-0.135} \rho_a^{0.12} B^{0.131} \quad (2.12)$$

$$\frac{dT_l}{dt} = \frac{1}{m_l C_{Pl}} \left\{ \pi D_l^2 h \cdot (T_2 - T_l) + \lambda \frac{dm_l}{dt} \right\} \quad (2.13)$$

$$\frac{dD_l}{dt} = \frac{2}{\pi D_l^2 \rho_l} \left\{ \frac{dm_l}{dt} - \frac{\pi D^3}{6} \frac{d\rho_l}{dt} \right\} \quad (2.14)$$

$$\frac{dm_l}{dt} = -\pi D_l^2 k \cdot \frac{Y_{AO} - Y_{A2}}{(1 + \xi) Y_{AO}} \quad (2.15)$$

$$m_{fg} = \frac{\pi}{6} (\rho_{l0} D_{l0}^3 - \rho_l D_l^3) N \quad (2.16)$$

Due to evaporation; the temperature of the zone will drop. This is calculated by Equation 2.17.

$$\Delta T = \frac{Q \cdot d - C_{Pf} \frac{dm_l}{dt} (T_2 - T_1)}{C_{Pl} m_{fg} + m_a C_{Pa}} \quad (2.17)$$

The ignition delay of the fuel is calculated depending on pressure, temperature and equivalence ratio. Equation 2.18 shows the equivalence ratio. Ignition delay is calculated using a time integral. When the condition shown in Equation 2.20 is satisfied, the ignition starts. So Equation 2.19 is calculated at each time step and these are added to each other until the integral becomes equal to one. The time at which the integral becomes one is the ignition delay time.

$$\phi_g = \frac{m_{fg}}{m_g \cdot F_{st}} \quad (2.18)$$

$$\tau = 4.0 \cdot 10^{-3} P^{-2.5} \phi_g^{-1.04} \exp\left(\frac{4000}{T_2}\right) \quad (2.19)$$

$$\int_0^{\tau_i} \frac{1}{\tau} dt = 1 \quad (2.20)$$

The combustion occurs at stoichiometric conditions and following condition shown in Equation 2.21 and Equation 2.22 is applied for the fuel mass burned during the steps. These equations show that fuel burn rate is limited by stoichiometry (subscripts:  $f_i$  > fuel ignited,  $f_{ui}$  > evaporated fuel,  $f_{ci}$  > stoichiometric fuel according to air available) if equivalence ratio is higher than one.

$$\Delta m_{f_i} = \Delta m_{f_{ui}} \quad (\Phi_\phi \leq 1) \quad (2.21)$$

$$\Delta m_{f_i} = \Delta m_{f_{ci}} \quad (\Phi_\phi > 1) \quad (2.22)$$

Heat release in a package for a time step and total spray heat release are given by Equation 2.23 and Equation 2.24, respectively.

$$\Delta Q_{pi} = H_u \Delta m_{f_i} \quad (2.23)$$

$$\Delta Q_B = H_u \sum_{i=1}^n \Delta m_{f_i} \quad (2.24)$$

$H_u$  is the calorific value of the fuel and  $n$  is the number of burning packages at that time step.

Heat transfer from the cylinder to the ambient is calculated by the simple convection formula by calculating the heat transfer coefficient ( $h_w$ ) using pressure, temperature and injected fuel quantity. Equation 2.25 and Equation 2.26 show the heat transfer correlation of the model.

$$Q_w = F \cdot h_w (T - T_w) \quad (2.25)$$

$$h_w = 110 \cdot B^{-0.2} P^{0.8} (C_1 \cdot C_m)^{0.8} T^{-0.53} \quad (2.26)$$



The net heat release is the difference of the heat released from the fuel and heat transfer loss to the ambient. This net heat release also gives the cylinder pressure. Equation 2.27 and Equation 2.28 show these calculations. These equations also show how heat release and cylinder pressure is related for general purposes such as back calculating heat release from cylinder pressure data.

$$\frac{dQ}{d\theta} = \frac{dQ_B}{d\theta} - \frac{dQ_W}{d\theta} \quad (2.27)$$

$$\frac{dP}{d\theta} = \frac{1}{V} \left( \frac{\kappa - 1}{A} \frac{dQ}{d\theta} - \kappa P \frac{dV}{d\theta} \right) \quad (2.28)$$

In DIjet model of GTpower, there are modifications in the equations used above for penetration, evaporation, ignition delay and combustion rate calculations. The modifications on the model are done by considering some modifications already done in [2]. Calculations for fuel jet velocity, penetration distance before break-up, break-up time and penetration distance after break-up are shown in Equation 2.29, Equation 2.30, Equation 2.31 and Equation 2.32, respectively taken from [3]. One of the main differences is that the penetration distance is time dependent both before and after break-up time. In the previous one; the penetration distance before break-up does not depend on time. Break-up time mostly depends on injector nozzle geometry (length and diameter), fuel jet velocity (i.e. injection pressure) and densities of fuel and air.

$$u_0 = C_n [2(P_{inj} - P_{cyl})/\rho_{finj}]^{0.5} \cdot (\rho_{finj}/\rho_{fcyl}) \quad (2.29)$$

$$S = u_0 t [1 - 0.06 \cdot (t/t_b)^7], \quad \text{for } t < t_b \quad (2.30)$$

$$t_b = 0.29(3 + L_n/D_n)(\rho_{fcyl}/\rho_a)(D_n/u_0) \quad (2.31)$$

$$S = u_0 t_b [(t/t_b)^{0.5} - 0.06], \quad \text{for } t > t_b \quad (2.32)$$

Swirl modifies the penetration distance as shown in Equation 2.33.

$$S_s = S \cdot \left( 1 + \frac{\pi r_s n S}{u_0} \right)^{-1} \quad (2.33)$$

In DIjet model, increase of the fuel jet temperature is also calculated, which is claimed to be significant in modern high pressure injectors. This increase is calculated using Equation 2.34. The increase of temperature depends on density of fuel during injection and inside the cylinder, injection and cylinder pressures.

$$\Delta T_f = \left[ 1 - \left( \frac{P_{inj}}{\rho_{fcyl}} \right) \left( \frac{\delta \rho}{\delta P} \right) - 1.02 C_n \left( \frac{\rho_{finj}}{\rho_{fcyl}} \right)^2 \right] \frac{(P_{inj} - P_{cyl})}{\rho_{finj} c_p} \quad (2.34)$$

Sauter mean diameter (SMD) for fuel droplets are calculated using the following correlation. All droplets are assumed to have same diameter in a subzone. There is a multiplier available for SMD calculation, which multiplies the right hand side of the given equation. Here the SMD is calculated as a function of Reynolds and Weber numbers and it also depends on fuel and air densities and nozzle diameter.

$$D_{32} = 60 D_n Re^{-0.22} We^{-0.31} (\rho_{fcyl} / \rho_a)^{-0.17} \quad (2.35)$$

Air entrainment calculation is same as the model of Hiroyasu *et al.* as explained previously, only the entrainment multiplier before combustion can be set also by the user.

Evaporation rate is assumed to depend strongly on relative velocity of the fuel droplet. Drag acting on the droplets is assumed to drop their velocity rapidly and the decrease of velocity is calculated based on the Stokes drag law.

$$\frac{\delta u_d}{\delta t} = -18 \frac{u_d \mu}{(\rho D^2)} - 3 \frac{u_d}{D} \frac{\delta D}{\delta t} \quad (2.36)$$

The relative velocity drops to zero in a very short time (in the order of 0.01 milliseconds). The evaporation is either diffusion or boiling limited. This is decided by calculating the fuel vapor pressure at the droplet surface. If the vapor pressure exceeds the cylinder pressure, the evaporation is switched to boiling limited mode and to diffusion mode otherwise. The diffusion limited evaporation rate is calculated by the following equations. G is the mass flux from liquid to vapor. It is strongly dependent on mass diffusivity, Sherwood number, droplet diameter, density and mass fraction of vapor at the

surface and away from the surface. As the droplets slow down both Sherwood and Nusselt numbers go to 2 since Reynolds number is almost equal to 0 (see Equation 2.40 and Equation 2.42).

$$\frac{dm_v}{dt} = G\pi D^2 \quad (2.37)$$

$$G = \rho \cdot Sh \cdot \alpha \cdot \ln(1 + \beta)/D \quad (2.38)$$

$$\beta = \frac{Y_0 - Y_\infty}{1 - Y_\infty} \quad (2.39)$$

$$Sh = 2 + 0.57 \cdot Sc^{1/3} Re^{1/2} \quad (2.40)$$

Then boiling limited evaporation rate can be calculated from heat absorbed divided by the heat of vaporization as shown.

$$G = Q/h_{fg} \quad (2.41)$$

Typically; heat transfer to the droplets is dominantly form convection mode (compared to radiation from walls and soot) and Nusselt number is calculated from the following correlation, which is very similar to the formula used to calculate Sherwood number (see Equation 2.40).

$$Nu = 2 + 0.57 \cdot Pr^{1/3} Re^{1/2} \quad (2.42)$$

Ignition delay calculation is very similar to the Hiroyasu model, but is shown again here with the multipliers available to correlate the ignition delay.  $C_{ign\#}$  parameters are correlation parameters for ignition delay. There are totally four parameters shown but parameter  $C_{ign1}$  has the most significant effect on ignition delay.

$$\tau = \frac{C_{ign1}}{\phi(3 - \phi)^2} \cdot P^{C_{ign2}} \cdot \exp\left(\frac{C_{ign3}}{T}\right) \cdot 1.2E - 6 \cdot f(Dilution, C_{ign4}),$$

$$\text{for } \phi < 3.0 \quad (2.43)$$

$$\tau = \infty, \quad \text{for } \phi \geq 3.0 \quad (2.44)$$

$$I = \int \frac{1}{\tau} dt \quad (2.45)$$

As can be seen, pressure and temperature constants can be modified. Ignition delay again depends on pressure, temperature and equivalence ratio and residual gas fraction affect is added. No ignition occurs in a package if the equivalence ratio is higher than 3.

Similar equivalence ratio condition used for ignition delay is also used for combustion rate calculation. No combustion event occurs when equivalence ratio is higher than 3. The pressure and temperature constants cannot be modified in this equation but there is an overall multiplier named as *cmbmult* (also CRATE) (short for combustion multiplier).

$$\frac{dm_k}{dt} = cmbmult \cdot \phi \cdot (3 - \phi)^2 \cdot P^{2.5} \cdot \exp\left(-\frac{4000}{T}\right), \quad \text{for } \phi < 3.0 \quad (2.46)$$

$$\frac{dm_k}{dt} = 0, \quad \text{for } \phi \geq 3.0 \quad (2.47)$$

There are some differences between DIjet and model by Hiroyasu *et al.* in terms of mathematical models used for calculations but the main modeling idea and assumption is the same, which is to divide the fuel jet into smaller zones and calculation of the air entrainment.

## 2.2. Emission Model

There is not much detail available for emission modeling for the models of Barba and Maiboom. Model of Hiroyasu, DIjet model in GTpower and Grill *et al.* as shown in [14] (Grill has conducted the work by using the model by Rether *et al.* for combustion) utilize extended Zeldovich mechanism for the estimation of NO<sub>x</sub> emissions, where chemical kinetics is considered only for three reactions related to NO<sub>x</sub> and other reactions are assumed to be in equilibrium. These reactions are reactions of nitrogen atom (N) with NO, O<sub>2</sub> and OH. These reactions are accepted to be the governing equations for formation of NO. Rate constants for GTpower model are taken from [5]. This method is widely used frequently in the literature for NO<sub>x</sub> emission predictions. Also a detailed model can be used by taking the chemical kinetics of other reactions into consideration, which may affect NO<sub>x</sub> formation. The extended Zeldovich mechanism reactions are shown below and the Table 2.1 from [5] shows the rates for these reactions and their reverse reactions.

Since this mechanism only calculates the NO formation in the end, a modification is used in GTpower to account for NO<sub>2</sub>. The most important parameter that NO<sub>x</sub> emission depends by using this model is the temperature.

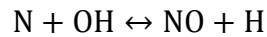
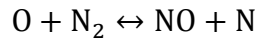


Table 2.1. – Reaction rates and temperatures for Zeldovich mechanism reactions [5].

Reaction	Rate Constant k [cm <sup>3</sup> /mol·s]	Temperature Range [K]	Uncertainty Factor or %
(1) O+N <sub>2</sub> → NO + N	$7.6 \times 10^{13} \exp(-38000/T)$	2000-5000	2
(-1) NO + N → O+N <sub>2</sub>	$1.6 \times 10^{13}$	300-5000	±20% at 300 K 2 at 2000-5000 K
(2) N+O <sub>2</sub> → NO+ O	$7.6 \times 10^9 \exp(-3150/T)$	300-3000	±30% at 300-1500 K 2 at 3000 K
(-2) NO+ O → N+O <sub>2</sub>	$1.5 \times 10^9 \exp(-19500/T)$	1000-3000	±30% at 1000 K 2 at 3000 K
(3) N + OH → NO + H	$4.1 \times 10^{13}$	300-2500	±80%
(-3) NO + H → N + OH	$2.0 \times 10^{14} \exp(-23650/T)$	2200-4500	2

For soot, formation and oxidation is modeled using one equation for each related to the conditions inside the fuel zones. The equations are Arrhenius type of equations. In GTpower; both NO<sub>x</sub> and soot models of Hiroyasu are available and also a modified version of the soot model is available in which oxidation model is modified according to the work of Nagle and Strickland-Constable. This modified version is recommended for use but it is also noted that the results can be meaningless in terms of quantity. NO<sub>x</sub> model is rather better since chemical kinetics is included together with reactions.

Following formation and oxidation equations are used by Hiroyasu for soot emission calculation. Subscript sf means formed soot, sc means consumed (oxidized) soot and s

means the mass of soot in the fuel jet package. The parameters  $A_f$  and  $A_c$  are correlation parameters for formation and consumption, respectively.

$$\frac{dm_s}{dt} = \frac{dm_{sf}}{dt} - \frac{dm_{sc}}{dt} \quad (2.48)$$

$$\frac{dm_{sf}}{dt} = A_f \cdot m_{fg} \cdot P^{0.5} \cdot \exp\left(\frac{-E_{sf}}{RT}\right) \quad (2.49)$$

$$\frac{dm_{sc}}{dt} = A_c \cdot m_s \cdot \frac{P_{O_2}}{P} P^{1.8} \cdot \exp\left(\frac{-E_{sc}}{RT}\right) \quad (2.50)$$

The oxidation part is modified by using the Equation 2.51 and Equation 2.52 to calculate oxidation and Equations 2.53-2.56 show the rate constants. The parameter  $w$  is the surface oxidation rate and  $x$  is the fraction of surfaces covered with type A sites. It has been assumed that there are two types of site surfaces where oxygen can attack. For the more reactive type A sites, the oxidation rate is controlled by the fraction of sites not covered by surface oxides (and therefore is of mixed order, between 0 and 1 in  $p_{O_2}$ , relative oxygen pressure). Type B sites are less reactive, and react at a rate which is first order in  $p_{O_2}$ .

$$\frac{w}{12} = \left(\frac{k_A P_{O_2}}{1 + k_Z P_{O_2}}\right) x + k_B P_{O_2} (1 - x) \quad (2.51)$$

$$x = \left(1 + \frac{k_T}{P_{O_2} k_B}\right)^{-1} \quad (2.52)$$

$$k_A = 20 \cdot \exp\left(-\frac{15100}{T}\right) \quad [g/cm^2 \cdot s \cdot atm] \quad (2.53)$$

$$k_B = 4.46 \cdot 10^{-3} \cdot \exp\left(-\frac{7640}{T}\right) \quad [g/cm^2 \cdot s \cdot atm] \quad (2.54)$$

$$k_T = 1.51 \cdot 10^5 \cdot \exp\left(-\frac{48800}{T}\right) \quad [g/cm^2 \cdot s] \quad (2.55)$$

$$k_Z = 21.3 \cdot \exp\left(-\frac{2060}{T}\right) \quad [1/atm] \quad (2.56)$$

The soot model used by Grill *et al.* is very similar to Hiroyasu, where formation and oxidation formulas are used in a slightly modified way, which are taken from [15]. The biggest difference is that the pressure is not directly used in the equations. The rate equations are shown in terms of crank angle instead of time. Similar to the model used by

Hiroyasu; the parameters  $A_f$  and  $A_o$  are correlation parameters for formation and oxidation, respectively.

$$\frac{dm_{sf}}{d\theta} = A_f \cdot \frac{dQ_B}{d\theta} \cdot \frac{1}{LHV} \cdot f \cdot \exp\left(\frac{-T_{sf}}{T_{Ff}}\right) \quad (2.57)$$

$$\frac{dm_{so}}{d\theta} = A_o \cdot m_s^{n_{ms}} \cdot (m_{Bz} \cdot x_{O_2, Bz})^{n_{o_2}} \cdot \exp\left(\frac{-T_{so}}{T_{Bz}}\right) \cdot \frac{1}{6n} \quad (2.58)$$

$$\frac{dm_s}{d\theta} = \frac{dm_{sf}}{d\theta} - \frac{dm_{so}}{d\theta} \quad (2.59)$$

There is also no standardized soot model widely used. Different modeling efforts have been carried out. Kennedy in [16] has investigated many of the soot models available in the literature and how the models were used. Soot models are investigated in three main categories: empirical, semi-empirical and detailed chemistry models. Empirical models try to relate the soot to a simple empirical function by correlating this function with a constant according to the application. It tries to include all parameters in the function, which have impact on soot formation. This modeling technique is very specific to the application. A more detailed approach is named as semi-empirical models, where soot formation and oxidation is modeled separately. There are also more detailed semi-empirical models dividing the emission of soot into more steps such as nucleation and growth of soot during formation. Some of these models take the chemical reactions into consideration. Models used in GTpower, model of Hiroyasu and model of Grill can be considered in this category. Detailed chemistry models take many chemical reactions into consideration, which take place during formation and oxidation of soot. These processes are nucleation, coagulation, surface growth and agglomeration. Number of chemical reactions included can change from model to model. Frenklach utilizes a numerical method called method of moments with interpolative closure (MOMIC) as explained in [17]. In other applications also Monte Carlo simulation methods are used for soot calculations as can be seen in [18]. It is hard to model soot formation with chemical reactions since soot particles are mixtures of different molecules such as phenol and polycyclic aromatic hydrocarbons (PAH). Also more detailed models with too much chemistry involved are not very practical for use with a predictive 0D combustion model since there will be more computational penalty. These models are more useful in a 3D CFD model.

Heywood in [5] gives Figure 2.13 showing the order of processes leading to net production of particulate emissions in diesel engines. As can be seen, there are many steps and dehydrogenation and oxidation reactions occur continuously during these steps.

Important parameters for the soot models used together with predictive combustion models are temperature, pressure and partial pressure of oxygen. It should be noted that partial pressure of oxygen depends on the air fuel ratio, which is an important parameter on soot emission.

There are mainly two correlation parameters for emission models. For  $\text{NO}_x$ , there is an overall multiplication multiplier and activation temperature multiplier and for soot there are formation and oxidation multipliers. These multipliers will be used for correlation as it will be explained further in the emission correlation part.

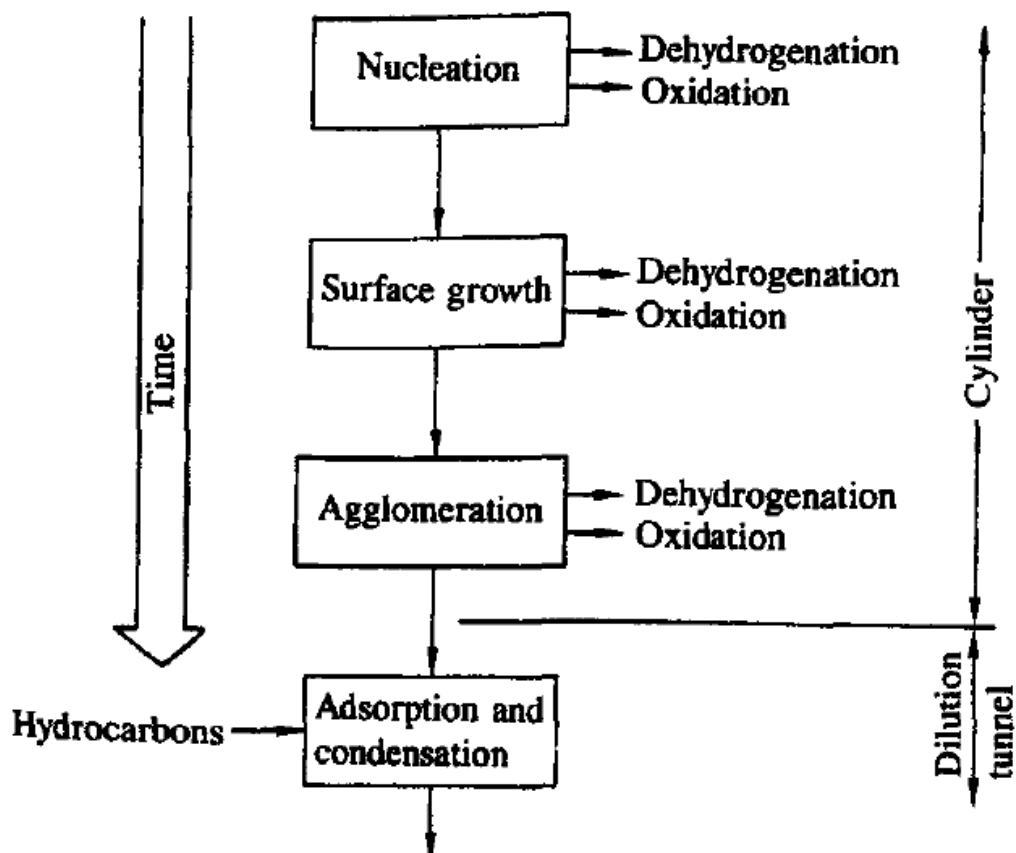


Figure 2.6. Process chart for net production of particulates in diesel engines [5].



GTpower DIjet model is one of the detailed models available in literature, which is a modified version of the work done by Hiroyasu. There are many numbers of parameters for the model to be optimized for different operating conditions. But mainly there are several parameters which have significant impact on the model and should be correlated. Main events for optimization are air entrainment, fuel evaporation (droplet) and ignition delay. It is also very important to have a correct injection profile input, which significantly affects the cylinder pressure, power output in turn and also emissions.

### 3. MODEL CORRELATION AND OPTIMIZATION

#### 3.1. Introduction

The DIjet model of GTpower requires test data for correlation in order to predict the combustion close to reality. It will be good to use as many operating points as possible for correlation however it gets harder to check too many operating conditions. Also the model loses its meaning if it needs too many points for correlation since it increases the number of tests to be done. 20-25 points are recommended to be chosen for correlation. These points should be chosen so that it covers the whole engine operation (i.e. different engine speeds and different engine torque). In this study; 24 points are chosen for 8 different engine speeds and 3 different load conditions (i.e. torque output) at each speed. The engine speeds are from 1000 to 4500 rpm with 500 rpm increments. The diesel engine used for this study is a mid-sized 4 cylinder diesel engine of 2.2 L with a fixed geometry turbocharger. Some of the technical details of the engine are given in Table 3.1.

Table 3.1. Engine properties.

Power	PS	125
Displacement	l	2.198
Bore	mm	86
Stroke	mm	94.6
Connecting Rod Length	mm	155
Compression Ratio	-	15.5

#### 3.2. Test Data and Pre-processing

The dynamometer data for this engine were available at many numbers of points (i.e. more than 24 points) but only 24 points are used since the goal is to use a predictive model correlated with limited amount of operating points. The tests are done on an AVL dynamometer designed for performance and emission purposes. In-cylinder pressures during the cycle are required for combustion correlation from the test, i.e. pressure vs. crank angle for 720 degrees. The cylinder pressures are gathered at steady state condition

for each cylinder. The cylinder pressures from the test results are generally very noisy and they can have both crank angle and pressure values shifted a certain amount. Therefore some pre-processing work is required before direct use for the correlation of the model. In this study it is observed that pressures of cylinder 4 have high crank angle shifts (compared to other cylinder pressures) at some of the operating points therefore it was disregarded. The average of the other 3 cylinders are taken and used as the cylinder pressure data for correlation. 1D simulation codes such as GTpower can also calculate the in-cylinder pressures and also can calculate burn rate and heat release from measured cylinder pressures. Therefore some matching work should be performed before further proceeding directly with predictive model correlation. This is an iterative process since a burn rate is calculated first from the test data which is not exactly correct having noise and shift. Therefore a burn rate is calculated first then a pressure is calculated by the program which should match with the test data. If errors are observed, necessary shifts and/or smoothing are done and a new burn rate is calculated which gives a new cylinder pressure. This process continues until both cylinder pressures match.

Since the combustion is a complex phenomenon and could affect the cylinder pressures measured, it is highly important that the cylinder pressure at the compression phase matches exactly. There can be some errors during the combustion phase. Also the pressure sensors are sensitive to high temperatures, where thermal shock can occur on the sensor. Therefore the maximum cylinder pressure and pressures close to this region can be somewhat erroneous. Pressure is shifted to match the re-calculated and measured cylinder pressures, which should especially match at the compression stroke if there is no any other error is present.

Another important fact during matching work is to apply the correct amount of smoothing on the cylinder pressure data. Low amount of smoothing means high noise and this propagates highly to the calculated burn rates. The risk of high amount of smoothing is to lose the real characteristic of the cylinder pressure. Care should be taken at this step and it should be kept in mind that different operating points may require different level of smoothing. The cubic smoothing algorithm in GTpower is used in this study for smoothing purposes. This algorithm fits a cubic curve by using certain number of neighbor points at each point. The number of neighbor points used defines the level of smoothing. An

alternative to this method can be taking the Fast Fourier Transform (FFT) of the cylinder pressure data and clear the undesired frequencies and then perform the reverse transformation. However this method also does not decrease the risk of losing real characteristics as mentioned before. The smoothing process eliminates some of the noise present in the measured cylinder pressure.

Figure 3.1 shows the differences before and after processing. First picture shows the noisy measured pressure data and smoothed pressure. Second one shows the final match between shifted and smoothed measured data and the recalculated pressure, which is calculated using the burn rate results of measurement cylinder pressures. There should not be any significant difference between the final two pressures.

After the pressure matching process is complete, the burn rate calculated by using the measured in-cylinder pressures can be used for combustion model correlation. In this correlation study; burn rates will be used for combustion correlation. Measured and calculated burn rates will be compared and an error will be calculated for different correlation parameter sets. The details of this process will be explained in the following sections.

All cylinder pressures are given as normalized values, where the cylinder pressures are normalized by the maximum cylinder pressure hardware limit.

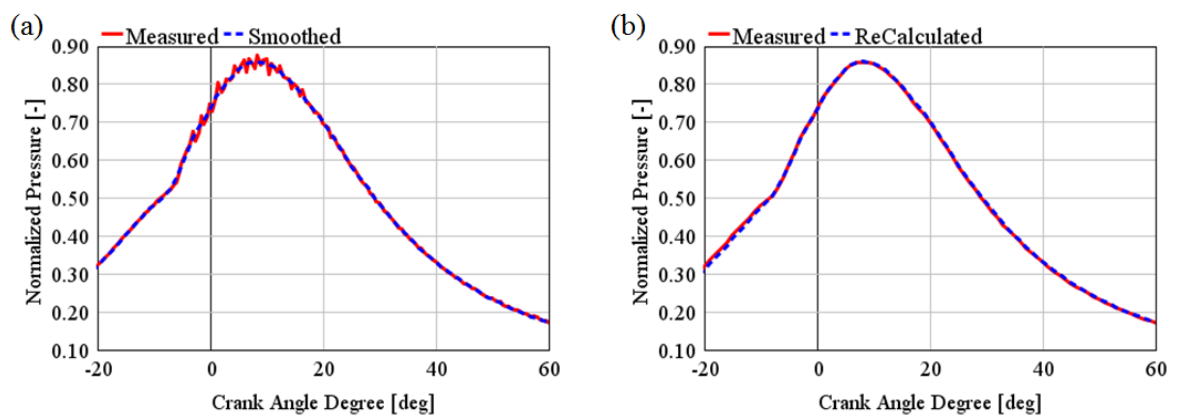


Figure 3.1. Pressures during processing (a) pressure with and without smoothing and (b) the comparison of measured vs. recalculated from burn rate.

Another critical test data are emissions data, which is the final goal of this study. The emissions are recorded as cycle averages. Especially  $\text{NO}_x$  and soot emissions are highly important on diesel engines.  $\text{NO}_x$  emissions are available in particles per million (ppm). Soot emissions are measured in an optical manner using a smoke meter in AVL test benches. A certain flow rate is sampled in a volume which passes through a filter and leaves smoke on the filter and the filter is blackened. A filter smoke number (FSN) is generated according to how much the filter is blackened. This is measured in an optical manner. FSN can be converted to soot density i.e.  $\text{mg}/\text{m}^3$ . GTpower can also give output of soot in terms of soot density in same units. Since the burn rates will be correlated and the fuel amount is an input, it is expected to have close  $\text{CO}_2$  emission results and therefore no work is carried out for that.

Other than engine dynamometer measurements for the correlation, the combustion model requires precise injection profiles since it models the injection event as explained in more detail in literature survey section. Simple trapezoidal shaped or square shaped injection profiles result in unrealistic burn rates from the model. Also this can be an issue during burn rate calculation from the measured cylinder pressure. Therefore injectors are tested to obtain the injection profiles at different rail pressures and different injection quantities. The test is done in a standard injection test bench with a 50 bar back pressure, i.e. the injection is done to a cylinder with a 50 bar pressure. The test is not done on a real engine, which will be much harder to conduct. The obtained profiles are put in a map in GTpower, where the injection profiles are selected by looking at the rail pressure and injection quantity given (i.e. rail pressure and injection quantity are X and Y and injection profile is the Z in this map). GTpower can interpolate for points in-between. Since there can be multiple injections during one cycle in a diesel engine, it is highly important to have the correct values injected fuel quantity at each injection event. Figure 3.2 shows injection profiles at 1800 bar for different injection quantities. Fuel mass is normalized by the highest fuel flow rate at that rail pressure.

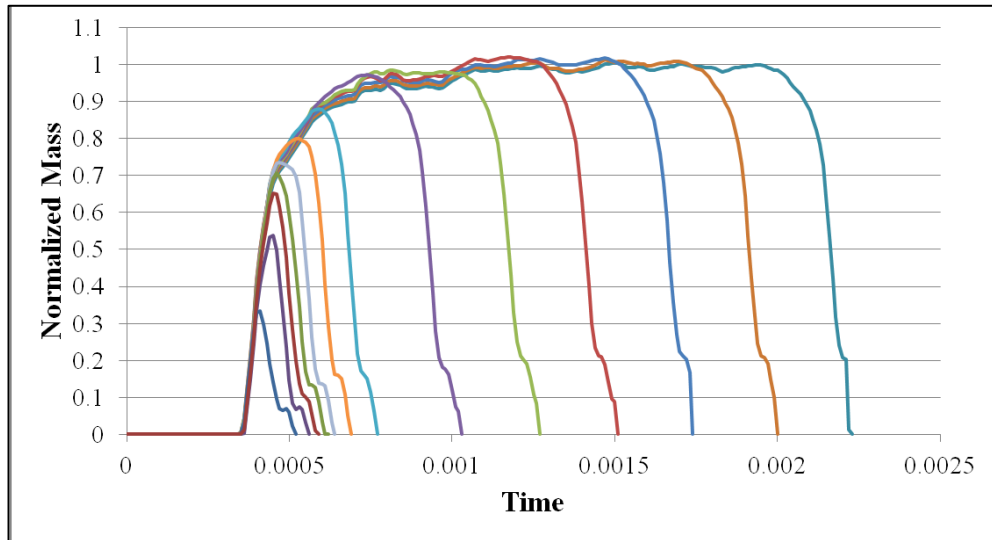


Figure 3.2. Injection profiles at 1800 bar rail pressure at different quantities.

Operating points used for correlation are shown in Table 3.2. The points are chosen to cover whole speed and torque range from low to high speeds and loads (part load and full load). 3 points at each 500 rpm are chosen from 1000 to 4500 rpm.

Table 3.2. Operating points chosen for correlation (Speed and Load).

Case No	Speed [rpm]	Load [%]
1	800	0
2	1000	3.5
3	1000	54.3
4	1000	100
5	1500	2.6
6	1500	40.7
7	1500	100
8	2000	2
9	2000	48.3
10	2000	100
11	2500	2.2
12	2500	65.7
13	2500	100
14	3000	2.6
15	3000	79.8
16	3500	14.2
17	3500	85.1
18	3500	100
19	4000	3.6
20	4000	82.7
21	4000	100
22	4500	5
23	4500	33
24	4500	100

### 3.3. Combustion Correlation

Mainly affecting combustion parameters were selected in the previous studies as shown in detail in appendix A and design of experiment (DOE) study is performed to find the optimum values of these parameters at each operation point separately for combustion correlation. The mainly affecting parameters used for the combustion correlation work are listed as follows:

- Entrainment multiplier before combustion (CBAIR): This multiplier affects the air entrained with fuel before combustion start (i.e. during ignition delay period)
- Entrainment multiplier after combustion start (CAAIR): This multiplier affects the air entrainment during the combustion phase
- Ignition delay multiplier (CIGN1): This multiplier modifies the ignition delay time.

Other parameters such as combustion rate multiplier, break-up time, entrainment multiplier after wall impingement and ignition delay multiplier for dilution effect are found to be less effective compared to the parameters listed above.

For the design of experiments (DOE) study; latin hypercube sampling method is used for DOE setup. As a first step in this method; number of experiments are chosen and the minimum and maximum values of the parameters are chosen. In this method; the points are chosen randomly but without using the value of a parameter if it is included in a previous case. For example; if one of the parameters is 0.15 in one of the experiments, this value will not be used in the next experiments. It is a two stage method. First, samples for each parameter are chosen strategically so that it represents the variable's probability density function. Then the samples for the parameters are ordered to match target correlations between variables as explained in [19]. The purpose of using latin hypercube is to decrease the number of experiments conducted for optimization but not losing too much resolution. In the case of a full factorial DOE; there will be a certain loss of resolution if the number of experiments is desired to be decreased since the parameters are evenly distributed between minimum and maximum. Therefore the increment of the parameter will change if the number of experiments is changed. However full factorial DOE is simple and it is



easier to use without any high knowledge on optimization. A more detailed description about DOE methods can be found in appendix C.

Burn rates are compared for combustion correlation. Cylinder pressures were processed as explained in the previous sections and burn rates are obtained from measurement results. These burn rates are compared with the burn rates calculated by the predictive model. To see the relation between burn rate and pressure recall Equation 2.27 and Equation 2.28 in literature survey section and Equation 2.46 and Equation 2.47 to see how the model calculates the burn rate. Equation 2.27 and Equation 2.28 are for overall cylinder pressure and burn rate but Equation 2.46 and Equation 2.47 are used for injected fuel parcels of the fuel jet, which is then summed to find the total burn rate. The burn rates shown in the equations are normalized by the total fuel injected per cycle; therefore the burn rates used in error calculation are normalized. It also means that the integral of the burn rate will equal to one since it is normalized by fuel mass.

The match of two burn rates are done in the following way: A root mean square (RMS) error in % is calculated from two burn rates by using Equation 3.1. Both burn rates in the equation are normalized as explained previously.

$$BurnRate\ RMS\% = 100 \cdot \sqrt{\frac{\int_{t_0}^{t_f} (BurnRate_{predicted} - BurnRate_{measured})^2 dt}{t_f - t_0}} \quad (3.1)$$

In this equation;  $t_f$  and  $t_0$  are final and start time for burn rate calculation, respectively. For each case this error is calculated, i.e. for different values of CAAIR, CBAIR and CIGN1. Then the optimum point with the lowest error is found. This is done by performing a regression analysis of the DOE data obtained. There are three independent parameters (CAAIR, CBAIR and CIGN1) and one dependent parameter (Burn Rate RMS Error). The purpose is to have an error equal to zero or close to zero. From that regression analysis; lowest error points are found and corresponding parameters are found. Figure 3.3 shows the optimum error values obtained at each case.

As can be seen from the Figure 3.3; cases 1, 2, 5, 8, 11 and 19 have errors higher than 1%. These cases correspond to low load (almost zero torque, load<5%) operation

conditions, where only a small amount of fuel is injected to overcome friction. This shows that the model can be erroneous at small injection quantities. Cases with errors lower than 1% have acceptable cylinder pressure match with measurement data. Figure 3.4 shows the comparison between cylinder pressures. The case numbers can be seen at top of each plot, where the engine speed is also written in parenthesis. For the cases having same engine speed value, higher case number means higher load. Deviation is high at the cases with an error higher than 1% as explained above. Cylinder pressures are given as normalized value, where all of the pressures are normalized by the maximum cylinder pressure hardware limit as mentioned before.

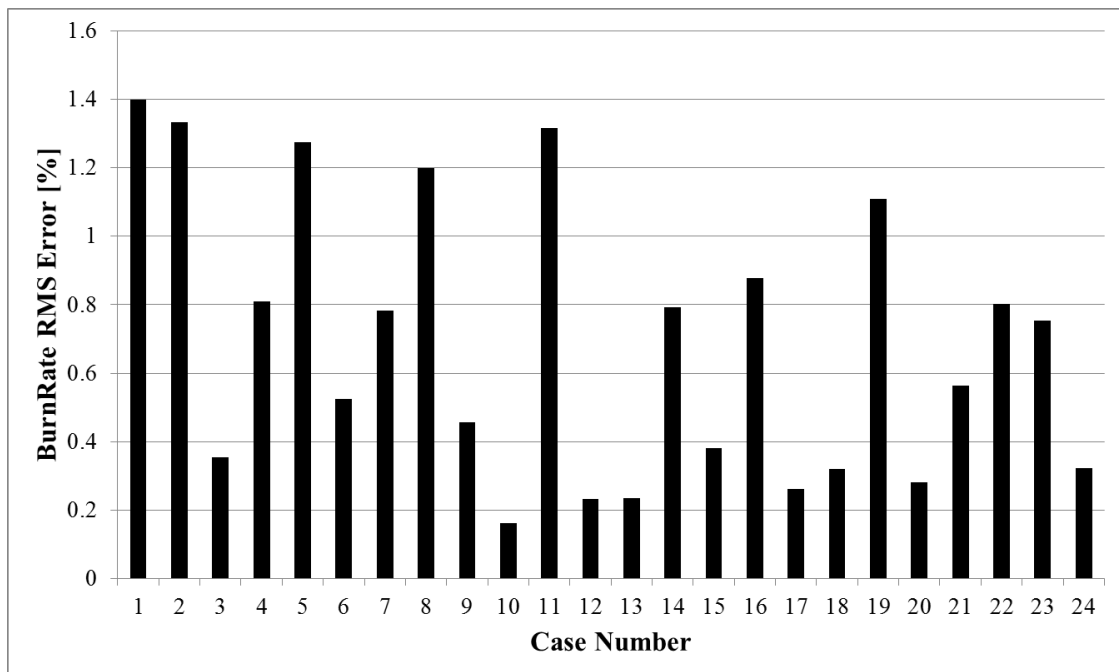


Figure 3.3. RMS errors at each case with optimum correlation parameters.

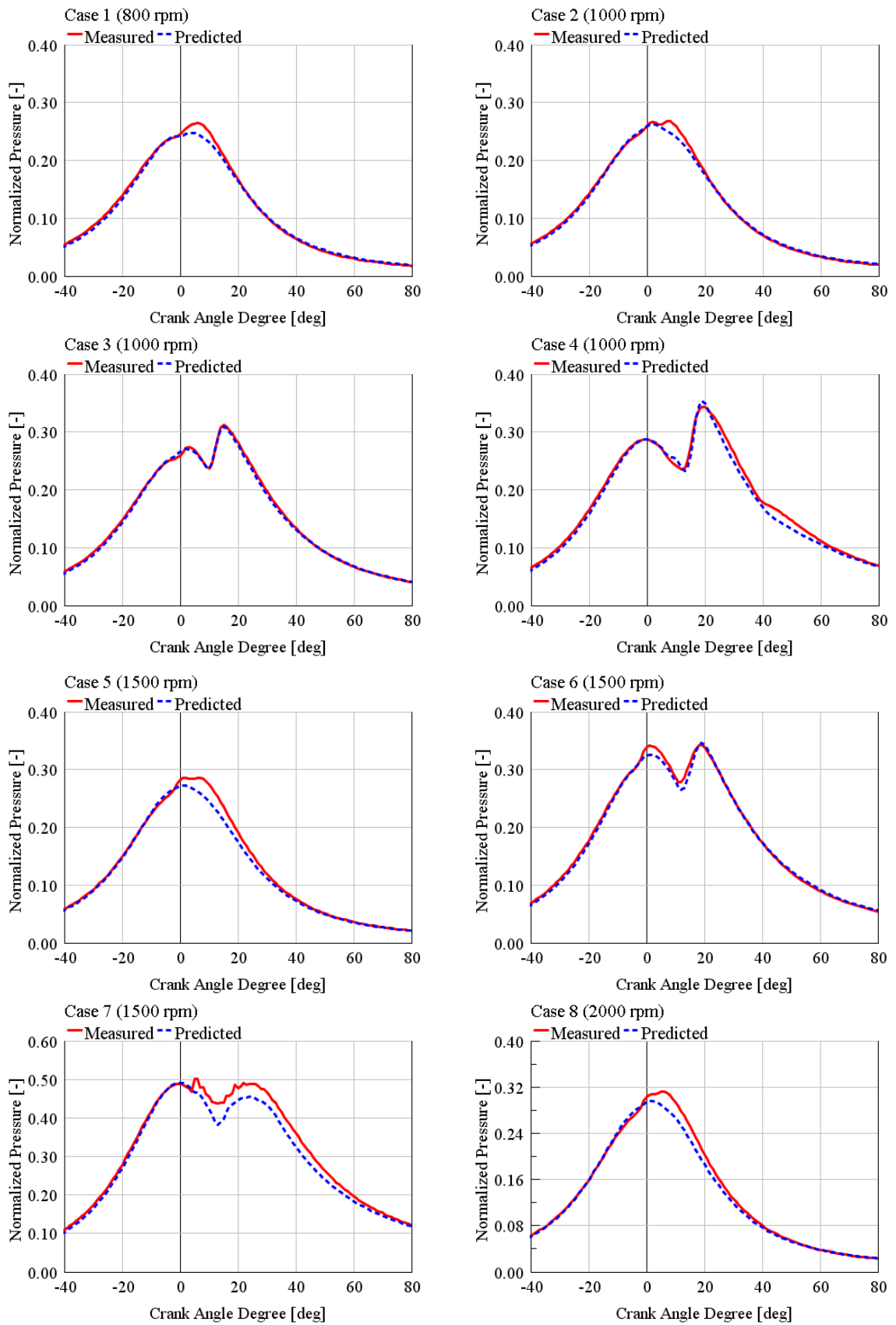


Figure 3.4. Cylinder pressure comparison for all cases (straight line – measured, dotted line – predicted).

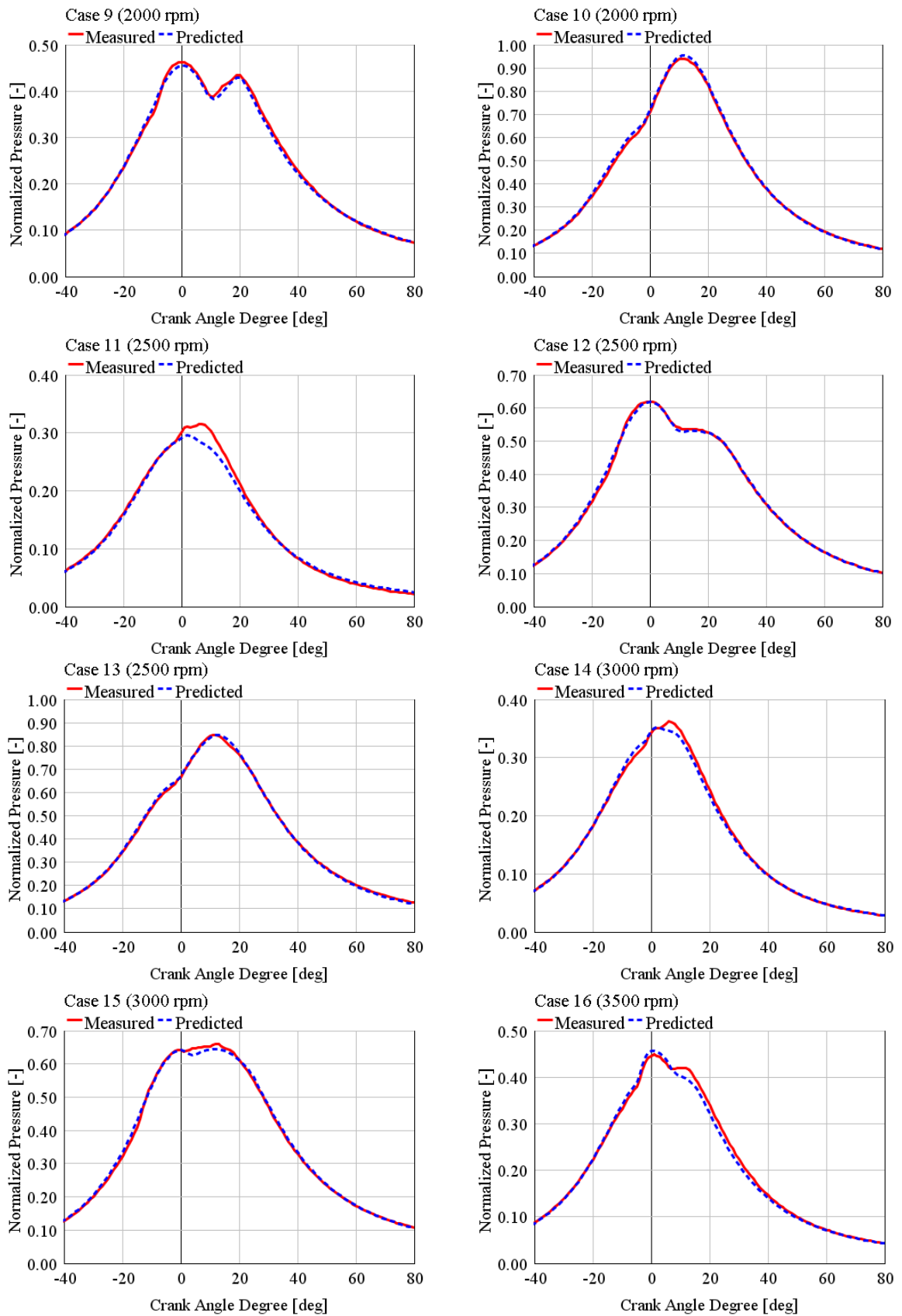


Figure 3.4. Cylinder pressure comparison for all cases (straight line – measured, dotted line – predicted) (cont.).

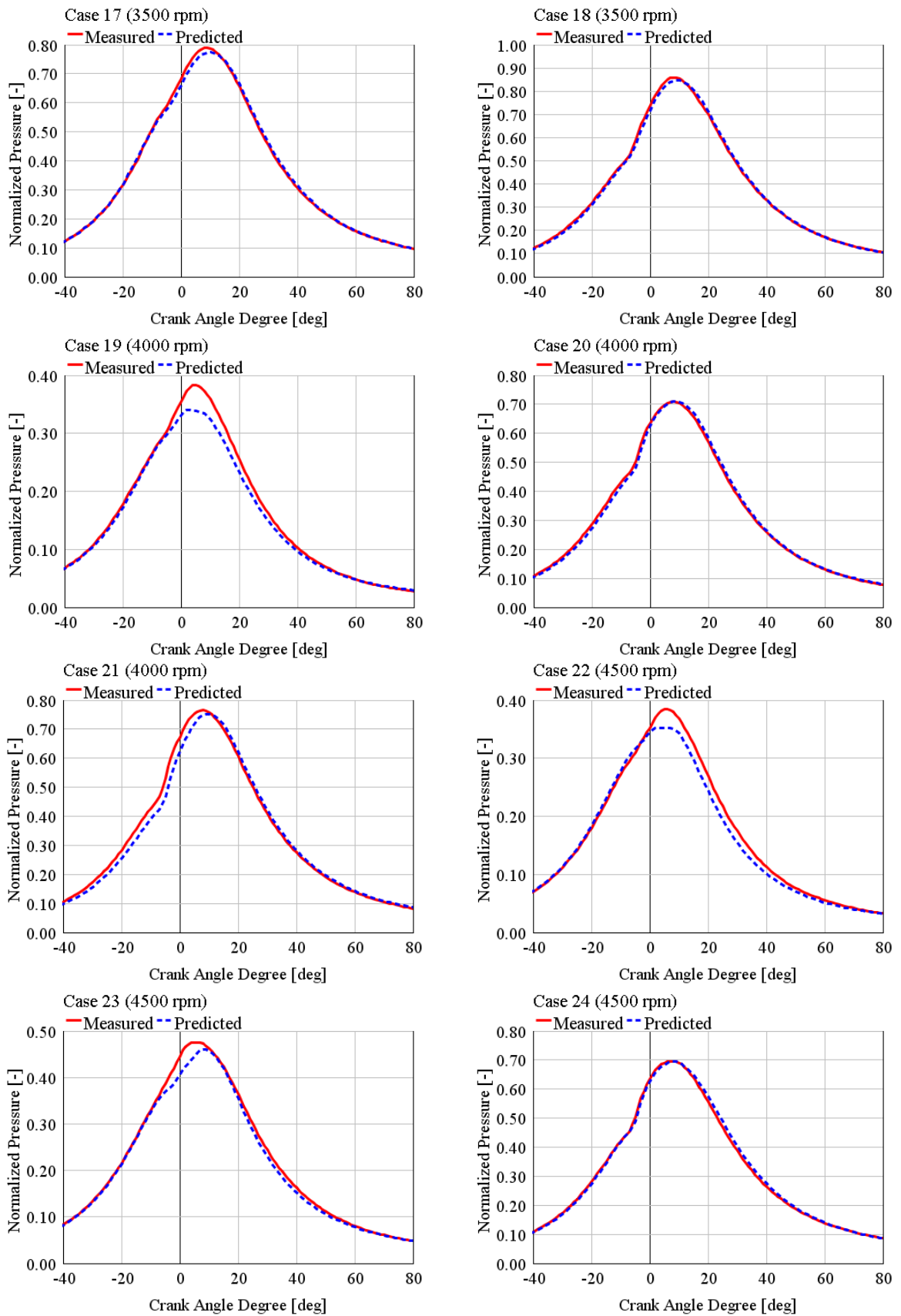


Figure 3.4. Cylinder pressure comparison for all cases (straight line – measured, dotted line – predicted) (cont.).

The error gets higher if the same parameter set is to be used in the whole operating region of the engine. Another optimization work is done by considering the DOE results for all of the cases and another regression analysis has been performed. Figure 3.5 gives the errors by using this single parameter set for all of the operating conditions. As can be seen from the figure, half of the cases have an error around 1% or higher. The cylinder pressure comparison plots are not plotted for this case since they are not better than the comparisons shown in Figure 3.4.

These results show that the model is generally good for higher fuel injection quantities i.e. closer to full load conditions of the engine.

As a next step; emission models for soot and  $\text{NO}_x$  are correlated as explained in the next section. Same 24 points are used for the emission model correlation and no operation point added.

As the final step, start of injection (SOI) and exhaust gas recirculation (EGR) sensitivity studies are performed to see if how close the combustion and emissions are predicted for changing EGR and SOI conditions at the same speed and load.

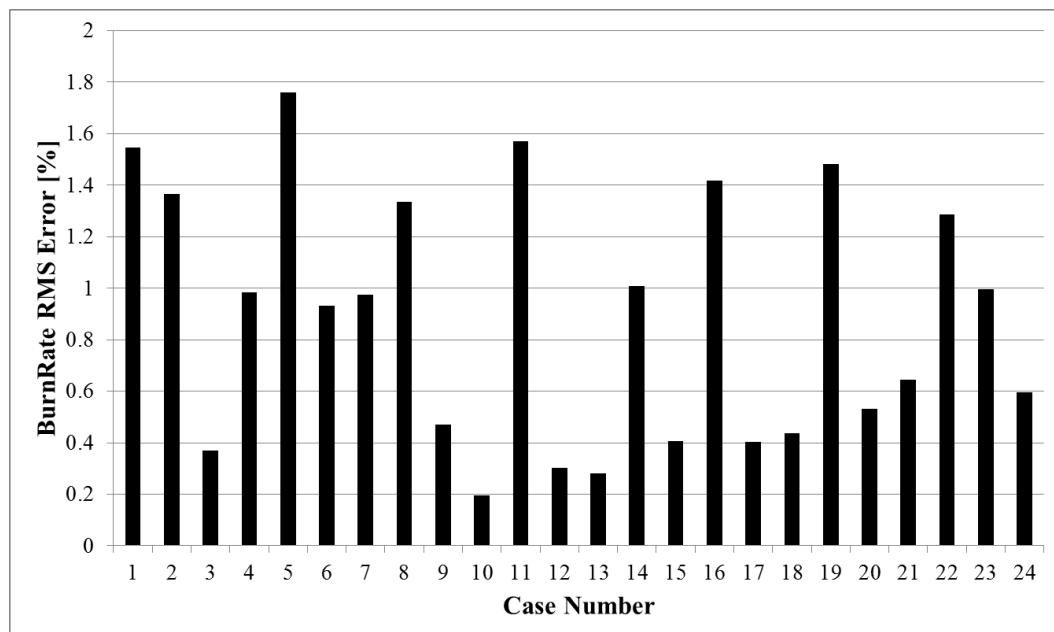


Figure 3.5. RMS errors by using a single optimized parameter set.

### 3.4. Emission Correlation

After the combustion model has been correlated meaning that pressure and temperature should match close to the real case, the emission parameters should be correlated with the test data. Again 24 cases selected will be used here and correlation will be made according to these points. Here the points with high RMS errors are also eliminated since this already will bring a certain error already not related to emission parameters. Therefore 6 cases are eliminated with an RMS error higher than 1%, where these points correspond to low load points being slightly higher than 0 load.

Two parameters are used for each emission (i.e. for  $\text{NO}_x$  and soot). For  $\text{NO}_x$ ; an overall multiplier parameter is used for multiplication of overall  $\text{NO}_x$  emission and activation temperature multiplier is used for changing the activation temperature at which  $\text{NO}_x$  emission reaction calculations are made (see extended Zeldovich mechanism in literature survey part). Temperature multiplier has a nonlinear behavior with  $\text{NO}_x$  emission since activation temperature is the power of Euler number in the equation.

For soot emissions; two parameters are multipliers for formation and oxidation. It has been observed that with the values of each multiplier being equal to one, the soot emissions are highly overpredicted compared to test results. Therefore it is already expected that oxidation parameter will be about ten times the formation parameter.

Full factorial DOE is setup for both emissions and corresponding parameters. It is observed that there is a curve obtained at each operation point, where the emission error is zero. Errors are calculated and curves for zero error are obtained for each case and both emissions ( $\text{NO}_x$  and soot). Figure 3.6 shows the zero error curves for  $\text{NO}_x$  emission for different cases.

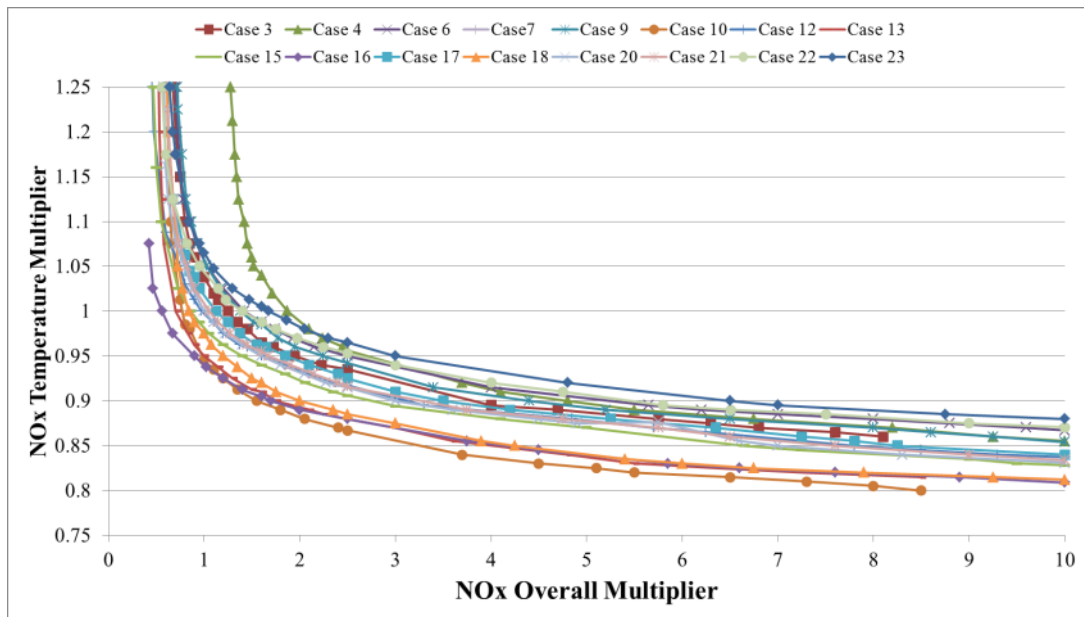


Figure 3.6. NO<sub>x</sub> emission zero error curves for different cases.

As it can be seen from Figure 3.6, the curves are close to each other after overall multiplier is equal to 2. The curves continue parallel to each other after that point. Below that value, most of the curves are very close but there are two curves as exceptions. Another fact is the nonlinear behavior of the temperature multiplier; therefore it is not desired to have a temperature multiplier far different from one, which is the default value. According to the facts explained, overall multiplier is selected as 2 where all curves are close and average temperature multiplier is calculated.

A similar approach is used for soot emission correlation. Again a zero error curve is obtained for different formation and oxidation multipliers. It is seen that the oxidation multiplier should have a value about 5-10 times the formation multiplier for most of the operating points with some exceptions. It is also observed that the zero error curves approach to each other for small values of both multipliers in the order of  $10^{-3}$ . Figure 3.7 shows the zero error curves for different cases.



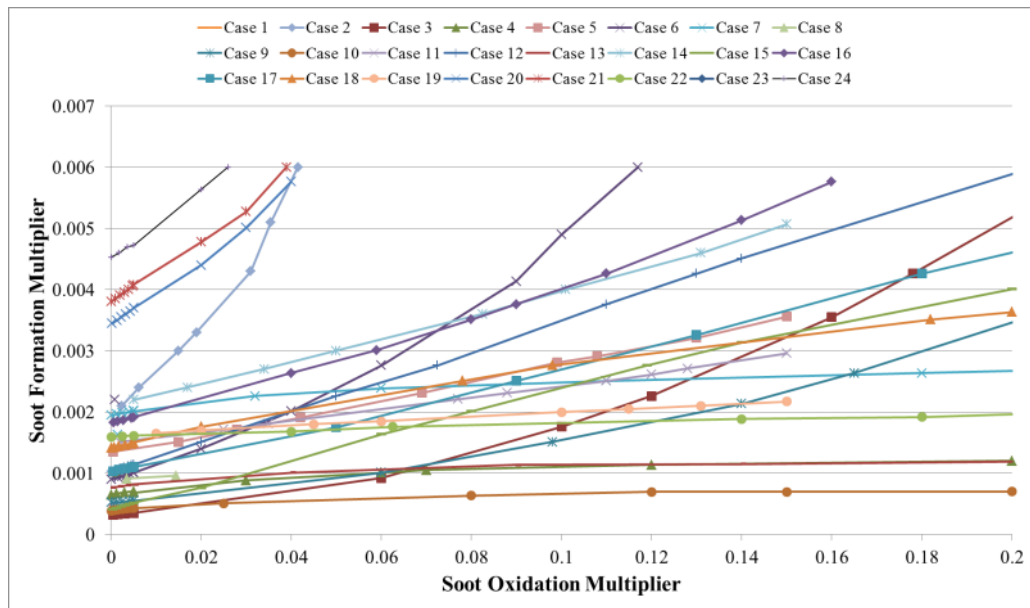


Figure 3.7. Soot emission zero error curves for different cases.

By looking at these curves, the oxidation multiplier is set as 0.005 where the curves are very close to each other and the improvement is not much as the multiplier is further decreased. Then an average formation multiplier is calculated. This is very similar what was done for  $\text{NO}_x$  emission correlation. However the correlation was not as good as expected therefore 3 cases are presented on the results section as follows

- (i) Single constant formation multiplier
- (ii) Four formation multipliers according to load and speed
- (iii) Formation multiplier function of load and speed

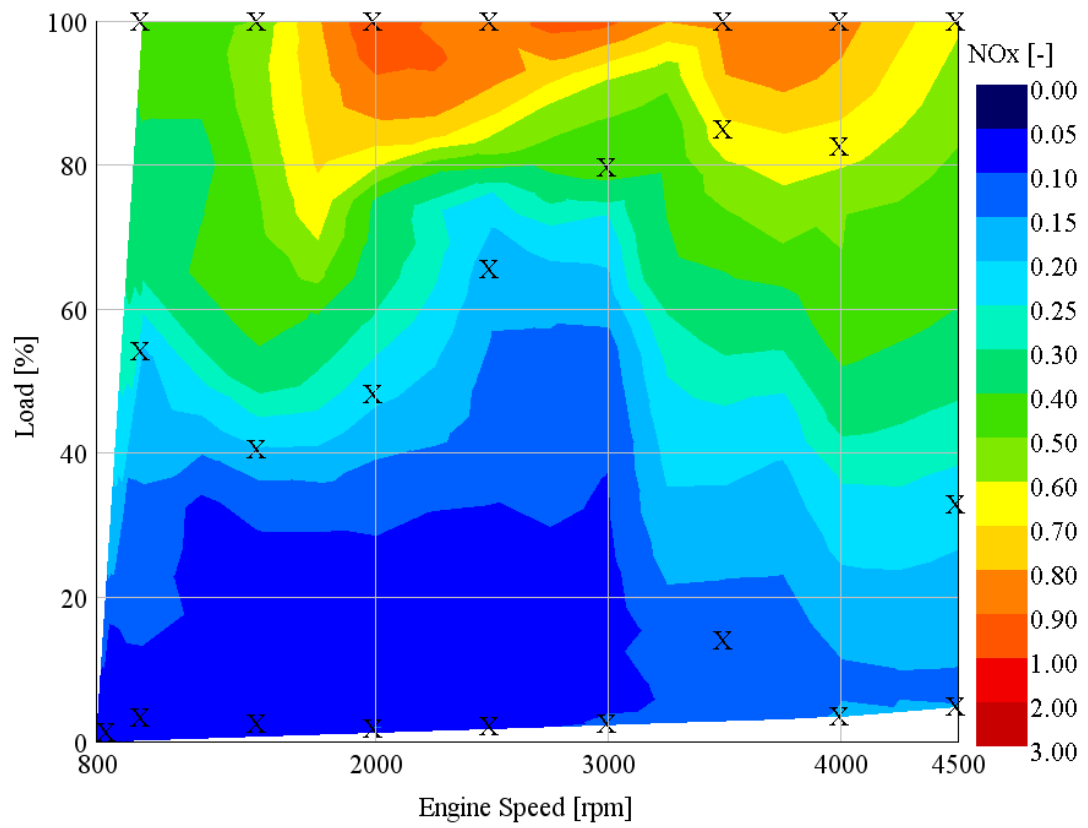
For the first case, a constant multiplier is calculated as explained. For the second case; the operating range is divided into four as load being below or above 50% and speed being above or below 3500 rpm. For each region a constant formation multiplier is calculated. In the third and the last case; formation multiplier is entered as a function, where multipliers calculated for 24 points were used and interpolated for other points. In all these cases, only 24 points are used as was used for combustion. No additional point is taken into account.

### 3.5. Results

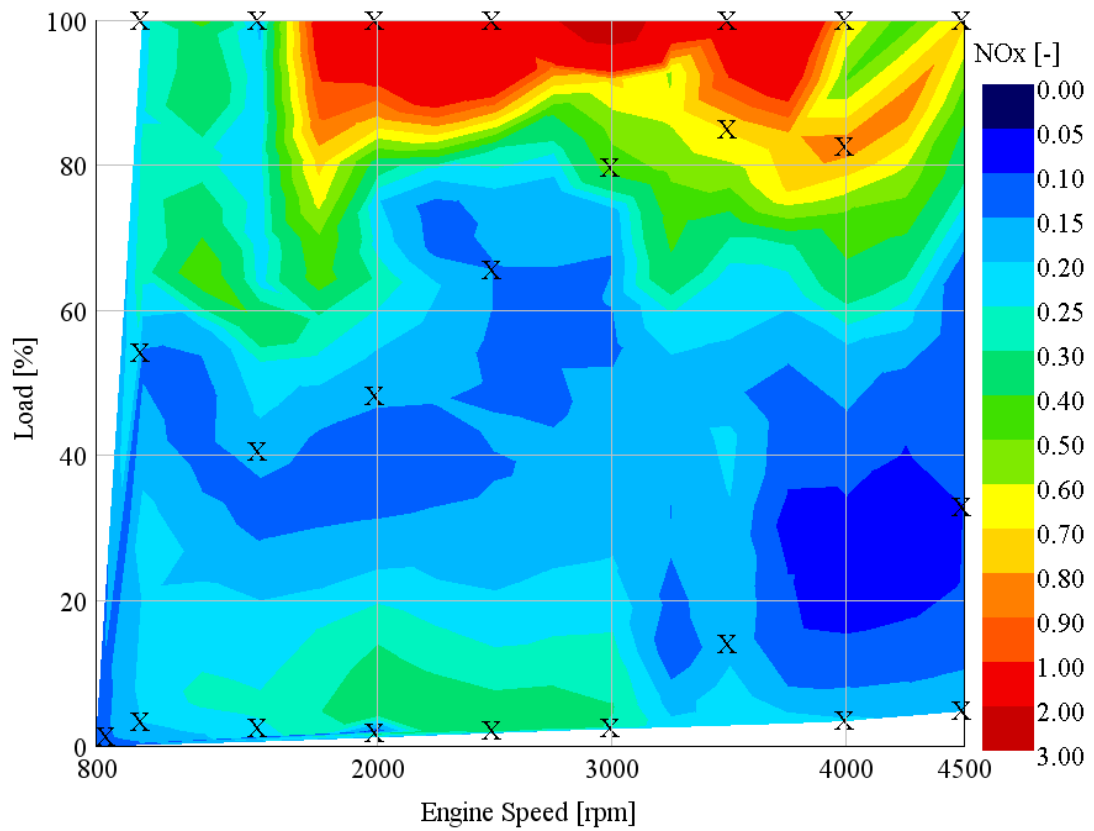
After all correlation work is done both for emissions and combustion, the model has run at a total number of 237 engine operating points, where test data for emissions are available. This is done to assess the performance of the correlation work done so far.

Figure 3.8a and 3.8b show the NO<sub>x</sub> emission contour plot as a function of load and engine speed for the test and model, respectively. Both plots have the same contour levels so same color means same amount of NO<sub>x</sub>. Comparing both plots; it can be said that the NO<sub>x</sub> model is directionally very good with some exceptions and there is a certain amount of overprediction at low speed and load region, which can also be related to the combustion model since it was not very good at low loads (Burn rate RMS error is high at low loads). This may result in different maximum cylinder temperature, which in turn directly affects the NO<sub>x</sub> amount produced. NO<sub>x</sub> emissions are normalized by maximum NO<sub>x</sub> amount observed in the test results and results are given as fractions. Points shown with X are the correlation points shown on the map.

The region between 1000 and 3000 rpm and below 25% load is overpredicted, but in terms of difference it is small since the NO<sub>x</sub> emissions are small at this area. Also there is an overprediction in the high NO<sub>x</sub> emission area, which is around 3000 rpm full load point. Figure 3.9 shows the error between test and the model. Error is given as the difference between model and test, i.e. model-test. Therefore positive values mean model is overpredicting and negative values mean underprediction. In general, the most of the engine operation is within +/- 0.25 range.



(a)



(b)

Figure 3.8. NO<sub>x</sub> emission map for (a) test and (b) model.

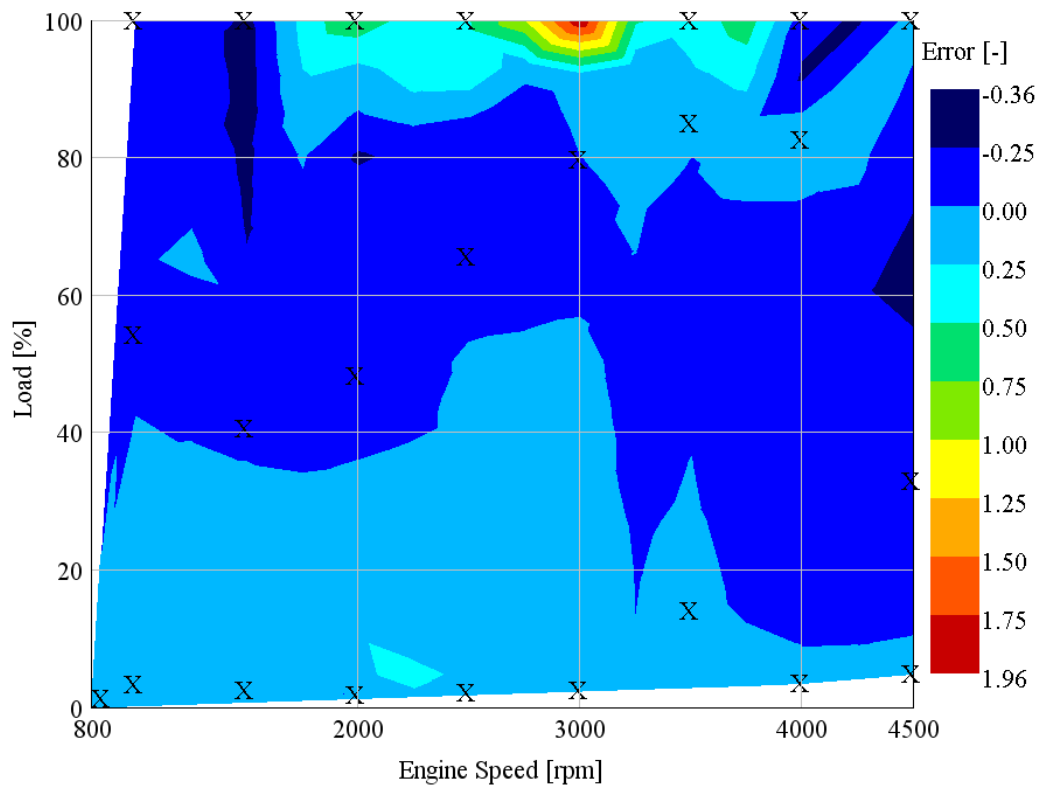
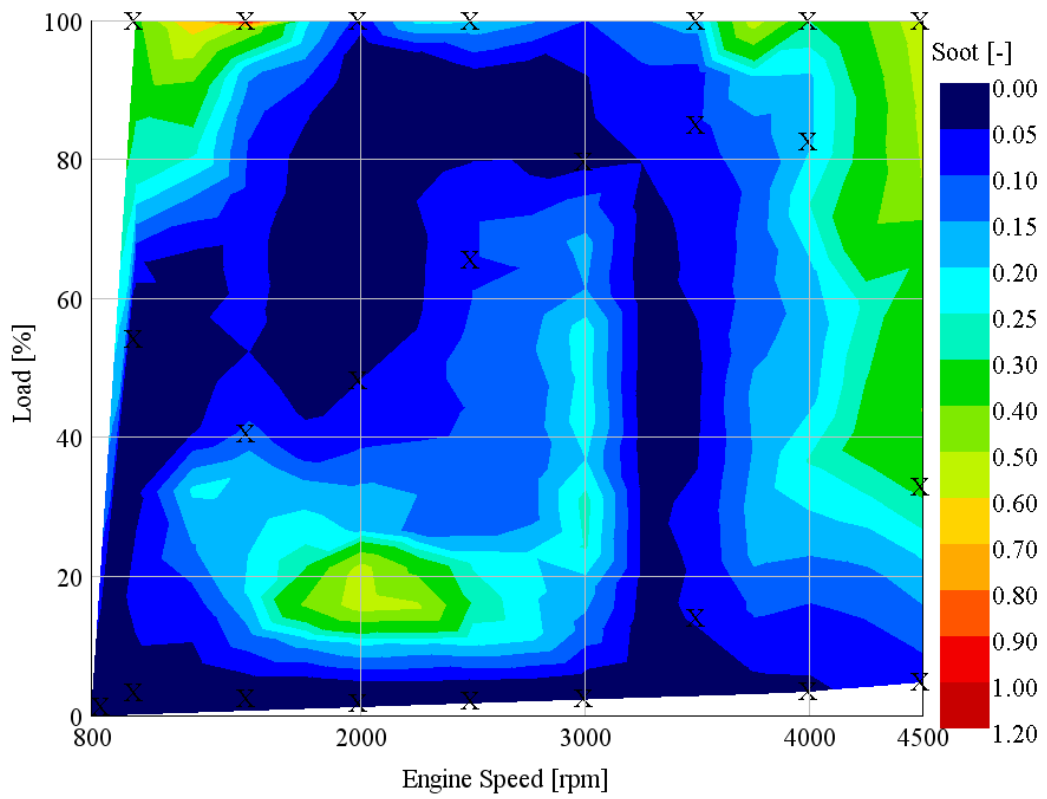


Figure 3.9. NO<sub>x</sub> error of the model compared to the test data.

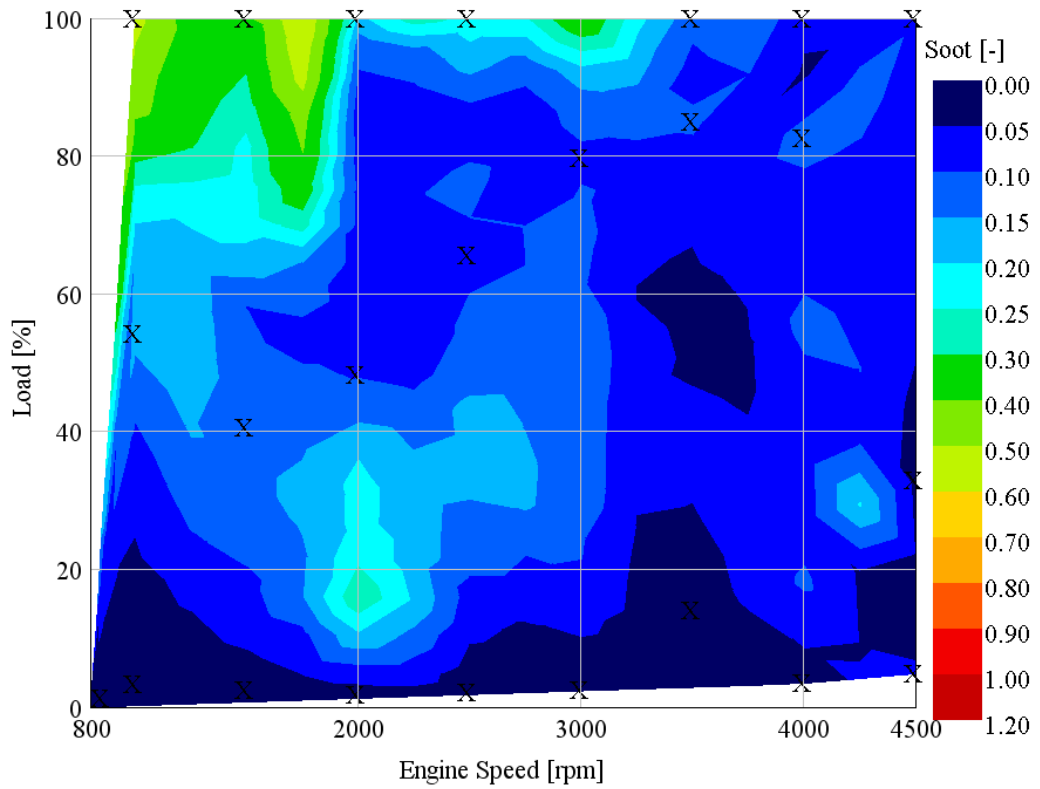
Highest error is about 1.96 and lowest error is -0.36. Since an average multiplier is used in all points, modifying the multipliers for improvement did not work. This can improve one of the regions of high and low error, where the other one will be worse than the current situation. Including additional correlation points at these regions will not change the average multipliers calculated since the two will affect the average in opposite directions, therefore canceling each other's effect.

As explained in the previous section, 3 model results will be presented for soot model results. Figures 3.10a, 3.10b, 3.10c and 3.10d show the test, single formation multiplier model, four formation multipliers model and interpolated formation multiplier model results, respectively. Again X-points show the 24 points used for correlation.

As the single multiplier model results are compared to the test results, the first area obviously not matching is the high engine speed area above 3500 rpm. Almost no change occurs at the model results but there is a soot increase towards higher engine speed in the test results. This area improves slightly when four set of formation multipliers are used and it is better when multiplier is a function of load and speed.

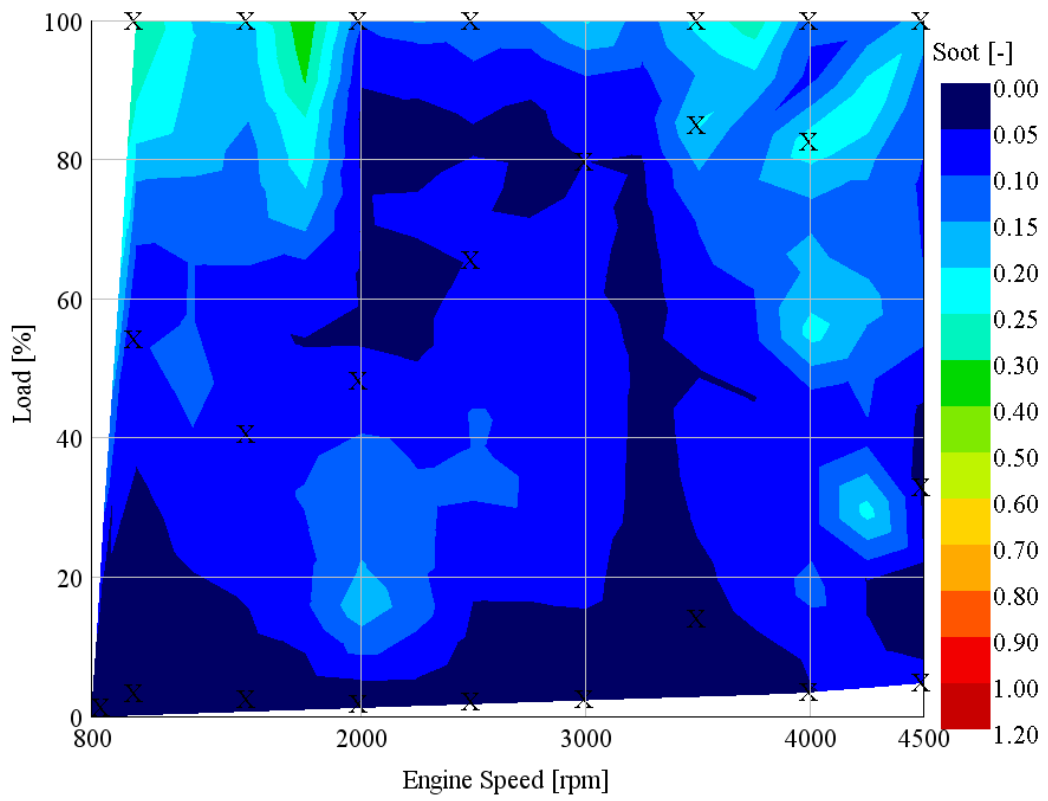


(a)

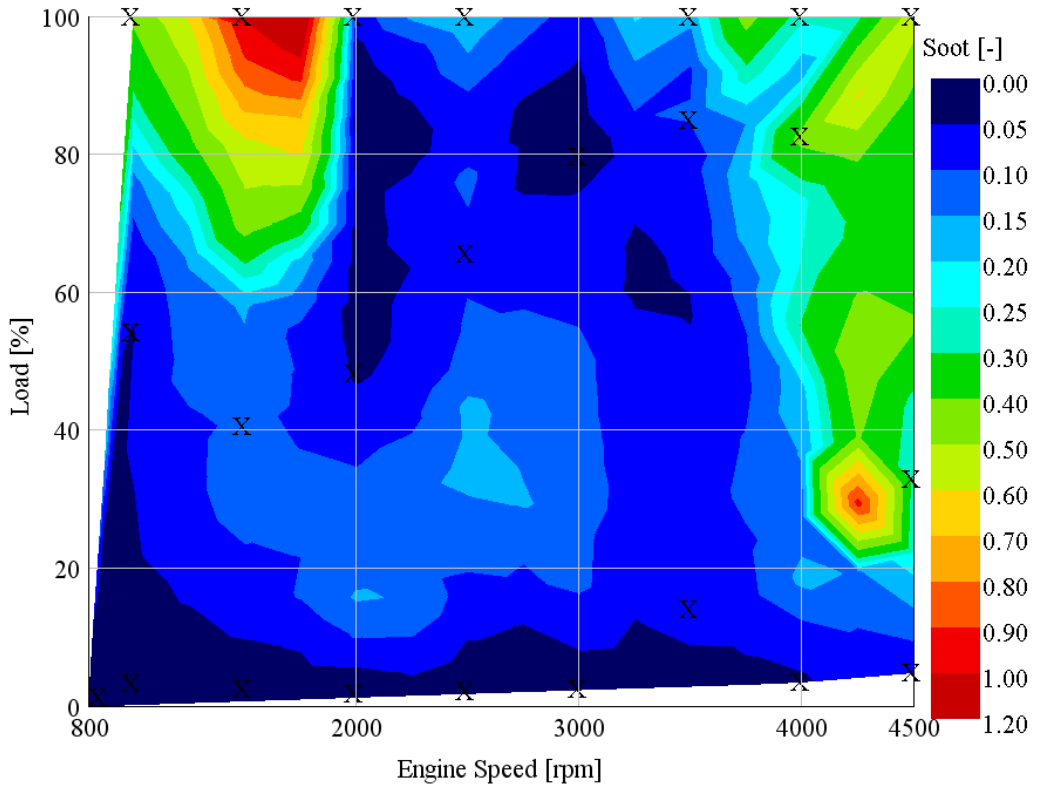


(b)

Figure 3.10. Soot emission map for (a) test, (b) single multiplier model, (c) four multipliers model and (d) interpolated multiplier model.



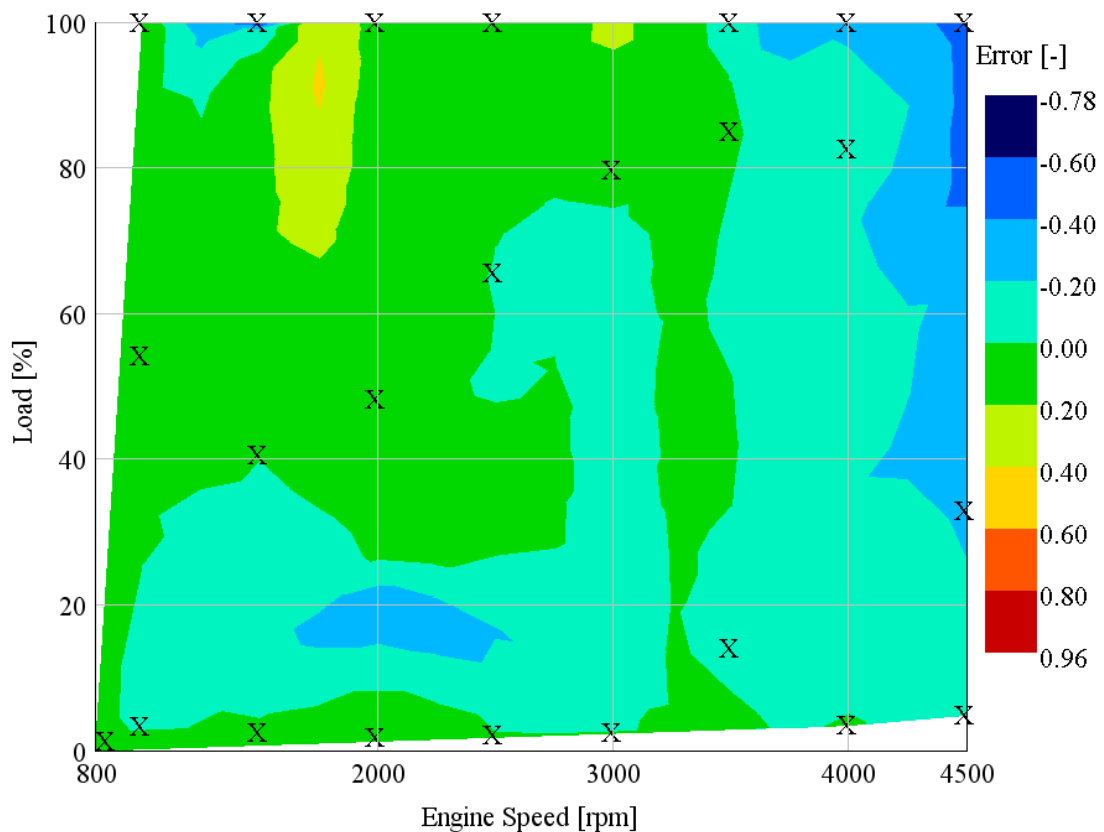
(c)



(d)

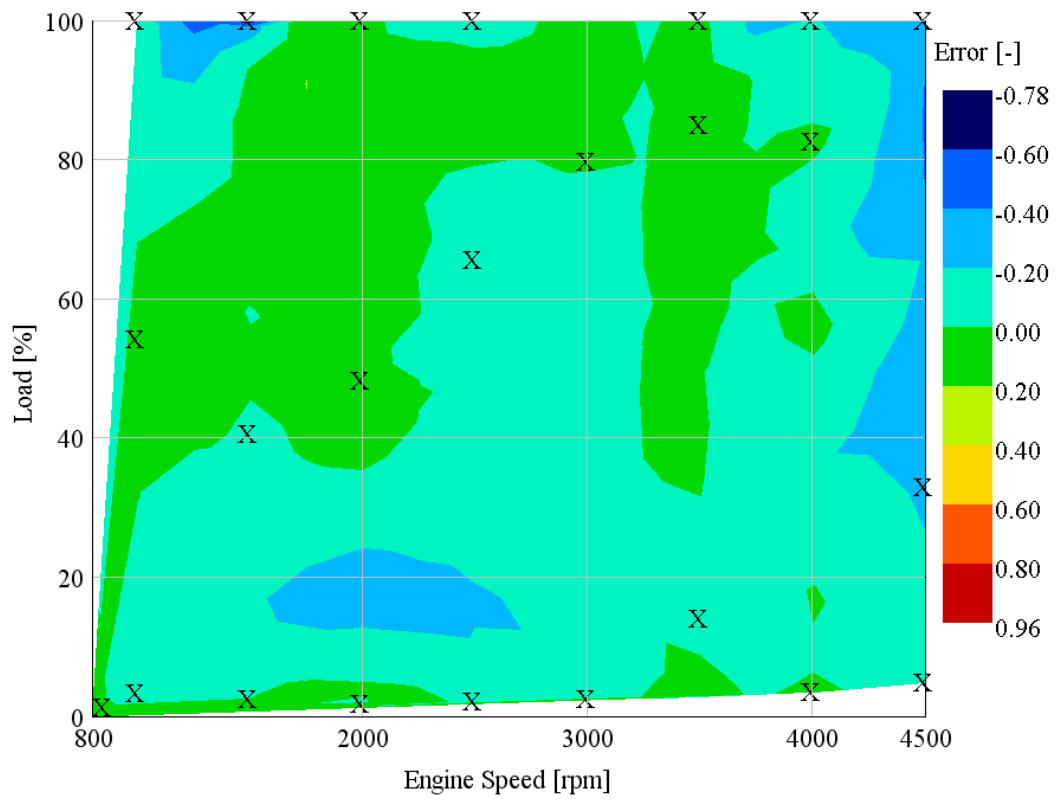
Figure 3.10. Soot emission map for (a) test, (b) single multiplier model, (c) four multipliers model and (d) interpolated multiplier model (cont.).

Figure 3.11a, 3.11b and 3.11c show the difference errors for single formation multiplier, four different formation multipliers and interpolated formation multiplier cases, respectively. Similar to  $\text{NO}_x$  case; the difference between model and test are given. Despite high engine speed area being predicted better with the last model, there are some areas slightly worse compared to the previous cases. High soot emission area around 1750 rpm 80% load is overpredicted, which was already problematic. Four formation multiplier case shows improvement in the overprediction area at 1750 rpm 80% load. High engine speed area improves as the formation multiplier is different in that region. Interpolated multiplier model gives the best results overall as already stated before. Low load points (load < 25%) are underpredicted, where  $\text{NO}_x$  was overpredicted, which again can be related to the combustion model being worse at low load points.

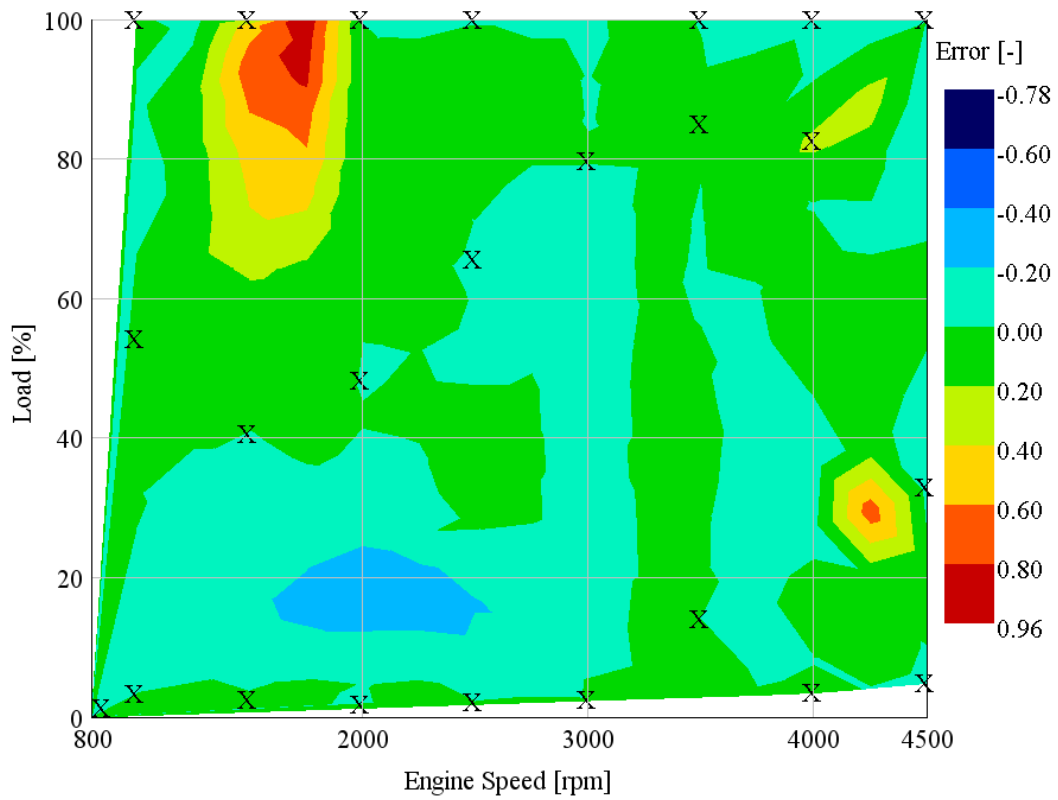


(a)

Figure 3.11. Soot error map for (a) single multiplier model, (b) four multipliers model and (c) interpolated multiplier model.



(b)

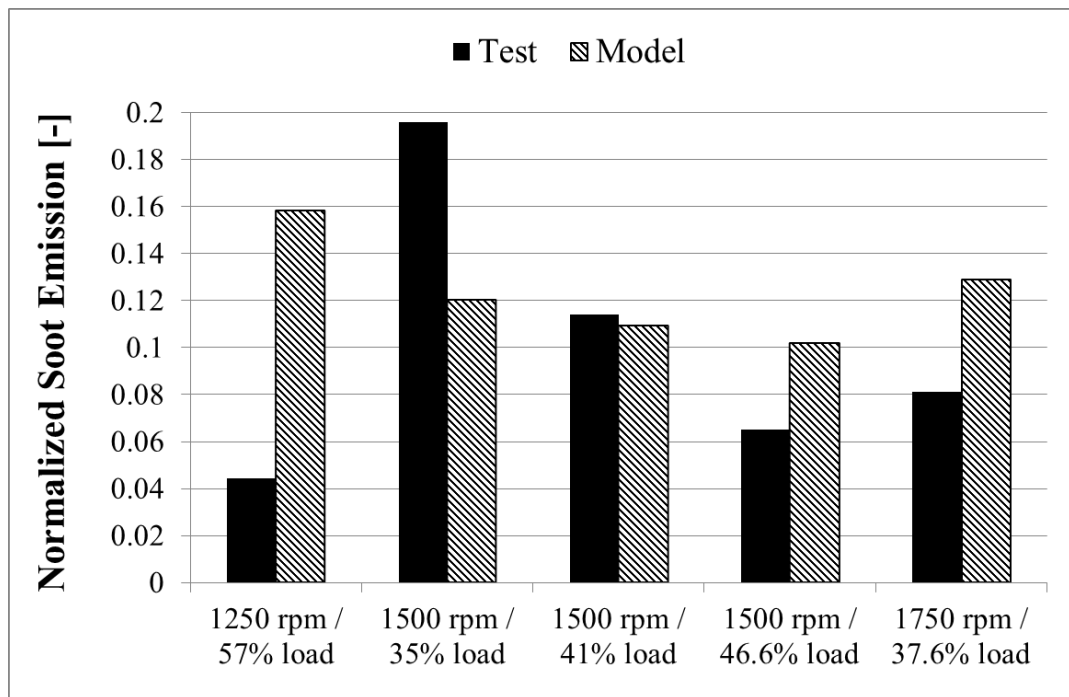


(c)

Figure 3.11. Soot error map for (a) single multiplier model, (b) four multipliers model and (c) interpolated multiplier model (cont.).



For the soot model; it is also observed that the correlation is not good enough for a constant parameter. A short sensitivity study was done by selecting a correlated point and comparing the soot emissions of this point and closest four points by using same soot model multipliers at the correlated point. The study is done at 1500 rpm 41% load and 4000 rpm at 83% load. Closest points are selected so that there are comparable test data available therefore two points at same speed slightly high and low load are selected. Other two points are selected from 250 rpm higher and lower engine speeds with same torque. The loads of these points are different slightly since load is determined by torque at that point divided by highest torque available at that speed. Figure 3.12a and 3.12b show the results for 1500 rpm and 4000 rpm, respectively. As can be seen, the model results differ highly at other operation points, which are very close to the correlation point. Another fact is that the test result change very rapidly but model results do not change too much.



(a)

Figure 3.12. Soot emissions for (a) around 1500 rpm 41% load and (b) around 4000 rpm 83% load.

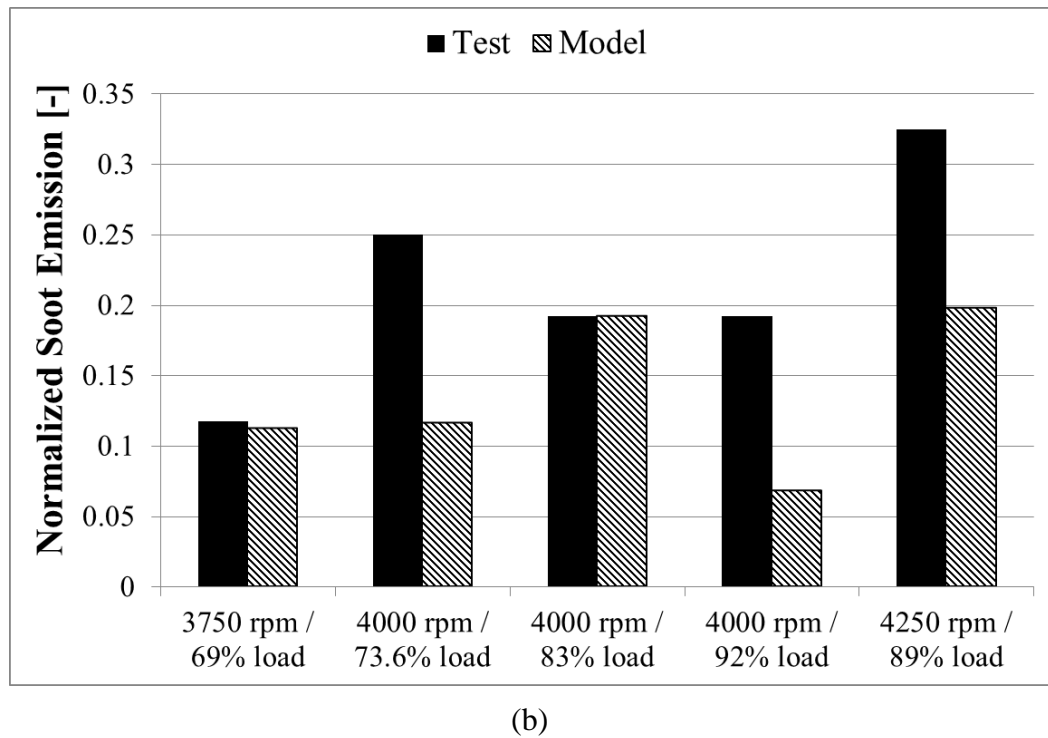


Figure 3.12. Soot emissions for (a) around 1500 rpm 41% load and (b) around 4000 rpm 83% load (cont.).

Another fact for the soot is the FSN to soot concentration ( $\text{mg}/\text{m}^3$ ) conversion. Measurements are taken in FSN and it is converted to  $\text{mg}/\text{m}^3$ . As it is explained in [23] in more detail, there is a correlation of FSN and opacity, where the soot is measured by using a reflectometer. The correlations are made by using different engines and in different test labs but it is also explained that there is a chance that this relation might not apply in all cases. This also creates an additional uncertainty on the measured test data. The formula for FSN to  $\text{mg}/\text{m}^3$  conversion is given in [23] by Equation 3.2.

$$"C" \left( \frac{\text{mg}}{\text{m}^3} \right) = \frac{1}{0.405} \cdot 4.95 \cdot \text{FSN} \cdot e^{0.38 \cdot \text{FSN}} \quad (3.2)$$

One of the differences between test and model are the fact that the measurement is done slightly from a different location where pressure and temperature will be different (after the turbine). Model gives emissions as whatever comes out of the cylinder. However  $\text{NO}_x$  compared is in particles per million and soot is given in density where both do not change with pressure and temperature. Normalized values are presented. Soot density does not change since soot particles are solid particles.

### 3.6. SOI and EGR Sensitivity

After the model is being correlated, the sensitivity of the correlated model is checked for start of injection (SOI) and different EGR percentages at the same engine speed and load point. A part load operating point at 2000 rpm is chosen for the sensitivity (2000 rpm 50% load). SOI is important in terms of fuel economy so it is important to correctly predict SOI effect on combustion. EGR is very important in terms of the emissions considered i.e.  $\text{NO}_x$  and soot.

In this study; the start of injection values represent the start of injection of the main injection but there is also a pilot injection which also shifts together with main injection. SOI sweep is done at no EGR condition. Figure 3.13 shows the burn rate RMS error values for start of injection changing from -9 to 9 after top dead center (ATDC) of the firing event. The error increases as SOI gets closer to -9 (i.e. advanced too much) which mean deviation from reality increases. Still the error is below an acceptable value, it is less than 1%. Highest error is 0.7%. This means that combustion is predicted close to reality during a start of injection sweep. So the model can be used to check SOI changes for performance and emission prediction purposes.

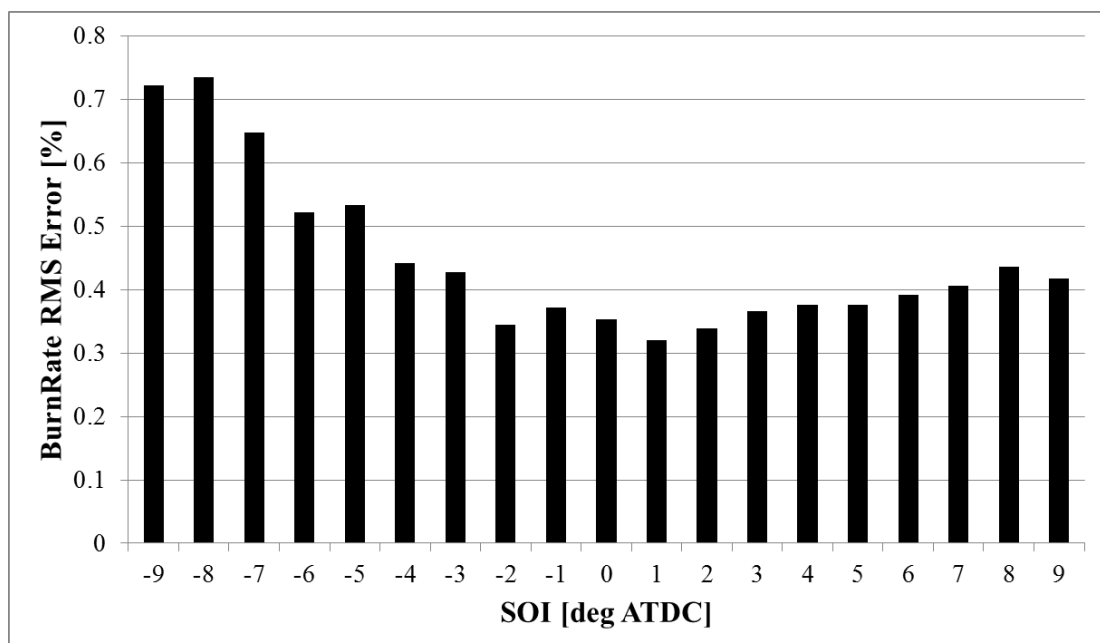


Figure 3.13. RMS errors when SOI changes at 2000 rpm 50% load.

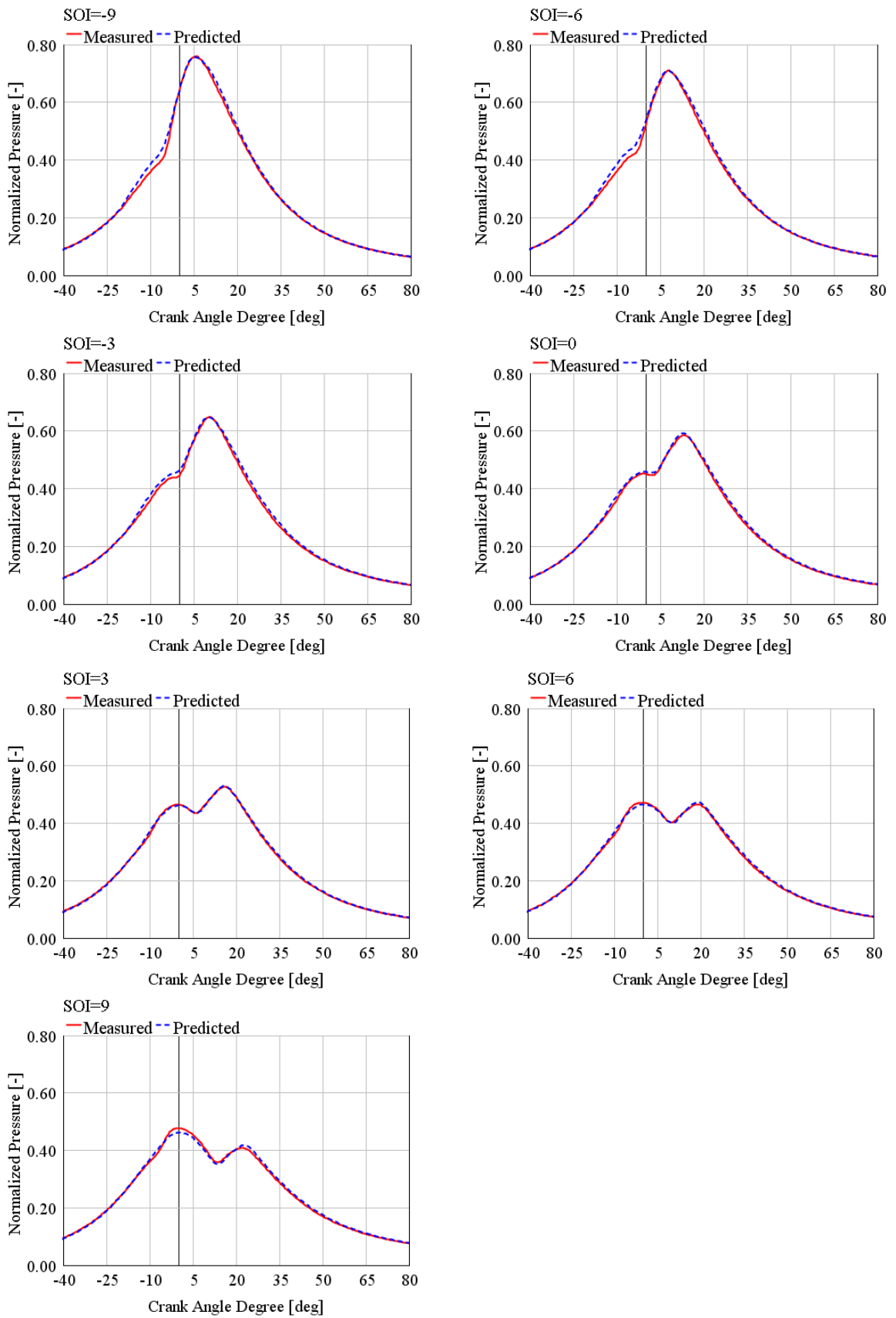


Figure 3.14. Cylinder pressure comparison for different SOI values.

Figure 3.14 shows the cylinder pressure comparison plots SOI starting from -9 to 9 ATDC by 3 degree increments. Cylinder pressures are very close especially during combustion. It can be concluded that SOI change can be predicted close to reality. The deviations are especially close to pilot injection event just before main combustion which is expected since it has been shown that small injection quantities cannot be predicted well enough as can be seen from low load points.

Another comparison is done to see if the emissions can be predicted closely in terms of direction and quantity. As can be seen from Figure 3.15 and 3.16, NO<sub>x</sub> emission prediction is very close but soot is not predicted very well. The results of the model does not show much change on soot emissions, but test results show that there is a rapid increase if the SOI is further advanced after -7 ATDC. Other than this, there are only slight changes in soot emissions. NO<sub>x</sub> emissions are very close, maximum error being 40% at SOI=9 and the average error being around -3.5%. Directionally, NO<sub>x</sub> behavior is predicted very well, a decreasing NO<sub>x</sub> emission due to lower in cylinder temperatures since SOI is retarded.

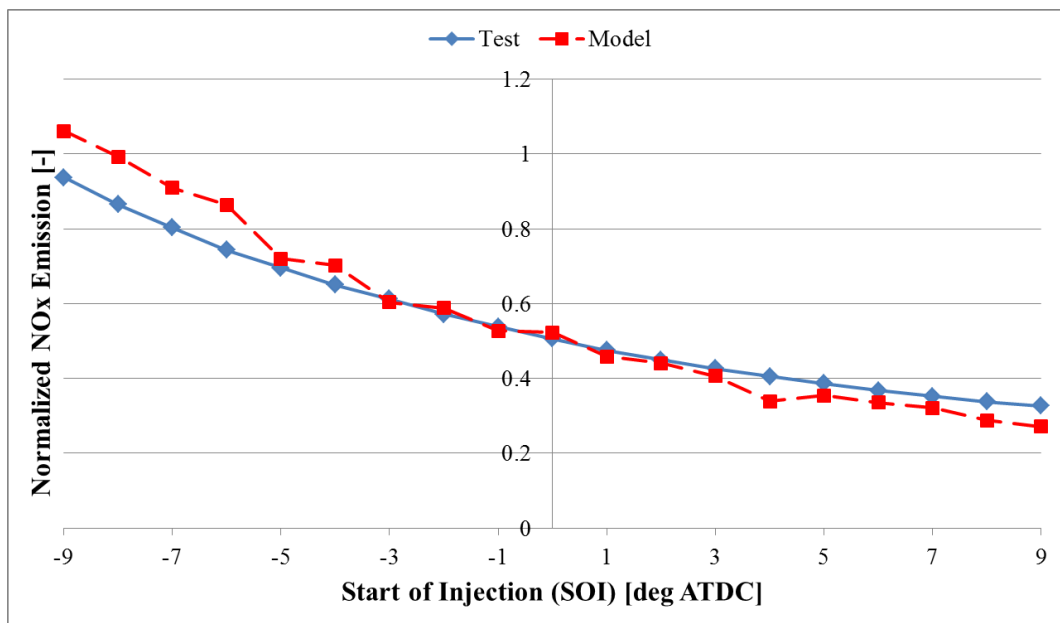


Figure 3.15. NO<sub>x</sub> emissions for different SOI values (test vs. model).

The poor match of the model and test results in terms of soot emissions is already expected, since the model cannot be correlated as well as the NO<sub>x</sub> model as discussed in

the previous section. It is interesting to observe that both  $\text{NO}_x$  and soot emissions drop together from SOI -9 to -5, when test values on Figures 3.15 and 3.16 are considered. After SOI=-5, soot emission behavior changes. Generally it is expected to have opposite behaviors for soot and  $\text{NO}_x$ . When SOI is advanced, the temperatures in the cylinder will be higher so that more  $\text{NO}_x$  is formed and soot particles formed should burn more easily. However soot does not show this expected behavior.

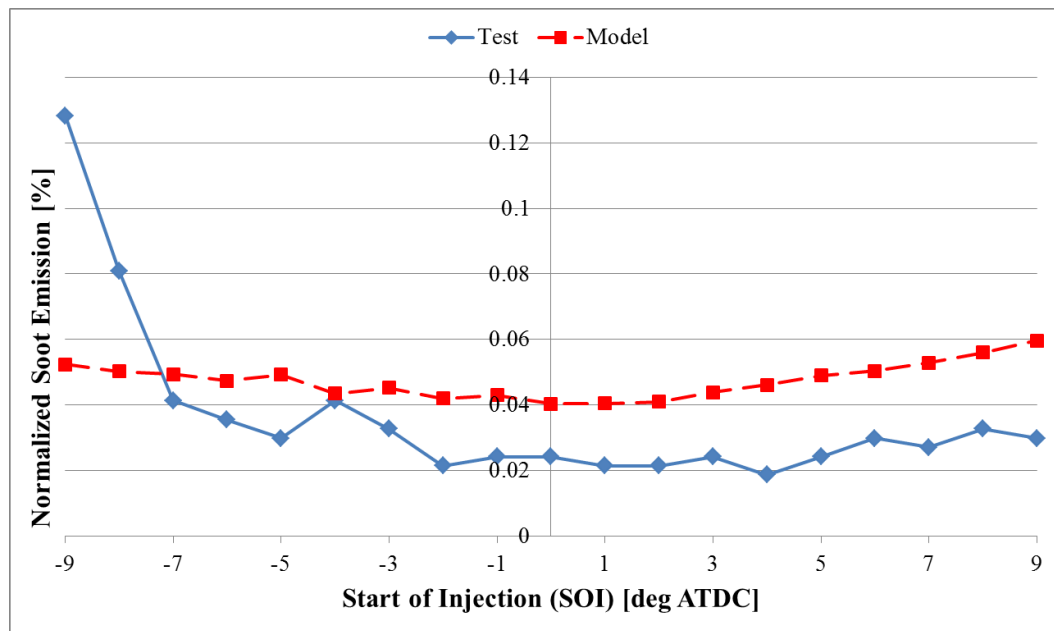


Figure 3.16. Soot emissions for different SOI values (test vs. model).

Another important sensitivity check of the model is the EGR sensitivity. It is highly important to closely predict combustion and emissions for different EGR percentages. EGR percentage is given as the fraction of the EGR flow to the total flow (i.e. EGR flow + air flow). Sweep study is done from 3% to 21% EGR cases again at 2000 rpm 50% load as was done for SOI sweep study. Again using the model correlated already, errors shown in Figure 3.17 are obtained for different EGR percentages. As can be seen, the prediction is close enough (error < 1%) up to 18% but error is above 1% for 21% EGR case. Figure 3.18 shows the pressure comparisons. It can be seen that the cylinder pressures are overpredicted for high EGR percentages. This means that the fuel is burning much faster than it should be. Since the fuel is predicted to be burn faster than in reality, higher peak pressures are observed when compared to the test values. Together with increased EGR, the duration for combustion increases but the model does not predict that very well.

Combustion model cannot be very precise for the prediction of very different EGR percentages at the same operating point (i.e. EGR sweep at the same load and speed). Figure 3.19 shows the  $\text{NO}_x$  emission comparison between test and model for different EGR rates. Directionally it is good but high errors observed for EGR rates higher than 15%. Actually this is expected since combustion model is giving higher burn rates, which in turn causes higher temperatures in the cylinder. This directly means that the  $\text{NO}_x$  emission will be overpredicted in the model, which is the case as it can be clearly seen from Figure 3.19. Figure 3.20 shows the comparison for soot emissions. It is good to observe that the trend of soot after 15% EGR rate is the same for measurement (test) and prediction (model) results, where both are increasing. Test results show that soot is very sensitive to increasing EGR since it suddenly increases rapidly after 15% EGR; however this increase is not as rapid as the test in the model. In the test; soot density suddenly increases to 200 and then 800 from values below 50%. Therefore two y-axes are used, where primary one is for the test on the left and secondary axis on the right is for the model, where the highest value is 110%. Otherwise it will be hard to see the behavior of both data on the same graph.

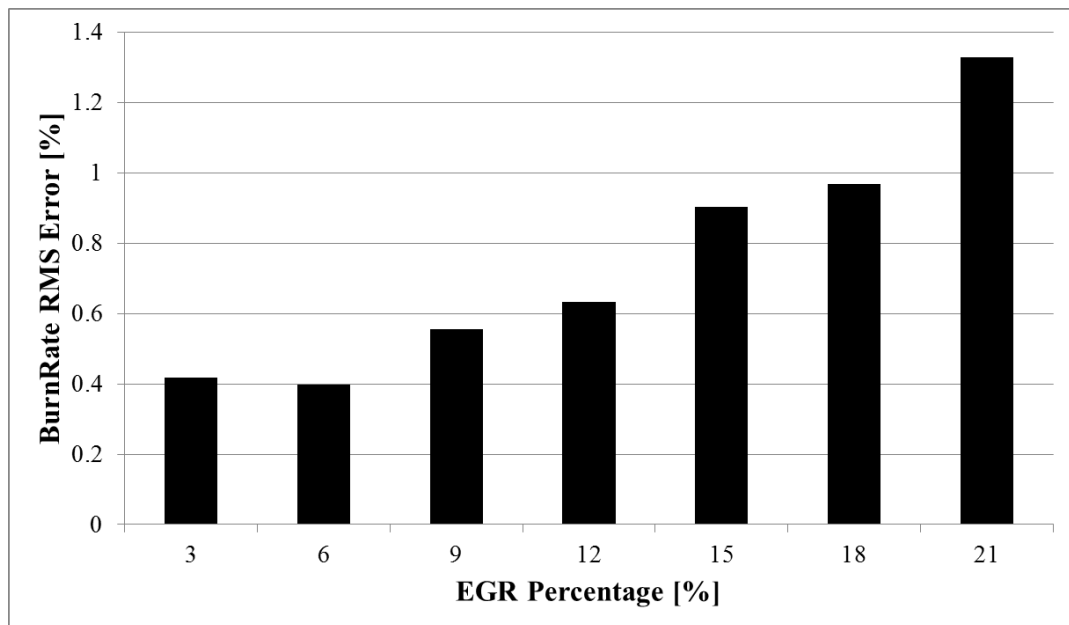


Figure 3.17. Burn rate RMS errors for different EGR rates (in percentage).

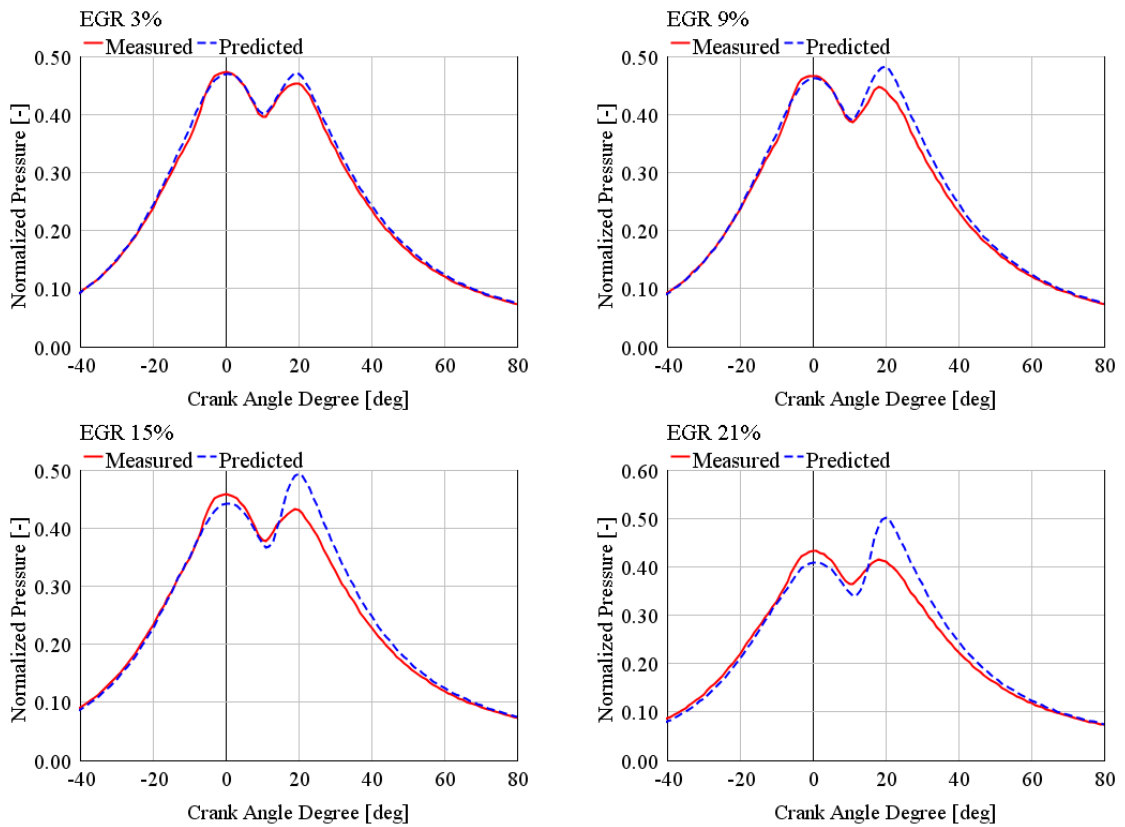


Figure 3.18. Cylinder pressures for different EGR rates (test vs. model).

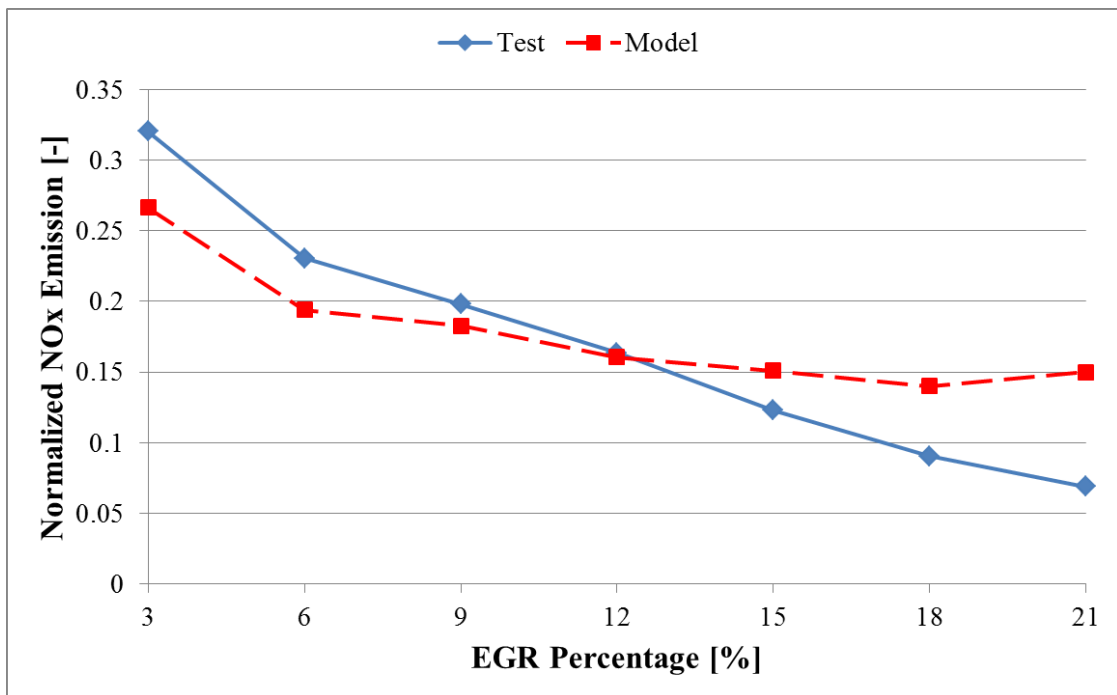


Figure 3.19. NO<sub>x</sub> emission for different EGR rates (test vs. model).



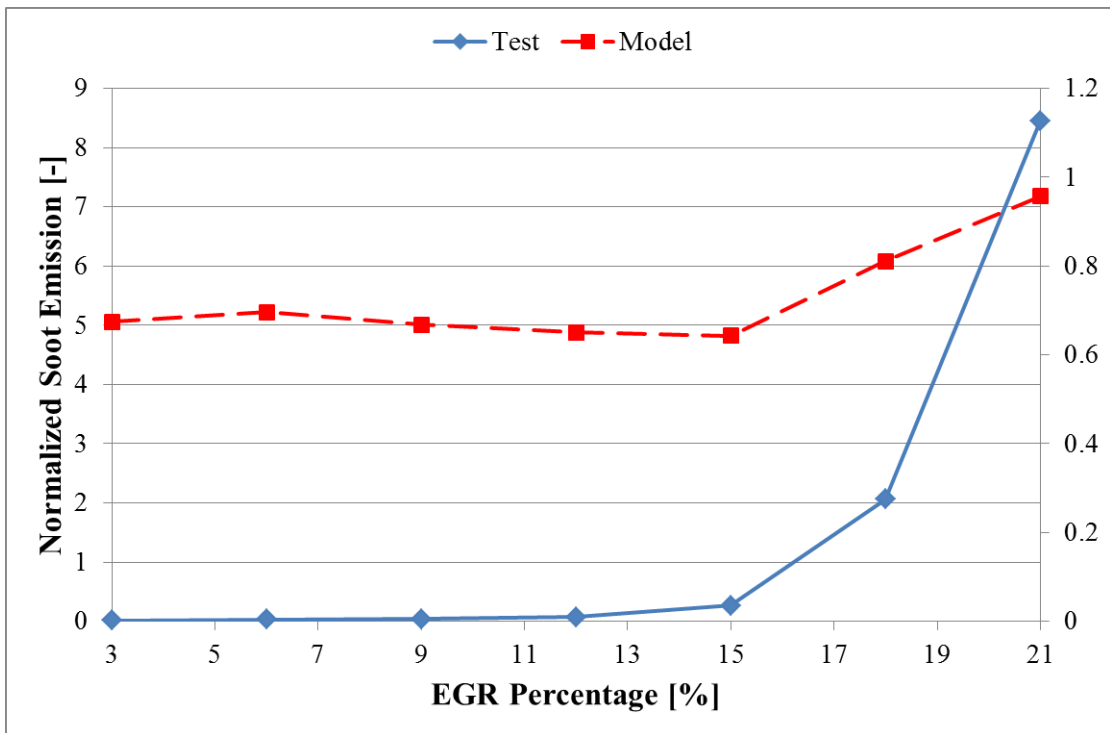


Figure 3.20. Soot emission for different EGR rates (test vs. model).

## 4. CONCLUSION

A phenomenological diesel combustion model is correlated and used for the prediction of engine out emissions of  $\text{NO}_x$  and soot. First important combustion parameters are determined and these are correlated for combustion to correctly predict physical conditions such as pressure and temperature inside the cylinder. Secondly emission models are investigated and correlated with the limited data available and then the emission results are compared at a higher number of operation points of the engine. As the final step; model sensitivities for SOI and EGR are investigated.

One of the crucial steps at this study was the preparation steps such as gathering test data for injection and cylinder pressure from the dynamometer. Since the data cannot be used directly, pre-processing of the data was needed. This step depends on how good the test data are. The cylinder pressures can be smooth or very noisy with high oscillations according to how well the pressure sensor is calibrated. There will be some amount of noise in cylinder pressure due to combustion process itself. However this noise can be minimized if the sensor is properly calibrated. This allows the pressure data to be used with a less amount of smoothing. Similarly injection profiles have noises due to pressure waves in the injection system. Since these two facts are the results of physical conditions, it is hard to eliminate all the noise, but noise from sensor or measurement setup should be eliminated.

Combustion is correlated using 3 parameters eliminated from 7 correlation parameters. Combustion correlation is good except low load operation points. There are high RMS error and therefore high deviation of cylinder pressures between test and model. This fact has also an effect on emission correlation.

Investigating the emission results for  $\text{NO}_x$  and soot, it can be first concluded that the emissions can be predicted directionally correct meaning that increase and decreases between different operating conditions are predicted well. Soot is more problematic compared to  $\text{NO}_x$ .  $\text{NO}_x$  is also very close to test values in terms of values predicted with the exception of some areas, such as low load and 3000 rpm full load. However since the

emissions are low in the low load region, this will not contribute too much and this is also related to the fact that the combustion correlation is poor compared to other operation points. For soot emissions; model with different correlation strategies are compared with the test data. It is observed that oxidation is much slower compared to formation and therefore it should have a higher multiplier than formation. The issue with the soot model can be related to the kinetic rate of the model equations. Also it can be related that many simplifications and assumptions are done, where important parameters for soot may be neglected in the model. In the SOI sensitivity investigation; it is observed that soot was increasing, where it was expected to decrease since the in cylinder temperatures are increasing.

Another important observation about the soot model is that it cannot show the changes in the close operating points around a point where the model is correlated. Test results show rapid changes at 1500 rpm with load change, where soot doubles with load increase at 1500 rpm. The model does not show so high changes.

Combustion and  $\text{NO}_x$  emission prediction was good for different SOI, slightly worse for different EGR, especially at high EGR rate. Soot prediction was worse as expected from previous observations.

Another issue with soot is the correlation of FSN to opacity and conversion to density. The formulation is obtained by different tests on different engines but it is also stated that the correctness of the correlation is not fully guaranteed.

More number of points will not improve the current model too much as explained in the main text. For the low load region; the error does not drop below a certain value, which is above 1%. Therefore increasing number of correlation points will not fix the issue at low engine load. Also using number of correlation points will increase number of tests needed.

Both models can be used for directional purposes during early design stage, but care should be taken with the soot model that it may not provide always the correct direction.

## APPENDIX A: PHENOMENOLOGICAL COMBUSTION MODELS

Four phenomenological models were listed at the literature survey part but only the model by Hiroyasu *et al.* and the modifications in GTpower are explained. The other three models are explained in this part in a brief manner without going into too much detail such as every single equation used.

### A.1. Model of Barba

Another predictive combustion model is the work done by Barba *et al.* explained in [4]. It is a simple zone model and does not model the fuel jet in detail. Three key processes modeled are ignition delay, premixed combustion and mixing controlled combustion. So it divides the combustion into two phases premixed and mixing controlled. These two phases are modeled in a different way. It is merely simpler compared to the model of Hiroyasu *et al.*. This model is developed using combustion data from 3 different diesel engines for which cylinder volumes are 320, 443 and 540 cc for one cylinder.

Fuel evaporation is modeled by using d2-law meaning that square of the droplet diameter decreases linearly with time. Initial Sauter mean diameter (SMD) depends on nozzle diameter, discharge coefficient, Re and We numbers of the fuel jet flow.

First part of the combustion is modeled as premixed combustion. For the main injection; this is the first part however pilot injections almost completely burn as premixed. Premixed stage of the combustion is simulated by a mixing and combustion model. The pre-mixed part can be summarized as follows shown in Figure A.1 from [4]:

1. Gaseous fuel of one jet forms one premixed zone
2. An initial amount of air and residual gas is entrained into the spherical zone.
3. After the end of injection (in case of a short pilot injection) air and residual gas is mixed into the zone because of the turbulence in the cylinder.
4. At combustion start a turbulent flame propagates from one ignition location → burning mode 1 forming the ascending trace of heat release.

5. During the first flame propagation other locations ignite  $\rightarrow$  burning mode 2 forming the descending trace of heat release.

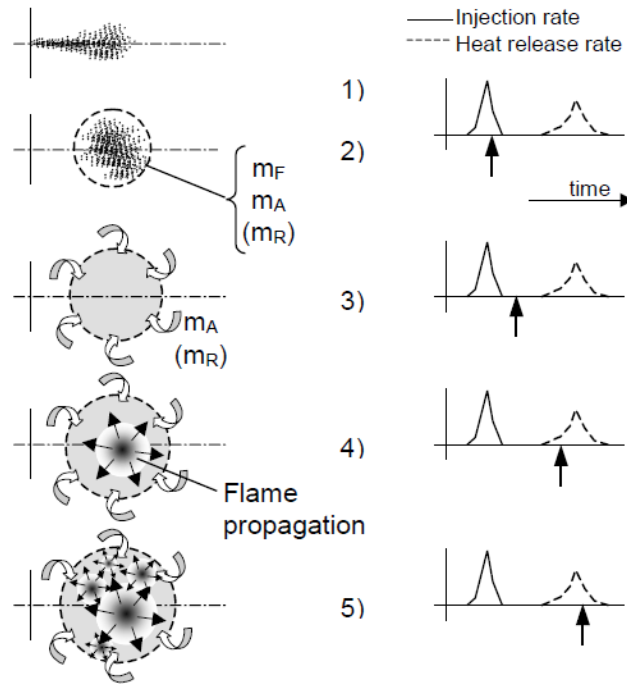


Figure A.1. Temporal sequence of the premixed combustion model [4].

Burning of the mixture depends on turbulent flame velocity. Turbulence intensity is assumed to be proportional to the mean piston speed. Laminar burning velocity is calculated by using previous calculations from [5] and [6]. Local equivalence ratio is also important for the rate of fuel burning.

The next part is the mixing controlled combustion model. A frequency model is used, where the aim is to determine the characteristic mixing frequency. Burn rate of the fuel is equal to the multiplication of this frequency times the fuel available. The mixing frequency is considered to be the quotient of a characteristic mixing velocity and a characteristic mixing length. Mixing length depends on equivalence ratio, actual cylinder volume and number of nozzle holes.

The characteristic mixing velocity is determined by the turbulence in the cylinder. There are many contributor mechanisms to turbulence such as intake flow, swirl, squish-flow, injection and combustion. It is hard to estimate the effects of these mechanisms

separately. Therefore it is only subdivided into two; first part considers the effect of injection and the second part considers other contributors. This is done due to the fact that injection pressure can be changed for almost any operating condition very easily and it can have a big impact. For the second part it is assumed that all velocities can be scaled by mean piston velocity. For the first part, a simple turbulence model is used. The homogeneous  $k-l_1$ -model assumes a homogenous turbulence field in the cylinder. Conservation of energy principle is used. Conservation of momentum, dissipation of energy and production of the kinetic energy are considered. The integral length scale  $l_1$  is chosen as the nozzle diameter. As dissipation occurs in a certain distance to the nozzle, the integral length scale is expected to be greater than the nozzle diameter therefore an exponential parameter in the equation is modified. The production of kinetic energy is derived directly from the kinetic energy of the injected fuel, scaled with the total amount of gas mass in the cylinder and multiplied with a pre-factor.

The fuel evaporated before combustion start is burned in the premixed part and fuel evaporated after combustion start is burned in diffusion combustion phase.

The last remaining important phenomenon is the ignition delay. It is treated as sum of three delay times: physical ignition delay, chemical ignition delay and an empirical ignition delay for correlation without any physical or chemical background. Empirical integral equation is used according to [6] starting at injection start and ending at combustion start. Physical ignition delay is related to the evaporation of the fuel and a characteristic evaporation time is used. The amount of evaporated fuel required for ignition start is unknown. A time proportional to evaporation time is used in the model. For chemical ignition delay, Arrhenius type of equation is used.

## A.2. Model of Maiboom

Another phenomenological model work is done by Maiboom *et al.* as explained in [7]. Combustion is modeled in two phases similar to the model of Barba *et al.*. But also the spray and entrainment is modeled as was done in the model of Hiroyasu *et al.*. In this work, there are totally 6 zones in the cylinder. Spray is divided into zones only in the axial

(injection) direction and not in the radial direction. The following submodels are included in the model:

1. An injection rate model based on measurements,
2. The spray models from Siebers *et al.* as explained in [8-10] for the description of the fuel jet (maximum liquid-phase fuel penetration, vapor-phase fuel penetration, spray spreading angle, lift-off length, and corresponding air-fuel equivalence ratio).
3. A model for the air entrainment by the fuel jet based on the spray model
4. A premixed and diffusion combustion model partially based on Barba's simplified 0D turbulent kinetic calculation
5. An energy balance in each zone to calculate corresponding mean temperatures.

The 6 zones in the cylinder are described as follows and shown in Figure A.2 taken from [7].

Zone 1: Liquid fuel zone, from the nozzle hole to the maximum liquid penetration  $L$ .

Zone 2: Air-fuel mixture between the maximum liquid penetration  $L$  and the lift-off length  $H$ . If  $H > L$ , zone 2 contains the fuel that is completely evaporated downstream of the liquid penetration. If  $H < L$ , zone 2 contains the liquid fuel downstream of the lift-off length.

Zone 3: Premixed combustion zone that consists of the combustion of the air-fuel vapor phase that has been prepared during ignition delay.

Zone 4: Diffusion combustion zone from the lift-off length to the vapor-phase fuel penetration.

Zone 5: Diffusion flame surrounding zones 3 and 4.

Zone 6: Surrounding gas (air and EGR).

The model assumes that the various jets are supposedly free and identical. No interaction is supposed between various jets (from the multiholes injector) and between jets and combustion chamber walls. Also no interaction is supposed between the pilot and principal sprays. Some modifications are made on the spray models from Siebers [8-10].

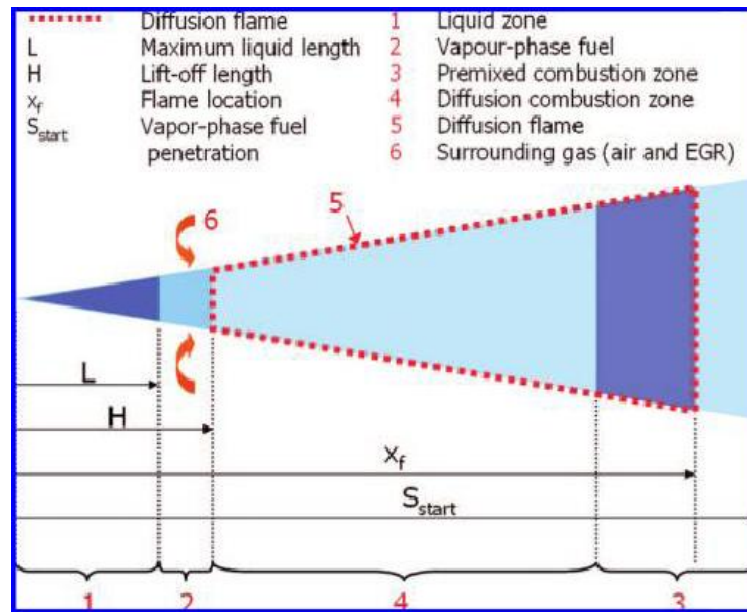


Figure A.2. Zone description [7].

In the six-zone model of Maiboom *et al.*; the ignition delay is used as input and not modeled but some modeling work is done in [11], where 5 zones are used. It is also assumed that pilot injections only affect the ignition delay of the main combustion and do not affect the emissions such as  $\text{NO}_x$  and soot.

### A.3. Model of Rether

The last and the most recent model investigated is by Rether *et al.* explained in [12]. The model is built to account for any number of injections during one cycle. The model is explained therefore for pre-, main- and post injections.

Ignition delay is modeled by using a single Arrhenius type of equation and a Magnussen type of equation, where it is not practical to use reaction mechanisms (detailed or even reduced). The approach is very similar to the approach explained in [13]. The effects of local excess air ratio, temperature, previous combustion events (if any) and injection turbulence are considered. Ignition delays from Arrhenius and Magnussen equations are summed and accordingly reaction rate is calculated. The reaction rate is calculated at each time step and then integrated from SOI to the actual time step. When the integral of the reaction rate from start of injection to the actual time reaches a certain limit, combustion starts.



The next part of the model is the pilot injection, which shortens the ignition delay of the main injection and therefore decreasing the pre-mixed part of the main combustion. As pre-mixed part gets less, combustion noise and component loads decrease. Each pilot injection is modeled as a separate air-fuel cloud. A simpler approach of the entrainment model by Barba *et al.* is used in this model. A constant entrainment rate is assumed after combustion start.

It has been pointed out that when too much excess air or few air is present, it is not possible that ignition will occur inside the mixture cloud or a combustion occurring extinguishes. In the model; if excess air ratio gets out of the range between 0.536 and 3, the laminar flame velocity gets negative which means flame quenching. DIjet model similarly assumes no burning at local equivalence ratios higher than 3. Pilot injection combustion is modeled as premixed totally by using the approach by Barba *et al.* and including laminar flame velocity as a function of excess air ratio. A spherical propagation of the combustion from one single ignition point is assumed and the increase rate of the radius of the sphere corresponds to turbulent flame velocity. By neglecting the time-based change in density, the current flame-sphere surface is determined and the mass flow is calculated, which flows into the flame sphere because of the propagation.

Mixture cloud is assumed to have a uniform velocity decreasing with time. Mixture cloud velocity is calculated from the mean injection velocity calculated from nozzle discharge coefficient, injected mass, number of nozzles, density of fuel, nozzle diameter and injection time. The mixture cloud velocity is used to determine specific turbulence.

The next part is the main injection. Slices are created in constant time steps. At the initialization stage; a fixed amount of combustion-air gas is admixed with each slice. During the ignition delay period fuel in the slices are diffused to two fuel pools: pre-mixed and diffusion pools. After the ignition delay slices only have diffusion pool. The assumption is that the mixing of fuel and air inside the premixed pool of each slice is already concluded at the ignition point. The combustion is modeled by means of an Arrhenius approach.

The fuel slices propagate through the combustion chamber and zones with different excess air ratios ( $\lambda$ ) are formed as can be seen in Figure A.3 from [12]. The first zone A is very rich in terms of fuel and therefore there is no combustion in this zone. The zone B has a stoichiometric excess air ratio (i.e.  $\lambda=1$ ) where combustion can occur (diffusion I). The zone C is lean but it contains areas where combustion can occur (diffusion II). Also the  $\lambda=1$ -line of the fuel zone is shown in the Figure A.3.

The decrease of fuel concentration in the slice is taken as constant. The calculated concentration is used to assign the unburnt fuel mass of the diffusion pool to one of the three zones in each slice: rich, diffusion I and diffusion II (i.e. A, B and C in Figure A.3, respectively). Also the velocity distribution in the slice can be calculated. When this is integrated over entire spray, mass-averaged spray velocity is obtained to calculate specific turbulence.

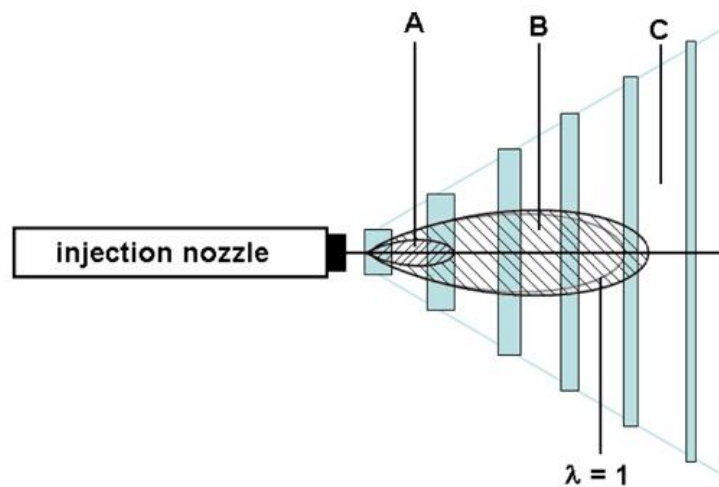


Figure A.3. Slice propagation through the combustion chamber [12].

The specific turbulence for diffusion pool I zone is calculated from velocity distribution of the spray and only the parts are taken into consideration, which are within the  $\lambda$  limits. To calculate characteristic length; current combustion chamber volume is used with the limitation that it is smaller than 2.5 times the compression volume. There is a maximum limit for the characteristic length, which is claimed to prevent combustion becoming too slow in the burn-out phase.

Slices or parts of the slices which are in the areas with a local excess air ratio above 1.1, the fuel is assigned to diffusion pool II. A weakening at a low global excess air ratio does not take place during diffusion combustion II. The burn rate of the main injection is finally obtained by adding up the slice conversion rates.

For post-injection; similar calculations as main injection are made and ignition delay step is repeated.

## APPENDIX B: SENSITIVITY STUDY

### B.1. Grid Sensitivity

First the model is tested for its sensitivity to calculation timestep. Default value of the model was 0.2 crank angle degrees. Runs are done for 0.05, 0.1 and 0.2 crank angle degrees (CAD for short). 0.05 CAD is the minimum timestep that can be applied in the model since smaller timesteps will increase truncation errors. Pressure and temperature vs crank angle for each case are compared with each other. Also emission results are compared. For each case operating conditions are kept the same only timestep has changed. Figure B.1 shows the pressure variation between -20 and 40 crank angle degrees relative to top death center of firing. Figure B.2 shows the temperature in the same time interval shown for the pressure plot.

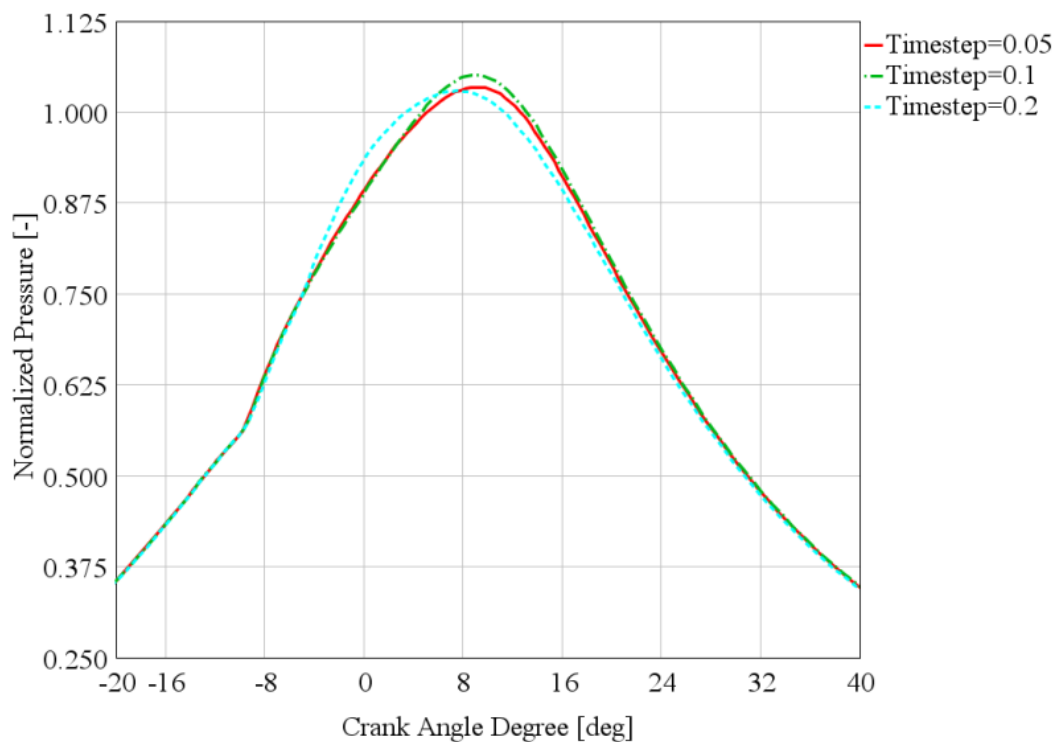


Figure B.1. Pressure vs crank angle plots for timestep sensitivity.

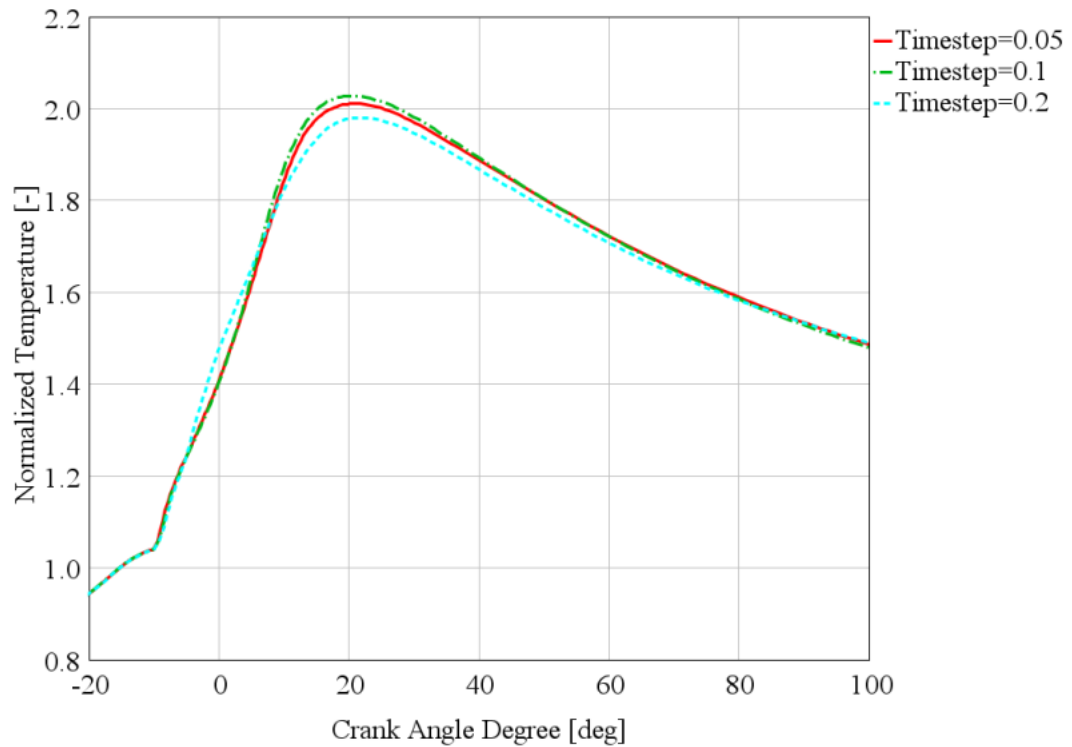


Figure B.2. Temperature vs crank angle plots for timestep sensitivity.

The two plots show significant difference between 0.2 CAD timestep and others. The general trend of pressure and temperature for this timestep is clearly different than others. Also there are differences still as the minimum timestep is approached. These are generally in terms of the maximum value observed in this interval for pressure and temperature. This is very critical however for the emissions. Especially,  $\text{NO}_x$  emission is almost directly determined by maximum temperature during the cycle. Therefore emissions are also plotted for each timestep. Figure B.3 and B.4 show the emissions of  $\text{NO}_x$  and soot for time sensitivity study. Again 0.2 CAD timestep is very different than others but there are also differences between other timesteps as well. Also the difference does not decrease as the minimum timestep is approached. According to the observations listed, it is concluded that 0.05 CAD timestep is the best choice since it is the smallest and therefore finest timestep expected to be more close to real case.

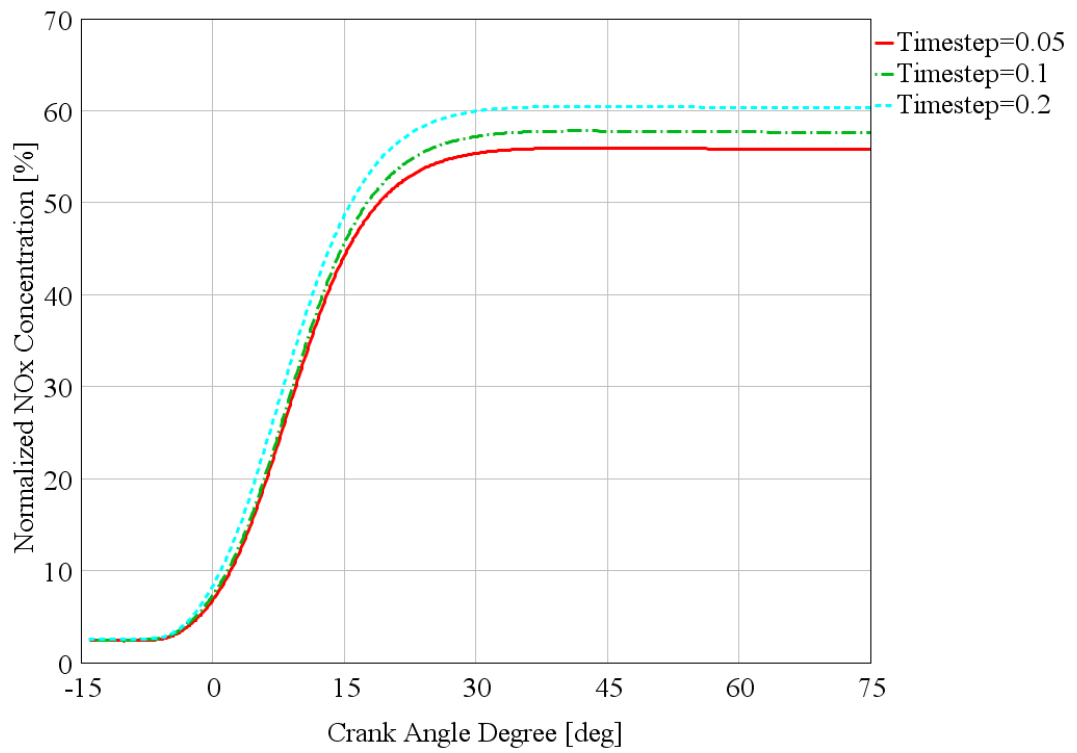
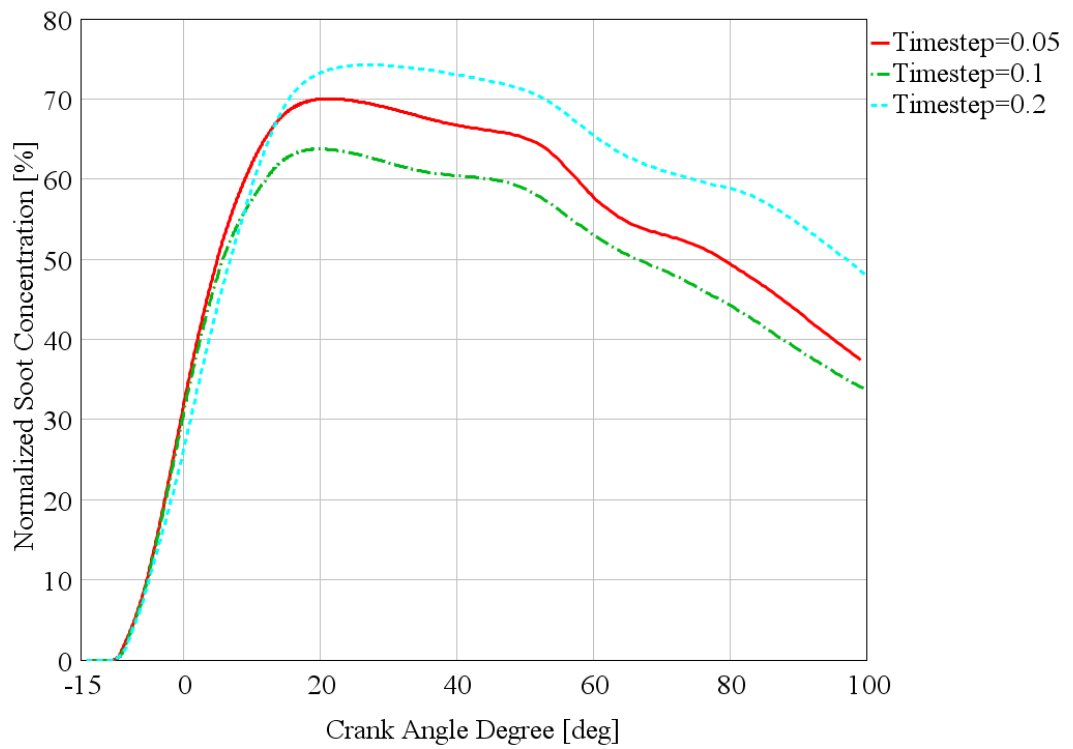
Figure B.3. NO<sub>x</sub> concentration vs CAD.

Figure B.4. Soot concentration vs CAD.

## B.2. Parameter Sensitivity

There are totally 20 parameters that can be used to correlate the model. Not all of them have the same effect on the model and the sensitivity of the model to each parameter is different. Here are 7 parameters investigated, which are suggested to be the most relevant parameters for correlation by GTpower manual. These parameters are listed as follows with their default (def) values

- 1) Entrainment Multiplier Before Combustion: CBAIR (def value=1.2)
- 2) Entrainment Multiplier After Combustion: CAAIR (def value=0.5)
- 3) Entrainment Multiplier After Wall Impingement: CWALL (def value=1.2)
- 4) Overall Ignition Delay Multiplier: CIGN1 (def value=1.0)
- 5) Dilution Effect Multiplier: CIGN8 (def value=1.0)
- 6) Break-up Time Multiplier: TBMULT (def value=0.9)
- 7) Combustion Rate Multiplier: CRATE (def value=1.7)

Sensitivity is done by increasing and decreasing the default values by 0.2 except CBAIR since it is small compared to other multipliers. CBAIR multiplier is increased/decreased by 0.1. So there are 3 cases for each multiplier and 4 for TBMULT and CRATE multipliers by default case being the same case for each multiplier. The effect of the multipliers to fuel burn rate and emissions are observed.

Case setup and change of parameters for each case is given in Table B.1. There are 17 cases in total.

It should be noted that dilution effect will be dominant when EGR is present in the cylinder. The sensitivity case was conducted for full-load where there is no EGR. Therefore the sensitivity for dilution effect multiplier (CIGN8) is repeated for 2000 rpm part load, where EGR is present in the cylinder.

Table B.1. Case setup for parameter sensitivity.

Case	CAAIR	CBAIR	CWALL	CIGN1	CIGN8	TBMULT	CRATE
1 (Def)	0.5	1.2	1.2	1	1	0.9	1.7
2	0.4	1.2	1.2	1	1	0.9	1.7
3	0.6	1.2	1.2	1	1	0.9	1.7
4	0.5	1	1.2	1	1	0.9	1.7
5	0.5	1.4	1.2	1	1	0.9	1.7
6	0.5	1.2	1	1	1	0.9	1.7
7	0.5	1.2	1.4	1	1	0.9	1.7
8	0.5	1.2	1.2	0.8	1	0.9	1.7
9	0.5	1.2	1.2	1.2	1	0.9	1.7
10	0.5	1.2	1.2	1	0.8	0.9	1.7
11	0.5	1.2	1.2	1	1.2	0.9	1.7
12	0.5	1.2	1.2	1	1	0.75	1.7
13	0.5	1.2	1.2	1	1	1.05	1.7
14	0.5	1.2	1.2	1	1	1.2	1.7
15	0.5	1.2	1.2	1	1	0.9	1.4
16	0.5	1.2	1.2	1	1	0.9	2
17	0.5	1.2	1.2	1	1	0.9	2.3

### B.2.1. Entrainment Multiplier Before Combustion: CBAIR

Burn rate comparison plot is shown at Figure B.5 for CBAIR multiplier.

As air entrainment rate decreases, the burn rate decreases as expected. Also the maximum temperature observed in the cylinder decreases, which has a high impact on NO<sub>x</sub> emissions. NO<sub>x</sub> is formed mostly at the earlier phases of the combustion and during rapid temperature decrease, NO<sub>x</sub> chemistry freezes. Especially in diesel engines; the temperature drop is very rapid compared to gasoline engines [5]. At the Table B.2; emissions and maximum temperatures for each case is given. As expected; NO<sub>x</sub> emission decreases as maximum temperature decrease. Soot shows the opposite behavior compared to NO<sub>x</sub>, which is commonly observed in diesel engine emissions.



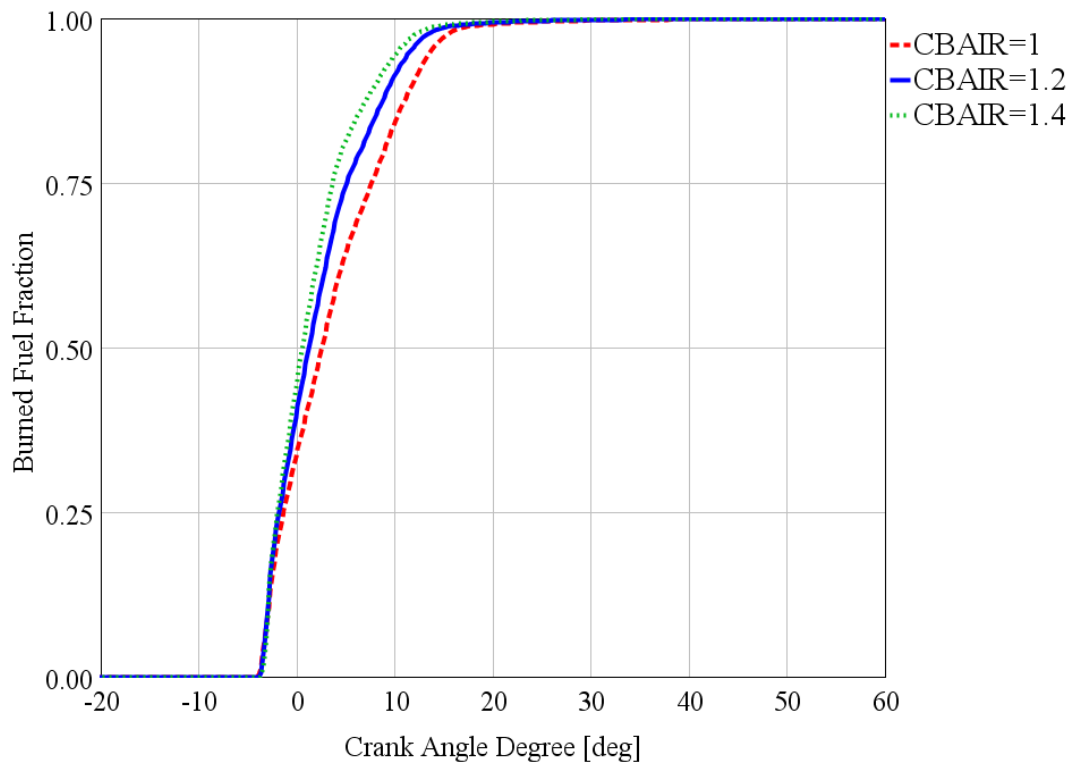


Figure B.5. Change of burn rate with CBAIR multiplier.

Table B.2. Emissions and maximum temperature for CBAIR sensitivity.

		CBAIR=1	CBAIR=1.2	CBAIR=1.4
Case No		4	1	5
Brake Specific NO <sub>x</sub>	g/kW-h	4.25	5.50	6.91
Brake Specific Soot	g/kW-h	8.97	5.28	2.54
Temperature, Maximum	K	1844	1965	2063

### B.2.2. Entrainment Multiplier After Combustion: CAAIR

Burn rate comparison plot is shown in Figure B.6 for CAAIR multiplier.

Compared to entrainment multiplier before combustion, CAAIR has a bigger impact on main combustion (see burn rate change after 5 crank angle degrees). Burn rates are almost the same up to a certain time, since this multiplier takes effect after combustion start and its effect increases as more sub-region fuels start to ignite. Also the premix region rate is mostly determined by entrainment before combustion start. This multiplier has also a higher impact on maximum temperatures and therefore on NO<sub>x</sub> emissions. Comments

about the emissions made in the previous section are also valid and observed in this case. Table B.3 gives the comparison when CAAIR changes.

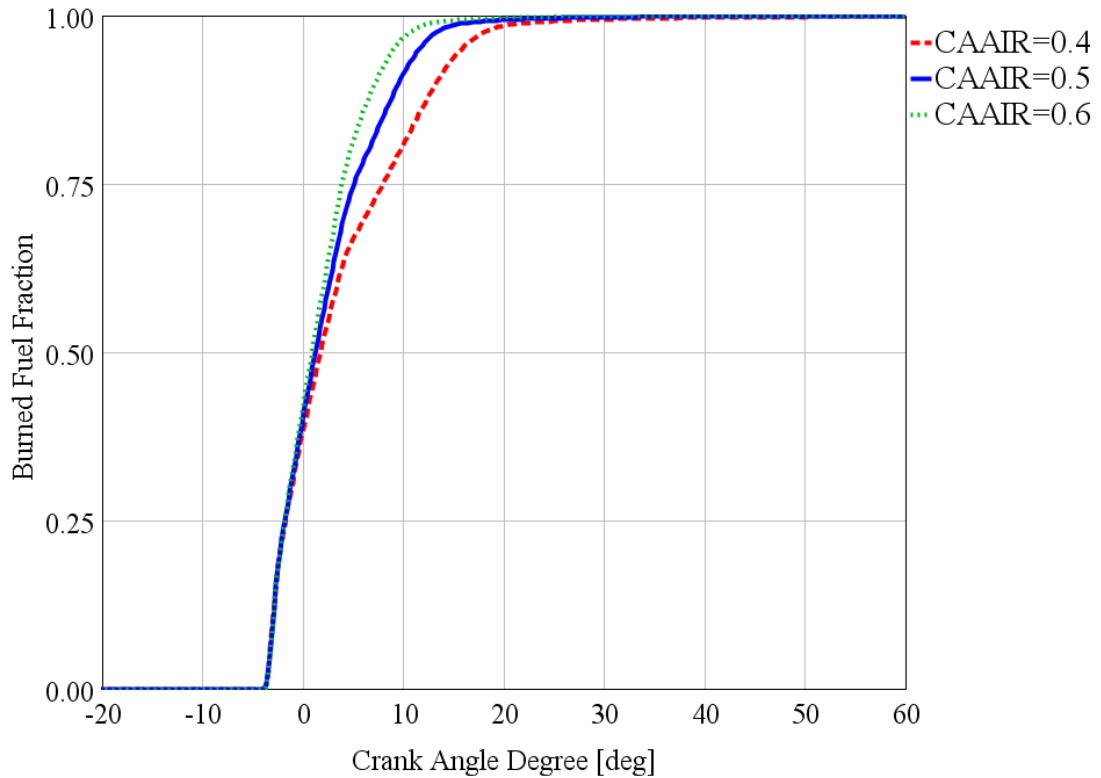


Figure B.6. Change of burn rate with CAAIR multiplier.

Table B.3. Emissions and maximum temperature for CAAIR sensitivity.

		CAAIR=0.4	CAAIR=0.5	CAAIR=0.6
Case No		2	1	3
Brake Specific NO <sub>x</sub>	g/kW-h	3.38	5.50	7.82
Brake Specific Soot	g/kW-h	17.17	5.28	0.96
Temperature, Maximum	K	1915	1965	2012

### B.2.3. Entrainment Multiplier After Wall Impingement: CWALL

Burn rate comparison plot is shown in Figure B.7 for CWALL multiplier.

This multiplier has much less effect compared to previous air entrainment multipliers. It can be observed that the wall impingement happens at a late stage and burn

rates are the same even after the half of the fuel is burned. But there is still some impact at the later stage on burn rate in the cylinder. However it is not as high as CAAIR and CBAIR. Table B.4 gives the comparison of emissions for this multiplier.

Table B.4. Emissions and maximum temperature for CWALL sensitivity.

		CWALL=1	CWALL=1.2	CWALL=1.4
Case No		6	1	7
Brake Specific NO <sub>x</sub>	g/kW-h	4.21	5.50	6.88
Brake Specific Soot	g/kW-h	11.66	5.28	1.47
Temperature, Maximum	K	1894	1965	2027

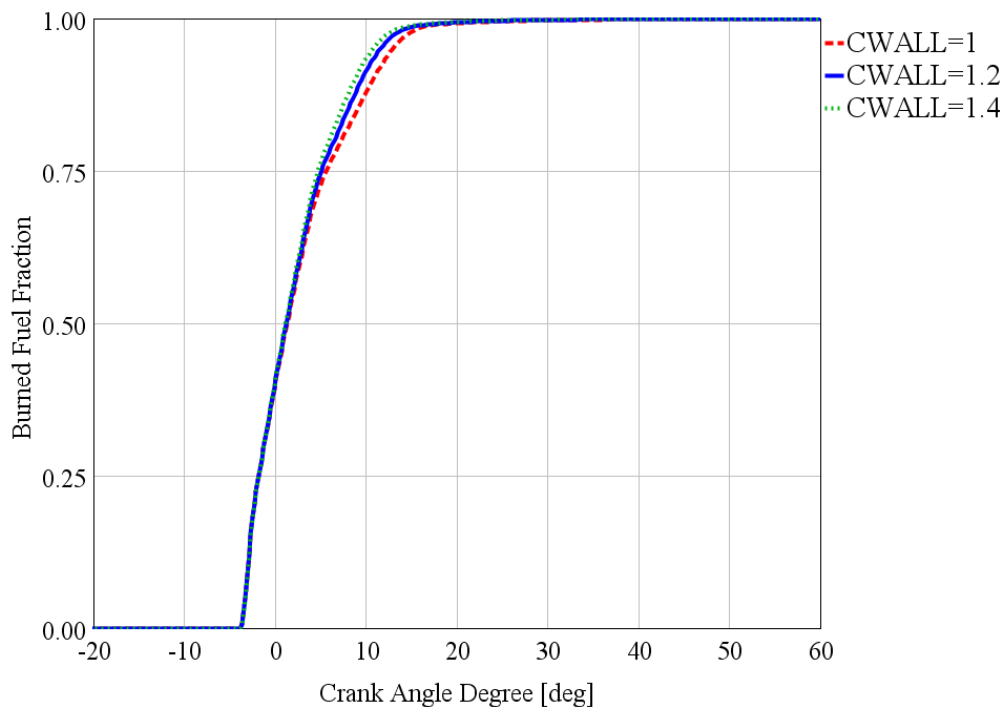


Figure B.7. Change of burn rate with CWALL multiplier.

#### B.2.4. Overall Ignition Delay Multiplier: CIGN1

Burn rate comparison plot is shown in Figure B.8 for CIGN1 multiplier.

Ignition delay multiplier directly affects the start of the combustion and that in turn affect how the combustion burn rate proceed throughout the cycle. A slower burn rate is observed when ignition delay is minimum. Since more fuel is evaporated and mixed with

the air during a longer ignition delay, it is logical to expect a more rapid burn rate when ignition delay increases. This means a higher percent of premixed combustion compared to main part. However, this rapid burn rate does not affect the maximum temperatures observed in the cylinder as can be seen by looking at Table B.5, where emission and maximum temperature results for CIGN1 multiplier are shown. This means effect on  $\text{NO}_x$  emission is not too high as it was for the first two parameters for air entrainment (CBAIR and CAAIR).

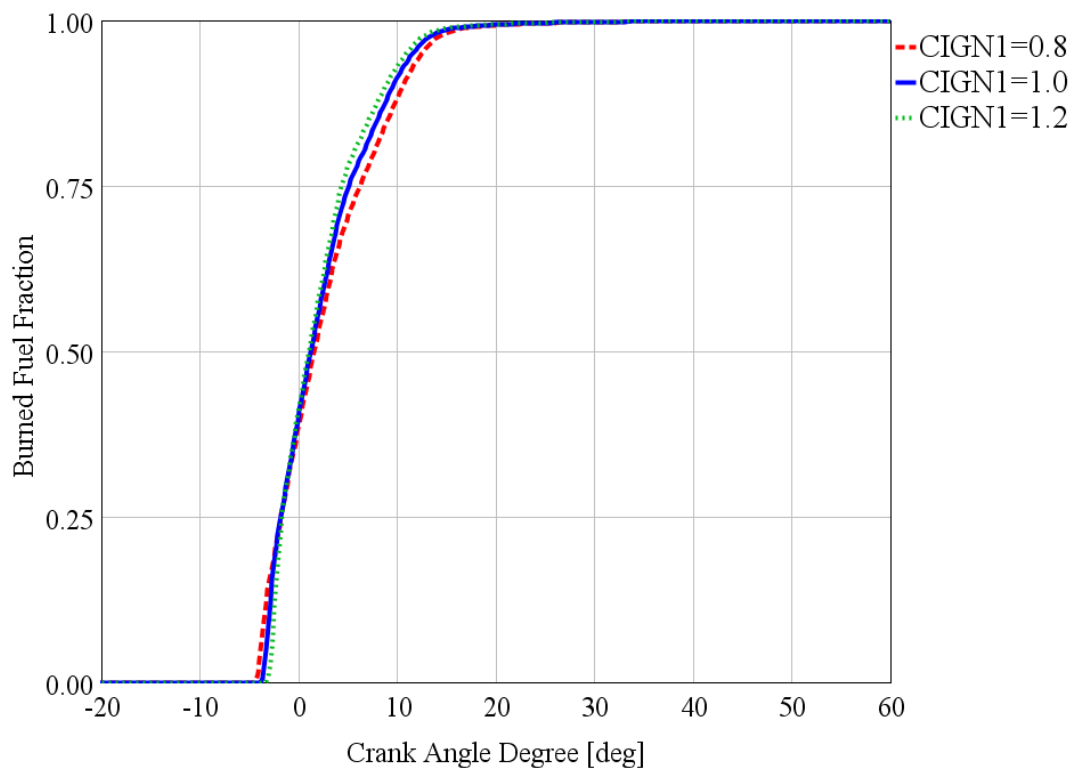


Figure B.8. Change of burn rate with CIGN1 multiplier.

Table B.5. Emissions and maximum temperature for CIGN1 sensitivity.

		CIGN1=0.8	CIGN1=1	CIGN1=1.2
Case No		8	1	9
Brake Specific $\text{NO}_x$	g/kW-h	5.14	5.50	5.85
Brake Specific Soot	g/kW-h	6.46	5.28	4.24
Temperature, Maximum	K	1947	1965	1981

### **B.2.5. Dilution Effect Multiplier: CIGN8**

Burn rate comparison plot is shown at Figure B.9 for CIGN8 multiplier.

Dilution effect is defined as the effect of substances other than air (i.e. O<sub>2</sub> and N<sub>2</sub>) on ignition delay. This means that dilution effect multiplier will affect the combustion when substances other than air are present before combustion. This concludes that the multiplier will be effective when a certain amount of EGR is present. Therefore the sensitivity for this parameter is repeated at a part load condition, where a significant amount of EGR is present in the cylinder (20% EGR is used, meaning  $EGR/(EGR+Fresh\ Air)=20\%$ ). Burn rate results for this study are shown in Figure B.10. There is more effect compared to the full load case but the effect is still small compared to CIGN1, which is shown in the previous section. The burn rates are almost the same for all cases, only the start of the combustion is changed.

Table B.6 gives the results of emissions for full load case and Table B.7 shows the results for part load case with EGR. As expected, no change for full load case and more significant changes observed for part load case.

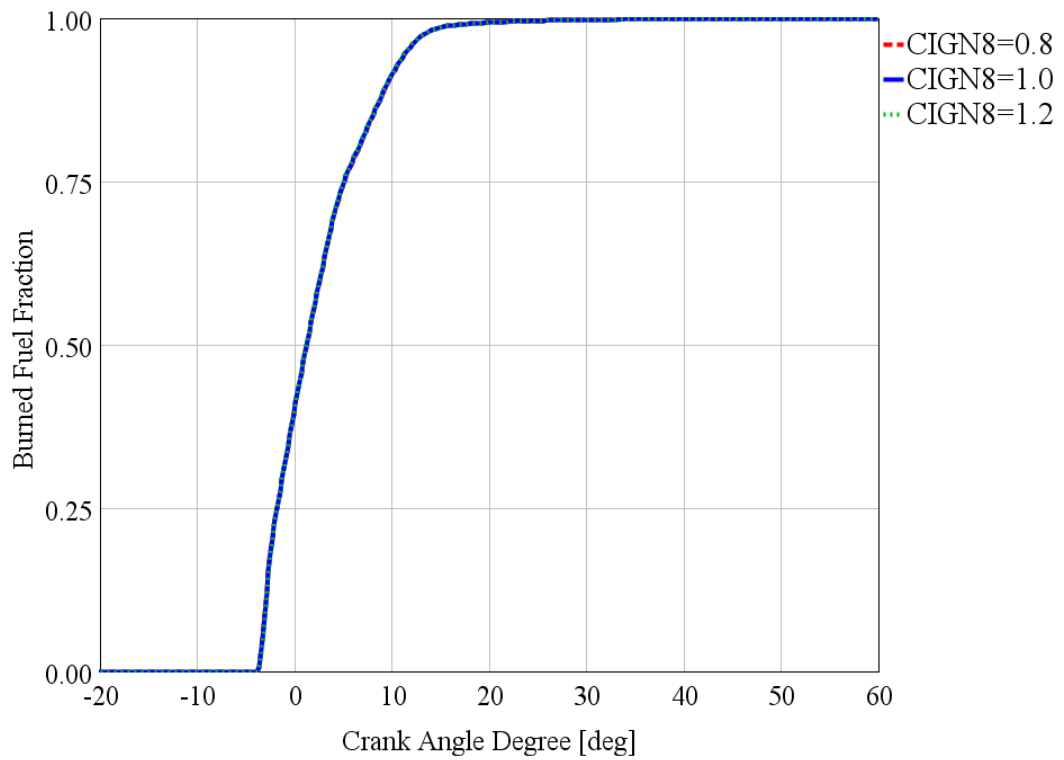


Figure B.9. Change of burn rate with CIGN8 multiplier (full load).

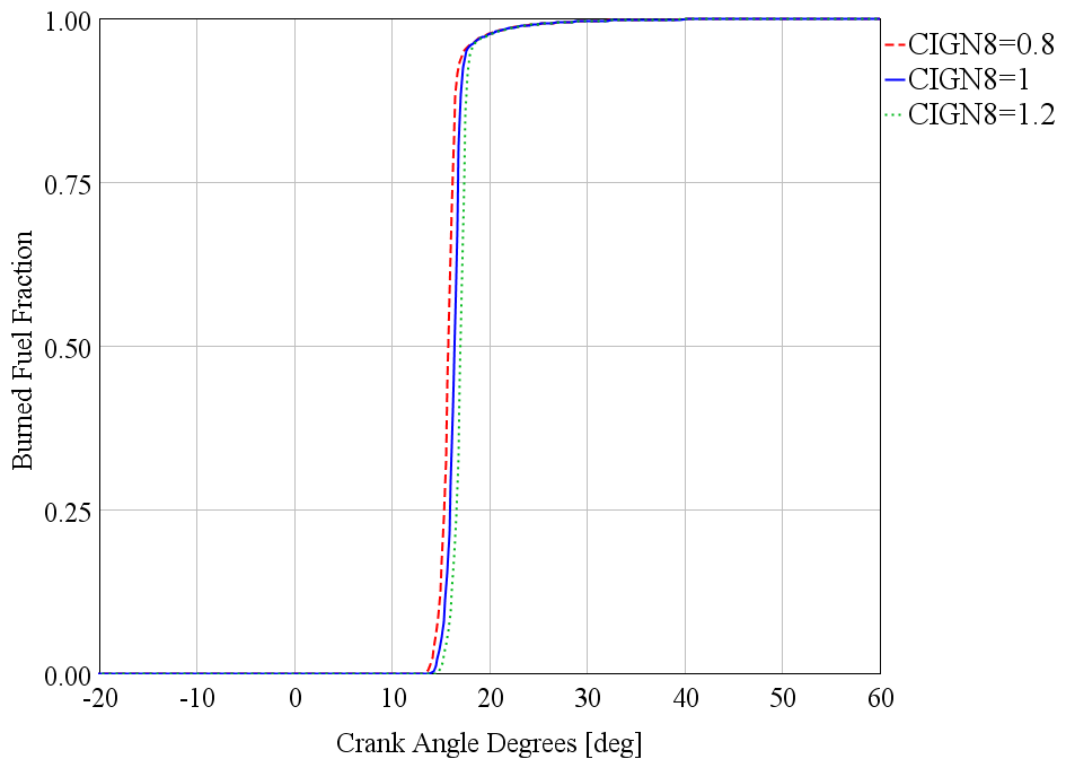


Figure B.10. Change of burn rate with CIGN8 multiplier with 20% EGR.

The aim of the study is to do the combustion correlation with as few parameters as possible and the effect on emissions is very little as can be seen from both tables. There is also an overall ignition delay multiplier to correlate the ignition delay so that this parameter can be neglected.

Table B.6. Emissions and maximum temperature for CIGN8 sensitivity (full load).

		CIGN8=0.8	CIGN8=1	CIGN8=1.2
Case No		10	1	11
Brake Specific NO <sub>x</sub>	g/kW-h	5.47	5.50	5.52
Brake Specific Soot	g/kW-h	5.35	5.28	5.18
Temperature, Maximum	K	1964	1965	1966

Table B.7. Emissions and maximum temperature for CIGN8 sensitivity (part load).

		CIGN8=0.8	CIGN8=1	CIGN8=1.2
Brake Specific NO <sub>x</sub>	g/kW-h	4.50	4.65	4.88
Brake Specific Soot	g/kW-h	0.0068	0.0068	0.0058
Temperature, Maximum	K	1878	1903	1930

### B.2.6. Break-up Time Multiplier: TBMULT

Burn rate comparison plot is shown at Figure B.11 for TBMULT multiplier.

Break-up of the fuel jet into droplets is a very important part of the model. The effect of the break up time multiplier can also be seen from the change of the burn rate. No effect is observed at the start, where up to 15% of the fuel is burned but then there is a significant difference in burn rates. Increasing this multiplier increases the break up time so the burn rate is slower. Table B.8 shows the changes in emissions for change in break up time multiplier. The impact of the multiplier can also be observed on the change of emissions.

This parameter has a similar effect as entrainment multiplier after combustion. So it is logical to keep one of these parameters and to left the other one as default since it will be

more complicated to use two parameters having similar effect and it is intended to use minimum number of correlation parameters.

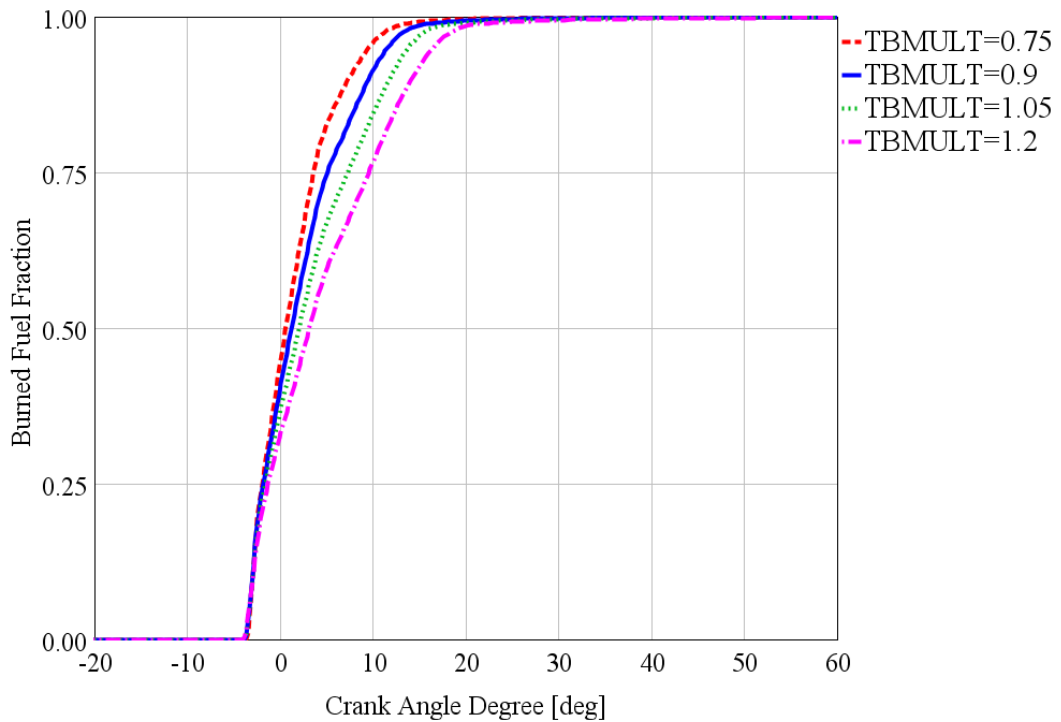


Figure B.11. Change of burn rate with TBMULT multiplier.

Table B.8. Emissions and maximum temperature for TBMULT sensitivity.

		TBMULT =0.75	TBMULT =0.9	TBMULT =1.05	TBMULT =1.2
Case No		12	1	13	14
Brake Specific NO <sub>x</sub>	g/kW-	7.37	5.50	4.16	3.15
Brake Specific Soot	g/kW-	1.30	5.28	11.79	18.37
Temperature, Max.	K	2040	1965	1899	1842

### B.2.7. Combustion Rate Multiplier: CRATE

Burn rate comparison plot is shown at Figure B.12 for CRATE multiplier. It can be observed that CRATE multiplier is the least effective multiplier compared to the other multipliers considered. There is really very small change in burn rates and similarly in emissions and maximum temperatures as can be seen at Table B.9.



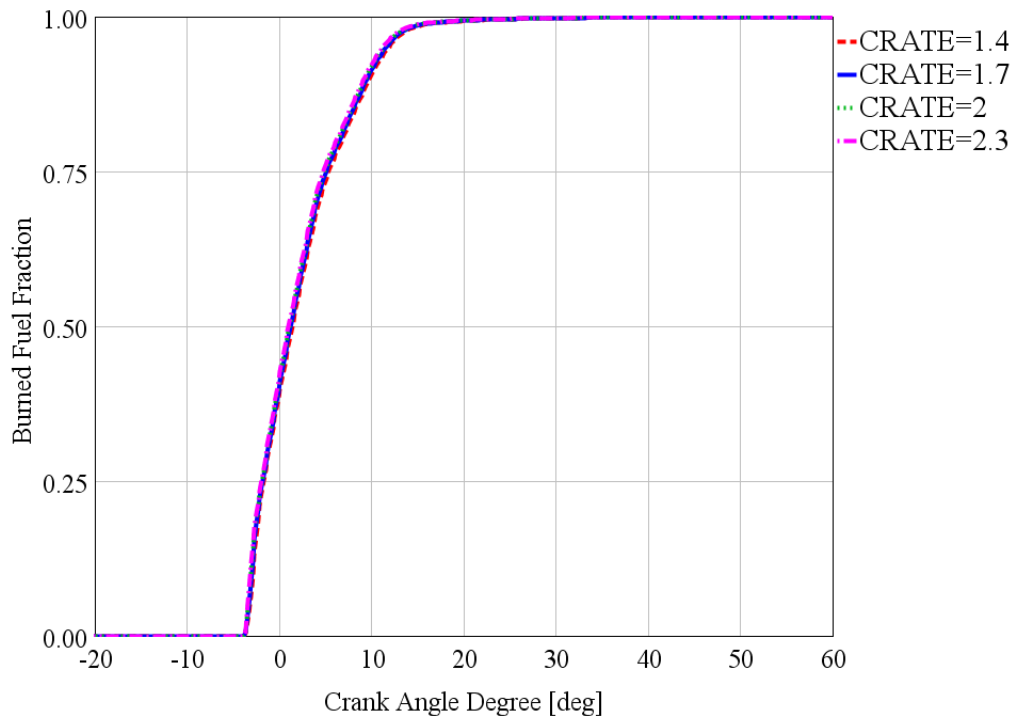


Figure B.12. Change of burn rate with CRATE multiplier.

Table B.9. Emissions and maximum temperature for CRATE sensitivity.

		CRATE =1.4	CRATE =1.7	CRATE =2	CRATE =2.3
Case No		15	1	16	17
Brake Specific NO <sub>x</sub>	g/kW-h	5.50	5.50	5.50	5.51
Brake Specific Soot	g/kW-h	5.48	5.28	5.10	4.95
Temperature, Maximum	K	1964	1965	1965	1966

### B.3. Conclusion

It can be concluded that CRATE is the least effective parameter among the parameters considered. Air entrainment rates are highly important for the model and the most effective parameters are CBAIR, CAAIR and TBMULT (i.e. entrainment multipliers before and after combustion and break up time multiplier). Dilution effect becomes important when EGR is present therefore for ignition delay prediction, different EGR conditions at the same operating point of the engine is necessary. Ignition delay multiplier

can be used for the wide range of operating points for ignition delay purposes. Emissions are directionally correct meaning that they show the expected behavior for changing conditions.

To decrease the number of parameters to be used for combustion correlation, combustion rate multiplier can be eliminated since no significant effect is observed. Dilution multiplier can also be eliminated since there is an overall ignition delay multiplier, which can also account for ignition delay for the whole engine operating region with or without EGR. CAAIR and TBMULT have similar effect on the combustion therefore it is logical to use one of these two. It can be seen that emissions are more sensitive to CAAIR multiplier compared to TBMULT. Therefore CAAIR is selected for combustion correlation. Lastly, CAWALL only effects the end of the combustion process and has very little effect compared to CAAIR and CBAIR, therefore it is also neglected. So three parameters are selected for combustion correlation as listed below.

- Entrainment multiplier before combustion CBAIR
- Entrainment multiplier before combustion CAAIR
- Overall ignition delay multiplier CIGN 1

## **APPENDIX C: TEST SETUP**

### **C.1. Injection Profile Measurement**

For injection rate measurements, IAV injection analyzer is used. The test is conducted at different rail pressures and different fuel injection quantities (fuel mass per cycle). The analyzer has the following technical properties as shown in [21]:

- Direct shot-to-shot measurement of injection rates
- Direct shot-to-shot measurement of injection masses or injected fuel volumes
- Measurement of injection delays
- Up to seven partial injection events per stroke
- Measurement ranges: 0.3 to 150 mg/stroke
- Measuring accuracy: +/- 1% of the value measured
- Application temperature range: -30°C to +125°C
- Adjustable fuel backpressure: 5-180 bar
- Suitability for diesel and gasoline fuels (biofuels etc.) on request

50 measurements are made at the same conditions and averages of these profiles are used. The variance was very low between the profiles as it is written in the measurement accuracy i.e. about +/- 1%.

### **C.2. Dynamometer Measurements**

Dynamometer test are conducted using an AVL performance and emission test rig dynamometer. On this rig; pressures and temperatures on different locations of the engine are measured and cylinder pressure sensors are installed for each cylinder. All of the measurements are done at steady state i.e. enough time is allowed at each operating condition so that the engine comes to a steady point. AVL Concerto is used for post processing the dynamometer measured data and exporting the data to excel.

Figure C.1 from [22] shows a typical diesel engine layout schematic with turbocharger, intercooler and EGR systems. Cylinder pressure measurement and emission measurements are critical for our study. Emissions are measured after the turbine as shown on the layout.

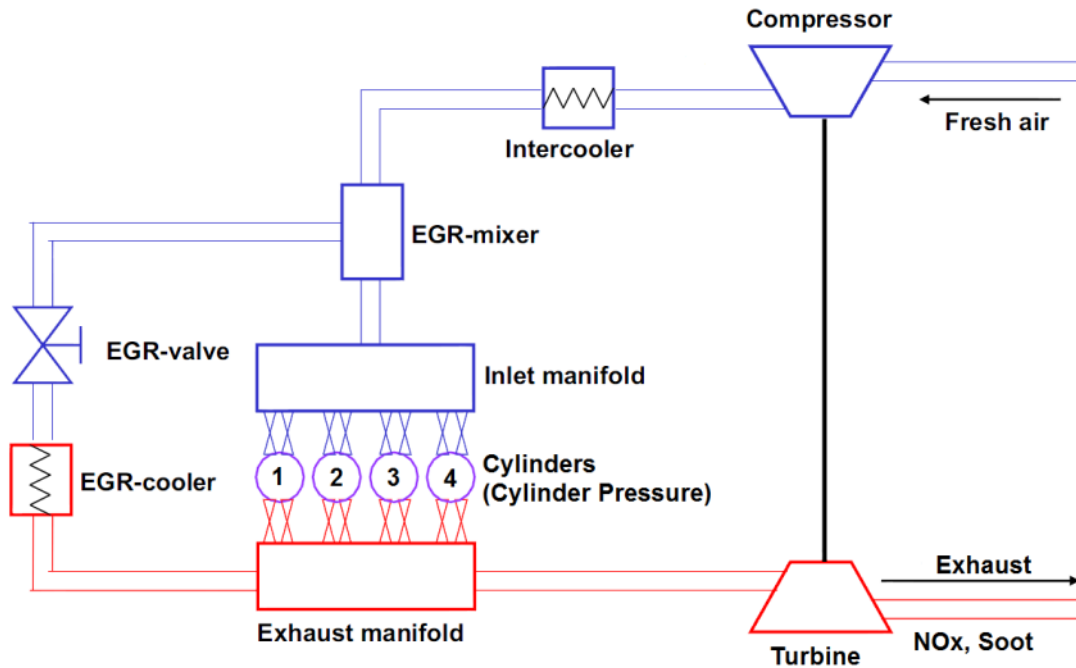


Figure C.1. Diesel engine flow layout schematic [22].

Soot emissions are measured using AVL type smoke meter. However NO<sub>x</sub> emissions are measured by using HORIBA NO<sub>x</sub> analyzer.

AVL smoke meter measures the soot via an optical manner. There is a sampled volume of the exhaust gas, which passes through a filter paper inside the sample volume. According to the blackened paper, a filter smoke number (FSN) is generated. Filter smoke number can be converted to soot density in mg/m<sup>3</sup>, which is explained in the main text. Table C.1 from [23] gives some of the technical properties of the smoke meter.

Table C.1. Smoke meter properties [23].

Measured Value	filter smoke number (FSN) or soot concentration ( $\text{mg}/\text{m}^3$ )
Measurement Range	0 to 10 FSN
Detection Limit	0.002 FSN or $\sim 0.02 \text{ mg}/\text{m}^3$
Resolution	0.001 FSN or $0.01 \text{ mg}/\text{m}^3$
Maximum Temperature	600 °C
Sample Flow	$\sim 10 \text{ l}/\text{min}$

HORIBA type  $\text{NO}_x$  measurement analyzer has a sensor directly inserted into the exhaust flow so there is no sampling as was the case for soot measurement. Zirconia type sensors are used [24]. Table C.2 shows some of the technical specifications of the device taken from [24].

Table C.2. HORIBA  $\text{NO}_x$  Analyzer properties [24].

Measurement Range	0-3000 ppm
Resolution	0-1000 ppm: $\pm 30 \text{ ppm}$ 1001-2000 ppm: $\pm 3\%$ of reading 2001-3000 ppm: $\pm 3\%$ of reading
Sample Conditions	Stoichiometric to lean burned gas Measured Gas Temperature -7 to 800 °C

## **APPENDIX D: DESIGN OF EXPERIMENTS**

Design of experiments (DOE) as the name implies is the name for experiment setup in terms of the input parameters. Different DOE techniques exist to get information about a system by input parameters at hand. Two techniques are used in this study mainly which are full factorial and latin hypercube. Both methods are explained separately.

### **D.1. Full Factorial DOE**

Full factorial is the most used and simplest DOE technique. The minimum and maximum values of the input parameters are determined by the user and additionally user determines how many levels between maximum and minimum values should be tested. So therefore if there are 3 parameters with a, b and c number of levels to be tested, a full factorial test setup results in n number of experiments, where n is the multiplication of a, b and c. This method is good to use for small number of input parameters since high number of input parameters will result too many number of tests. It is a simple method and therefore high knowledge is not required as also explained in [25]. The method is good since the input parameters are divided into evenly increasing levels and each parameter change can be observed while the others are constant. Therefore this technique is also widely used.

This technique is used for emission model correlation work, where two parameters for each emission model were present and it was easier to investigate the models with full factorial DOE and find out the minimum error curves.

### **D.2. Latin Hypercube Sampling**

As explained in the previous section, full factorial DOE results in too many experiments for high number of input parameters. This number increases further if a fine resolution is required by some of the input parameters. Increase of levels of one input parameter multiplies and therefore this affects the total number of experiments drastically.

There is another DOE creation method called latin hypercube sampling, where a more randomized experiment setup in terms of input parameters is used. In this method, again the minimum and maximum values of the input parameters are required but the input parameters are not divided into levels separately. Instead total number of experiments is defined. After that the test grid of input parameters is again divided into a grid of evenly divided squares and defined numbers of tests are picked from that grid randomly, where one value of one input parameter only occurs once in the whole test setup. Figure D.1 from [25] shows this matrix division both for full factorial and latin hypercube methods for 2 input parameters with 9 total number of experiments.

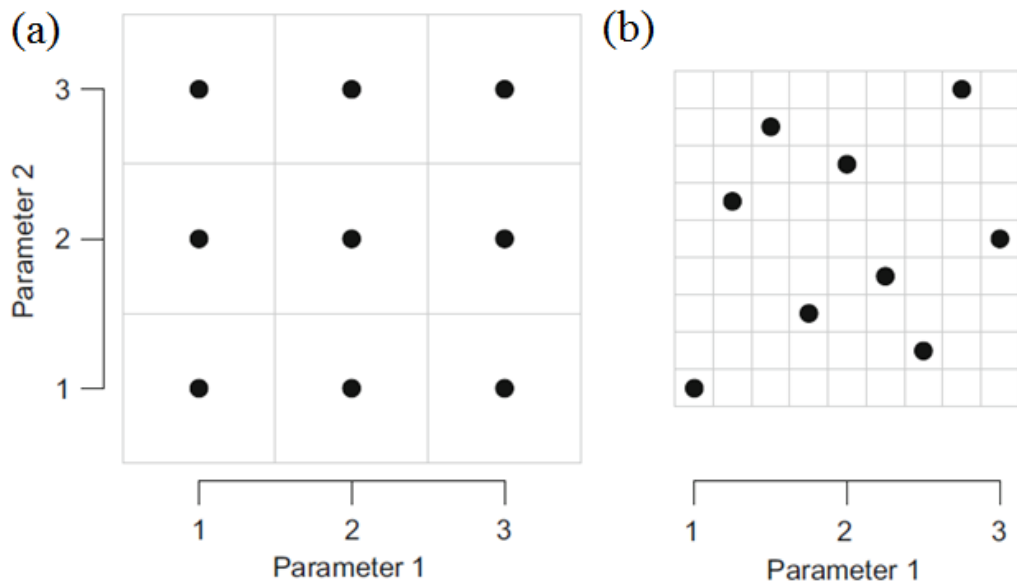


Figure D.1. Test matrix for full factorial (a) and latin hypercube (b) methods [25].

Latin hypercube method is used for correlation of the combustion model, where three correlation parameters were selected and therefore full factorial DOE will increase the number of experiments with the same resolution level. In [25]; it is also stated that there is no obvious advantage of full factorial DOE over latin hypercube design.

## REFERENCES

1. Hiroyasu, H., T. Kadota, and M. Arai, "Development and Use of a Spray Combustion Modeling to Predict Diesel Engine Efficiency and Pollutant Emissions", *Bulletin of the Japan Society of Mechanical Engineers*, Vol. 26, No. 214, 1983.
2. Yoshizaki, T., K. Nishida, and H. Hiroyasu, "Approach to Low NO<sub>x</sub> and Smoke Emission Engines by Using Phenomenological Simulation", *Society of Automotive Engineers Technical Paper Series*, No. 930612, 1993.
3. Morel, T., and S. Wahiduzzaman, "Modeling of Diesel Combustion and Emissions", *The International Federation of Automotive Engineering Societies World Automotive Congress*, Prag, 17-21 June 1996.
4. Barba, C., C. Burkhardt, K. Boulouchos, and M. Bargende, "A Phenomenological Combustion Model for Heat Release Rate Prediction in High-Speed DI Diesel Engines with Common Rail Injection", *Society of Automotive Engineers Technical Paper Series*, No. 2000-01-2933, 2000.
5. Heywood, J. B., *Internal Combustion Engine Fundamentals*, McGraw-Hill, New York NY, USA, 1988.
6. Rhodes, D. B., and J. C. Keck, "Laminar Burning Speed Measurements of Indolene-Air-Diluent Mixtures at High Pressures and Temperatures", *Society of Automotive Engineers Technical Paper Series*, No. 850047, 1985.
7. Maiboom, A., X. Tazua, S. R. Shah, and J-F Hétet, "New Phenomenological Six-Zone Combustion Model for Direct-Injection Diesel Engines", *Energy & Fuels*, Vol. 23, No. 2, pp. 690–703, 2009.



8. Siebers, D. L., “Scaling Liquid-Phase Fuel Penetration in Diesel Sprays Based on Mixing-Limited Vaporization”, *Society of Automotive Engineers Technical Paper Series*, No. 1999-01-0528, 1999.
9. Higgins, B. S., C. J. Mueller, and D. L. Siebers, “Measurements of Fuel Effects on Liquid-Phase Penetration in DI Sprays”, *Society of Automotive Engineers Technical Paper Series*, No. 1999-01-0519, 1999.
10. Siebers, D. L., B. Higgins, and L. M. Pickett, “Flame Lift-Off on Direct Injection Diesel Fuel Jets: Oxygen Concentration Effects”, *Society of Automotive Engineers Technical Paper Series*, No. 2002-01-0890, 2002.
11. Maiboom, A., X. Tauzia, J-F Hétet, and M. A. Cormerais, “5-Zones Phenomenological Combustion Model for DI Diesel Engine for a Wide Range of Operating Conditions”, *The International Federation of Automotive Engineering Societies World Automotive Congress*, Yokohoma, 22-27 October 2006.
12. Rether, D., A. Schmid, M. Grill, and M. Bargende, “Quasi-Dimensional Modeling of CI-Combustion with Multiple Pilot- and Post Injections”, *Society of Automotive Engineers Technical Paper Series*, No. 2010-01-0150, 2010.
13. Pirker, G., F. Chmela, and A. Wimmer, “ROHR Simulation for DI Diesel Engines Based on Sequential Combustion Mechanisms”, *Society of Automotive Engineers Technical Paper Series*, No. 2006-01-0654, 2006.
14. Grill, M., M. Bargende, A. Schmid, and D. Rether, “Quasi-Dimensional and Empirical Modeling of Compression Ignition Engine Combustion and Emissions”, *Society of Automotive Engineers Technical Paper Series*, No. 2010-01-0151, 2010.
15. Kožuch, P., *Ein Phänomenologisches Modell zur Kombinierten Stickoxid- und Rußberechnung bei Direkteinspritzenden Dieselmotoren*, Ph.D. Thesis, University of Stuttgart, 2004.

16. Kennedy, I. M., “Models of Soot Formation and Oxidation”, *Progress in Energy and Combustion Science*, Vol. 23, No. 2, pp. 95-132, 1997.
17. Frenklach, M., “Method of Moments with Interpolative Closure”, *Chemical Engineering Science*, Vol. 57, No. 12, pp. 2229–2239, 2002.
18. Mitchell, P., and M. Frenklach, “Monte Carlo Simulation of Soot Aggregation with Simultaneous Surface Growth”, *Proceedings of the Combustion Institute*, Vol. 27, No. 1, pp. 1507–1514, 1998.
19. Huntington D. E., and C. S. Lyrintzist, “Improvements to and Limitations of Latin Hypercube Sampling”, *Probabilistic Engineering Mechanics*, Vol. 13, No. 4, pp. 245-253, 1998.
20. AVL, *AVL Smoke Value Measurement with the Filter-Paper-Method Application Guide*, 2005, [https://www.avl.com/company?p\\_p\\_id=20&p\\_p\\_lifecycle=1&p\\_p\\_state=exclusive&p\\_p\\_mode=view&\\_20\\_struts\\_action=%2Fdocument\\_library%2Fget\\_file&\\_20\\_folderId=15583&\\_20\\_name=DLFE-301.pdf](https://www.avl.com/company?p_p_id=20&p_p_lifecycle=1&p_p_state=exclusive&p_p_mode=view&_20_struts_action=%2Fdocument_library%2Fget_file&_20_folderId=15583&_20_name=DLFE-301.pdf), accessed at December 2011.
21. IAV GmbH, *IAV Injection Analyzer*, 2011, <http://www.iav.com/sites/default/files/handouts/2011/en/iav-injection-analyzer.pdf>, accessed at December 2011.
22. Maiboom, A., X. Tauzia, and J-F Hétet, “Experimental Study of Various Effects of Exhaust Gas Recirculation (EGR) on Combustion and Emissions of an Automotive Direct Injection Diesel Engine”, *Energy*, Vol. 33, No. 1, pp. 22–34, 2008.
23. AVL, *AVL Smoke Meter Specifications*, 2011, <https://www.avl.com/smoke-meter>, accessed at December 2011.
24. HORIBA, *HORIBA MEXA-720 NO<sub>x</sub> Emission Analyzer Specifications*, 2011, <http://www.horiba.com/automotive-test-systems/products/emission-measurement-systems/portable-emission-analyzers/details/mexa-720-nox-860/>, accessed at December 2011.

25. Urban, N. M., and T. E. Fricker, “A Comparison of Latin Hypercube and Grid Ensemble Designs for the Multivariate Emulation of an Earth System Model”, *Computers & Geosciences*, Vol. 36, No. 6, pp. 746–755, 2010.